Strong edge zero modes in interacting systems

Jack Kemp

St John's College

University of Oxford

A thesis submitted for the degree of

Doctor of Philosophy

Trinity 2019

Abstract

I will discuss how edge spins in certain one-dimensional spin chains retain memory of their initial state for very long times, even with interactions and at infinite temperature. These long coherence times do not require disorder or integrability. I will show how this is a consequence of an "almost" strong edge zero mode that almost commutes with the Hamiltonian, and explain how to compute this operator explicitly with computer-aided algebra. I will examine the effect of this almost strong zero mode on the behaviour of a wide variety of one-dimensional systems analytically, from the ground state to infinite temperature, and from finite size to the thermodynamic limit. I will also examine the effect of the almost strong zero mode on the eigenstate spectrum and the matrix elements of the edge spin, and show that despite the long coherence time of the edge spin, the almost strong zero mode does not induce degeneracies in the entire spectrum, unlike its counterpart exact strong zero mode in non-interacting systems. At special values of the couplings, resonances dramatically limit the coherence time. I will explain how these resonances are related to physical processes which flip the edge spin for no change in the energy of the system, and calculate the coupling strengths for which they appear. I will propose an experimental test of the almost strong zero mode and the long coherence time of the edge spin in a trapped ion chain which is feasible to implement with current technology. Lastly, I will explain how these almost strong edge zero modes in a system with symmetry-protected topological order can be used to form a boundary qubit with both long decoherence and dephasing times.

Acknowledgements

I am sincerely grateful to my supervisor Paul Fendley for his invaluable guidance, advice and support over the four years of my DPhil, both in carrying out the research and in preparation of this thesis. I have deeply enjoyed our weekly conversations on physics.

I would also like to thank to our collaborators Dominic Else, Chris Laumann, Chetan Nayak, Frank Verstraete and Norm Yao for their contributions, and for many interesting discussions.

The EPSRC and St John's College, University of Oxford, financially supported my DPhil and I am grateful to them for making this work possible. I would also like to thank the Theoretical Physics sub-department of the University of Oxford for providing additional funding in the final year of my DPhil.

Finally, my friends and family offered support and encouragement throughout my DPhil. In particular, I would like to thank my mother, Sandra Kemp, for all her help, and for always being there to talk.

Contents

1 Introduction

In this thesis, we will consider 'strong edge zero modes' in interacting and non-integrable quantum systems. We will show how the existence of these strong edge zero modes leads to long coherence times for degrees of freedom localised at the edge of these systems.

We are motivated by a key objective for quantum information processing: to find measurable, local quantum observables which maintain coherence for long times. This would allow the construction of stable qubits. One well-known approach to this problem exploits topological phases of matter. In particular, non-Abelian anyons can be used for complete quantum computation, and there has been much focus on systems in which they could manifest [1–3]. At zero temperature, qubits constructed from such anyons are protected up to terms exponentially small in their separation. However, once the temperature is raised, thermally excited quasi-particles can interact with the anyons, dephasing the qubits. Such quasiparticles will be suppressed by the gap Δ present in topological phases. Thus at temperatures greater than $T > \Delta$ we should expect the topological protection to break down completely [1, 4].

Indeed, at non-vanishing temperatures, we run into a fundamental obstacle to constructing locally conserved quantities: thermalisation. Although quantum systems are unitary, and therefore conserve information, there is no guarantee that memory of the initial state will remain local, and thus no guarantee that it will remain recoverable. Instead, generic quantum systems are expected to obey the so-called 'eigenstate

thermalisation hypothesis', which implies that the statistical properties of physically measurable quantities are given by the microcanonical ensemble [5, 6]. Systems obeying the eigenstate thermalisation hypothesis relax to a time-independent thermal equilibrium in which the expectation values of local observables can be calculated from equilibrium stastical mechanics.

One well-known special class of systems which evade the eigenstate thermalisation hypothesis are integrable systems. Integrable systems have a macroscopic number of (quasi)-local conserved quantities [7]. Note that all quantum systems governed by Hermitian Hamiltonians have an extensive number of conserved operators given by projectors onto the Hamiltonian's eigenbasis – the key difference in integrable systems is the locality of the conserved operators. This suggests we could use integrability to avoid memory loss of the initial state, and construct stable qubits. However, any perturbation which breaks the quantum integrability will ultimately lead to thermalisation [8].

Many-body localisation allows one to obtain pseudo-integrability which is stable to perturbations via the introduction of strong quenched disorder [9]. It can be shown that as the disorder strength is increased, certain systems undergo an eigenstate phase transition from a thermal phase obeying the eigenstate thermalisation hypothesis to a many-body localised phase which never reaches thermal equilibrium [10]. The term eigenstate phase transition is used here because the transition is in the entire energy spectrum, rather than just the ground state. In this many-body localised phase, the absence of transport means there are an extensive set of local conserved charges, called 'l-bits'. There are akin to the quasilocal conserved quantities in integrable systems, but are not sensitive to perturbations, because weak pertubations cannot delocalise the system. In fact many-body localisation is a stronger constraint than integrability, because while it may be shown that integrable systems relax to an equilibrium 'generalised Gibbs ensemble' which nevertheless carries more memory of its initial state than the thermodynamic equilibrium [11], many-body localised systems do not quantum thermalise in any sense [9].

However, in this thesis, we focus on systems without disorder. We will study long-lived, local operators which live on the edge of the one-dimensional quantum systems, called strong edge zero modes. They are called 'strong' edge zero modes because they

are stable even at infinite temperature, distinguishing them from 'weak' edge zero modes, which are protected only at low energy densities. The anyonic edge zero modes familiar from the study of topological phases are all by definition at least weak edge zero modes. They may also be strong edge zero modes, as we shall discuss. The converse is not true – there are weak and strong edge zero modes that are not topological. Indeed, we will for the most part focus on spin chains without topological order. We will often omit the term 'edge' from strong edge zero mode where it is clearly understood.

Strong edge zero modes are operators which are exponentially localised on the edge of a system, and which commute with a Hamiltonian up to exponentially small corrections in the system size. They are thus both local and conserved, at least up to these small corrections. The most famous example of a strong edge zero mode is Kitaev's Majorana zero mode [12]. In his original paper, Kitaev showed that in a certain parameter regime of a simple model of a spinless one-dimensional superconductor, now dubbed the Kitaev chain, stable, unpaired Majorana fermions lived on the edge of the chain. He proved that these Majorana fermions located on either end of the chain do not interact with the bulk of the system, but only with each other. We can construct a qubit by considering these two Majorana fermions as one, non-local Dirac fermion, with occupation zero or one as normal. Thus, as the separation between the two ends becomes infinite, the ground state becomes twofold degenerate.

As the Majorana fermions are localised at opposite ends of the system, this degeneracy is topological, and the phase in which they exist is topologically ordered. The Kitaev chain is equivalent by a Jordan-Wigner transformation to the one-dimensional transverse-field Ising model. Under this transformation, the topological phase of the Kitaev chain is equivalent to the global $\mathbb{Z}_2$ symmetry-broken phase of the transverse-field Ising model. Although the Jordan-Wigner transformation is non-local, which is what allows the symmetry-broken phase to transform into a topologically ordered phase, the edge spins and unpaired Majorana fermions are simply related, as we shall discuss formally below.

Kitaev was focussed on the degeneracy in ground state, because of the consequences for topological order. However, his proof was already sufficient to show that not only in the ground state, but the *entire* spectrum was twofold degenerate as a consequence of

the existence of his unpaired Majorana fermions. This condition is much stronger than is required for topological order, which only requires the ground state to be degenerate. Alicea and Fendley [13] coined the term 'strong zero mode' to distinguish strong zero modes, which commute with the Hamiltonian and thus provide this total spectrum degeneracy, from the 'weak zero modes' sufficient for topological order, which need only commute in the ground level subspace.

We stress that strong zero modes need not also be topological zero modes. For example, the Majorana zero mode in the Kitaev chain is both a topological zero mode and a strong zero mode, but the related strong zero mode in the transverse-field Ising spin chain is *not* topological. This is manifest, because there is no topological order in the transverse-field Ising model. This difference is critical for practical applications. While we can construct a qubit from Majorana fermions, by contrast the protection of the edge spin due to the strong zero mode is purely classical – it prevents depolarisation, but not dephasing. We will discuss a method of constructing an edge qubit in a spin chain, which will involve reintroducing topological order.

How does the strong edge zero mode dodge thermalisation? The answer appears to be that the only two known strong zero modes which are exactly conserved in the thermodynamic limit exist in integrable systems. The Kitaev chain is a free fermion system, so not only is it integrable but it lacks interactions. Fendley explicitly constructed the strong edge zero mode in the XYZ model, which has interactions but is still integrable [14].

It is the focus of this thesis to consider what happens to the strong zero mode when we perturb interacting systems away from integrability. We shall find that the exact strong zero mode is broken down to an almost strong zero mode. The almost strong zero mode does not commute exactly with the Hamiltonian in the thermodynamic limit, but instead commutes up to corrections exponentially small in the perturbation away from integrability. Crucially, this means that the coherence time of the edge spin or fermion remains long compared to the bulk, even in interacting, non-integrable systems at infinite temperature. This long coherence time for edge spins due to the almost strong zero mode is the key result of this thesis.

Notice that because the coherence time is not infinite, the almost strong zero mode does not prevent the system from ultimately thermalising. Instead, we observe that the autocorrelation of the edge spin relaxes quickly to a plateau, which itself decays on exponentially longer timescales. This is related to the concept of prethermalisation, in which local physical observables in weakly perturbed integrable theories relax to transient non-thermal values predicted by the nearby integrable theory [8, 15, 16], before thermalising on much longer timescales. Indeed, in order to prove the existence of the almost strong zero mode in the thermodynamic limit we shall rely on a theorem due to Abanin *et al.* [17], which establishes the existence and lifetimes of the prethermal regime for certain systems.

The main test Hamiltonian for this thesis will be the transverse-field Ising model with interactions. The model is equivalent by Jordan-Wigner transformation to the Kitaev chain with four-fermion interactions. In fact, strong zero modes have already been considered in this model by Kells [18]. Unfortunately, Kells erroneously concluded that the strong zero mode would remain exact under four-fermion perturbations as long they did not close the gap – that is, as long as they did not destroy the topological order. He did this by constructing perturbation theory for the change in the eigenstate spectrum, and showed that it remained exactly twofold degenerate to first order in the perturbation. However, Kells then assumes his construction remains valid to all orders, and that the perturbation theory converges. We will show rigorously that this is not the case, and that the exact strong zero mode is replaced by an almost strong zero mode which does not yield a twofold degenerate eigenspectrum in the thermodynamic limit. Indeed it would be very surprising if the exact strong zero mode survived, albeit not entirely impossible *a priori*, because it would mean that this interacting, non-integrable system would not thermalise.

The thesis compromises chiefly of my own contributions to three papers, [19–21], written in collaboration with my supervisor Paul Fendley, and the other co-authors Dominic Else, Chris Laumann, Chetan Nayak and Norman Yao. Other important work on strong zero mode includes Fendley's proof of the exact strong zero mode in the XYZ model already mentioned [14], and a significant body of work on strong edge zero modes in chiral Potts, or parafermionic, systems [13, 22–24]. In this thesis we will build on the

former by considering the physical consequences of the exact strong zero mode in the XYZ model. We will often compare the behaviour of the edge spin in the interacting but still integrable XYZ model to both the free transverse-field Ising model, and to the non-integrable transverse-field Ising model with interactions. We will also briefly revisit the work on parafermions using the analytical structure developed in the thesis, and show numerics illustrating that the long coherence time for edge spins due to the almost strong zero mode transfer to long coherence times for edge parafermions.

We shall confine ourselves to one-dimensional, closed quantum systems, with the sole exception of the pseudo-one-dimensional case of two coupled transverse-field Ising chains. In higher dimensions, Dominic Else and Chetan Nayak have constructed almost strong edge zero modes along a one-dimensional boundary of a two-dimensional toric code, as well as along Cheshire-charge carrying loops in the three-dimensional toric code [20]. Vasiloiu *et al.* have also constructed strong edge zero modes in a class of generalised Ising spin ladders with plaquette interactions [25]. For open, non-Hermitian systems, Vasiloiu *et al.* studied the strong zero modes in the transverse-field Ising and XYZ models and showed that the long coherence time for edge spins persists even when dissipation is included [26].

We will discuss the strong edge zero mode particularly in respect to its ability to generate long coherence times for local observables at the edge of the system which could be used in quantum information processing. However, other physical consequences are of course possible. For example, McGinley *et al.* [27] found a slow logarithmic growth in the late-time entanglement entropy of free, disordered systems with strong zero modes following a quench from an unentangled initial state.

The thesis is divided into eight chapters. Following this Introduction, in Chapter 2 we will review the construction of the exact strong zero mode in the transverse-field Ising model or Kitaev chain. In Chapter 3 we will discuss in detail the almost strong edge zero mode, and examine its effects both analytically and numerically. We will describe how it may be explicitly constructed in perturbation theory with help from a computer-aided algebra program. We will consider the general conditions for its existence, and examine why and when it breaks down, including at special points called ‘resonances’. We discuss

a rigorous method for showing where these resonances exist, extending greatly the previously published work in [19]. In Chapter 4 we will consider which general classes of systems strong edge zero modes can be expected to exist, and we shall discuss resonances in the chiral Potts model as an example. We also look at finite-size, boundary-condition and finite-temperature effects in much greater detail than in my contributions to [19, 20]. In Chapter 5, we will study the effects of exact and almost strong edge zero modes on the entire energy spectrum. We will look at both degeneracies in the spectrum and the structure of the matrix elements of the edge spin in the eigenstate basis, and show how these can give us insight into the behaviour of the almost strong zero mode, both with and without resonances. We shall also examine the effects of adding both weak and strong disorder to our spin chains, and the possibility of eigenstate phase transitions. Chapter 6 focuses on a particular model with $\mathbb{Z}_2 \times \mathbb{Z}_2$ symmetry-protected topological order which we use to construct a complete qubit enjoying the edge zero mode protection. We shall do this by showing that the topologically ordered system is unitarily equivalent to coupled transverse-field Ising chains in their symmetry broken phase, and we shall analyse the resonance structure of the two resulting almost strong zero modes. Chapter 7 explores possible experimental tests of the strong zero mode in a trapped ion chain with long-range interactions. Finally, following a summary of my results in this thesis, we will outline possible future avenues of research, including higher dimensions, and possible deeper connections between the strong zero mode and integrability.

2

Exact strong edge zero modes

2.1 The model

We study quantum spin chains with L sites and open boundary conditions. For simplicity, we focus on systems with two states per site. A convenient basis for operators acting on the 2^L-dimensional Hilbert space is given by products of σ_j^a, the Pauli matrix σ^a acting at site j and trivially on the others, i.e. $\sigma_j^a = 1 \otimes 1 \otimes \ldots 1 \otimes \sigma^a \otimes 1 \otimes \cdots \otimes 1$. We will generally study models with a $\mathbb{Z}_2$ symmetry under flipping all spins, where the operator

$$\mathcal{F} = \prod_{j=1}^{L} \sigma_j^x \tag{2.1}$$

commutes with the Hamiltonian. We focus on ordered phases where the spin-flip symmetry is spontaneously broken, i.e. in infinite volume the system has two distinct ground states $|g_+\rangle$ and $|g_-\rangle$ with $\mathcal{F}|g_\pm\rangle = \pm|g_\pm\rangle$. An important example is the transverse-field Ising chain, with Hamiltonian

$$H_{\text{Ising}} = -J \sum_{j=1}^{L-1} \sigma_j^z \sigma_{j+1}^z - \Gamma \sum_{j=1}^{L} \sigma_j^x \ . \tag{2.2}$$

The ordered phase occurs for $|\Gamma| < |J|$. Throughout the thesis we shall work in natural units with $\hbar = k_B = 1$.

We note that we may make a change of variables by a Jordan-Wigner transformation [28] to a Majorana-fermion representation

$$H_{\text{Kitaev}} = iJ \sum_{j=1}^{L-1} b_j a_{j+1} + i\Gamma \sum_{j=1}^{L-1} a_j b_j, \tag{2.3}$$

where the Majorana fermions a_j, b_j are given by

$$\begin{aligned} a_j &= \left(\prod_{k=1}^{j-1} \sigma_k^x \right) \sigma_j^z \\ b_j &= i a_j \sigma_j^x \end{aligned} \tag{2.4}$$

and have anticommutation relations

$$\begin{aligned} \{a_j, b_j\} &= 0 \\ \{a_j, a_k\} &= \{b_j, b_k\} = 2\delta_{jk}. \end{aligned} \tag{2.5}$$

The $\mathbb{Z}_2$ spin-flip symmetry is of course preserved by the transformation, and becomes fermion parity

$$\mathcal{F} = \prod_{j=1}^{L} \sigma_j^x = -i \prod_{j=1}^{L} a_j b_j.$$

This fermionic version of the Ising Hamiltonian (2.2) is often known as the Kitaev chain, and the $\mathbb{Z}_2$ spin order corresponds to topological order in this picture.

Although we choose couplings so that the ground state is ordered, our interest is in the behavior of highly excited states. We explain how under a certain set of conditions, long-time coherence in the edge spin occurs even when the initial state is at infinite temperature. The basic physical quantity we study is the autocorrelator of the edge spin magnetization

$$A_s(t) \equiv \langle s \,|\, \sigma_1^z(t) \sigma_1^z(0) \,|\, s \rangle \ , \tag{2.6}$$

where s is an eigenstate of the Hamiltonian. We will often be interested in this quantity at infinite temperature. With a slight abuse of notation, we dub this autocorrelator as

$$A_\infty(t) \equiv \frac{1}{2^L} \sum_s A_s(t) \ . \tag{2.7}$$

Notice that this infinite temperature autocorrelator is an equally weighted mean of the autocorrelator in each of the 2^L eigenstates. This means that the (twofold degenerate)

ground state has negligible impact at infinite temperature. This is important, because the familiar ground state has very different properties from typical states in the middle of the spectrum. In particular, gapped ground states in one dimension always exhibit area-law growth of entanglement entropy [29], while typical states in the middle of the many-body spectrum exhibit volume law growth of entanglement entropy [30]. If we were to break integrability so that our system obeyed the eigenstate thermalisation hypothesis, we should expect typical states in the middle of the spectrum to be 'thermal', lacking any quantum order present in the ground state [10].

2.2 Definition and explicit construction

The especially long lifetime of the edge-spin coherence arises as a consequence of a *strong zero mode* [13, 14, 22, 23].

A strong zero mode is an operator Ψ that satisfies the following conditions:

1. almost commutes with the Hamiltonian: $[H, \Psi] = \mathcal{E}$, where the "error" $\mathcal{E}$ is an operator with norm $|\mathcal{E}| < e^{-\alpha L}$ with α a positive constant,

2. exponentially localised at the edge of a system,

3. squares to the identity operator: $\Psi^2 = \mathbb{1}$.

The most famous example of a strong edge zero mode is that localised on the edge of the Ising chain [12, 31]. Trivially when $\Gamma = 0$, the operator σ_1^z obeys all three conditions above. It corresponds to the Majorana fermion operator a_1 on the edge, which does not appear in H_{Kitaev} when $\Gamma = 0$ and so commutes with it. In phases with topological order, edge zero modes mapping the ground states between each other are common (although not necessary). Having Ψ for *all* the states is thus a much stronger condition, hence the name [13].

A remarkable fact is that the strong zero mode survives throughout the ordered phase $|\Gamma| < |J|$ of the Ising chain. This is quite simple to derive following the iterative

procedure described in [12, 14], and we review this quickly here. We set $\Psi^{(0)} = \sigma_1^z$, since this commutes with H_0. However, it does not commute with the full Hamiltonian

$$[H, \Psi^{(0)}] = 2i\Gamma\, \sigma_1^y\, . \tag{2.8}$$

We then need to add a term to the zero mode of order Γ to cancel this; $\Psi^{(1)} = (\Gamma/J)\sigma_1^x\sigma_2^z$ does the trick. However, this now generates a term of order Γ^2

$$[H, \Psi^{(0)} + \Psi^{(1)}] = 2i(\Gamma^2/J)\, \sigma_1^x\sigma_2^y\, .$$

This in turn can be canceled by including a term $\Psi^{(2)} = (\Gamma/J)^2\sigma_1^x\sigma_2^x\sigma_3^z$, generating a new term of order Γ^3.

Continuing in this fashion gives

$$\begin{aligned}\Psi &= \mathcal{N}_{\text{Ising}} \left[\sigma_1^z + \frac{\Gamma}{J}\sigma_1^x\sigma_2^z + \left(\frac{\Gamma}{J}\right)^2 \sigma_1^x\sigma_2^x\sigma_3^z + \dots\right] \\ &= \mathcal{N}_{\text{Ising}} \sum_{j=1}^{L} \left(\frac{\Gamma}{J}\right)^{j-1} \sigma_j^z \prod_{k=1}^{j-1} \sigma_k^x\, .\end{aligned} \tag{2.9}$$

The operator Ψ satisfies all three conditions for the strong zero mode throughout the ordered phase. Because each term in the expansion (2.9) anticommutes with each other one, setting the normalization to obey

$$(\mathcal{N}_{\text{Ising}})^2 = \frac{1-(\Gamma/J)^2}{1-(\Gamma/J)^{2L}} \approx 1 - \left(\frac{\Gamma}{J}\right)^2\, . \tag{2.10}$$

makes $\Psi^2 = \mathbb{1}$. The norm is non-vanishing as $L \to \infty$ when $|\Gamma| < |J|$. In this phase, Ψ does indeed commute with the Hamiltonian up to an exponentially small correction

$$\mathcal{E} \equiv [H, \Psi] = 2\mathcal{N}_{\text{Ising}}\Gamma \left(\frac{\Gamma}{J}\right)^{L-1} \mathcal{F}\, \sigma_L^z. \tag{2.11}$$

Moreover, in this phase, the norm of each term in the expansion (2.9) decreases quickly with j, justifying the name of strong *edge* zero mode. We of course can construct another strong edge zero mode on the other end, by starting with σ_L^z instead of σ_1^z. The two edge zero modes anticommute with each other.

An intuitive way of thinking about the higher terms in the expansion of the strong zero mode is that they describe how information initially stored on the boundary "leaks"

into the bulk. All the higher-order terms contain σ_1^x and so flip the edge spin. Thus they partially, but not completely, decohere the edge spin. Indeed, their presences reduces $\mathcal{N}_{\text{Ising}}$, which we will show reduces the asymptotic value of $A_\infty(t)$.

As an example, using exact diagonalization, $A_\infty(t)$ is plotted for $\Gamma = 0.3$ for very long times in figure 2.1; note that the time axis is logarithmic. We see that initial

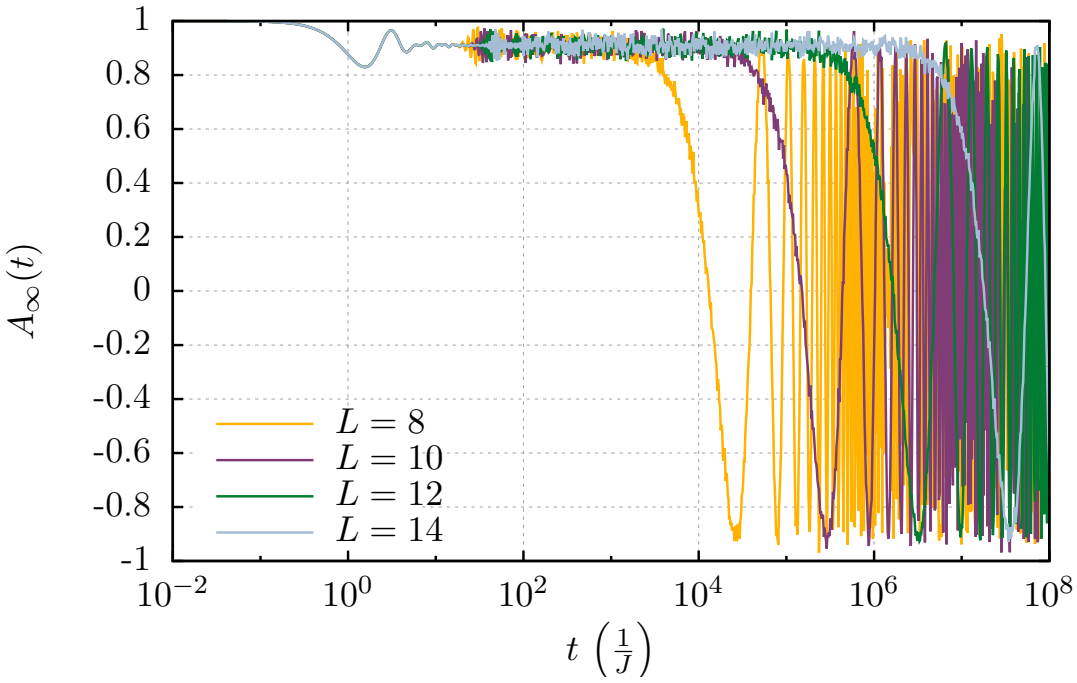

Figure 2.1: $A_\infty(t)$ from exact diagonalization for the transverse-field Ising model on a log axis for time for $\Gamma = 0.3$. Revivals appear at a time scale set by the finite size.

oscillating pieces die off very quickly in time to a long-lived plateau at the value $\mathcal{N}_{\text{Ising}}^2 = (1 - (.3)^2) = .91$. The coherence time indeed grows exponentially with increasing L, since the error term $\mathcal{E}$ has norm decaying exponentially. The plateau falls off at a time roughly $1/|\mathcal{E}|$, where the decay time arises from the "error" in (2.11). This gives the finite-size dependence of the coherence to be

$$T_{\text{Ising}} \sim \frac{1}{\sqrt{J^2 - \Gamma^2}} \left(\frac{J}{\Gamma}\right)^L . \tag{2.12}$$

This indeed goes to infinity as $L \to \infty$, but even for rather modest system sizes, the finite-size effects do not appear until very long times.

An phenomena apparent at finite sizes and long enough times is that the autocorrelator "revives", returning to its initial value. That this is visible in such a plot is a consequence

of the free-fermion nature of Ising: the energy differences in all Ising pairs are identical, and so sum up coherently at much shorter times than they would in an interacting system. We will discuss finite-size effects in more detail in section 4.6.

Since a single σ_j^z appears in each term, Ψ anticommutes with $\mathcal{F}$. Because $[\mathcal{F}, H] = 0$, eigenstates of H can be organized into sectors with $\mathcal{F} = \pm 1$. The presence of a strong zero mode guarantees that the *entire* spectrum in the $\mathcal{F} = 1$ sector is the same as that in the $\mathcal{F} = -1$ sector, up to corrections of order $e^{-\alpha L}$. Namely, eigenstates of H form "pairs" $|s_+\rangle$ and $|s_-\rangle$, with $E_{s_+} \approx E_{s_-}$ and $|s_\pm\rangle \approx \Psi|s_\mp\rangle$, up to these finite-size corrections.

Meanwhile, in the Majorana fermion picture, the strong zero mode takes on the particularly simple form

$$\Psi = \mathcal{N}_{\text{Ising}} \sum_{j=1}^{L} \left(\frac{\Gamma}{J}\right)^{j-1} a_j \ .$$

These is a fundamental difference between the strong zero modes in the two pictures related to the fact that global symmetry breaking in the spin picture becomes topological order in the fermion picture. The long coherence time in the spin picture is for a purely *classical* quantity: the edge magnetisation. The protection is against depolarisation, and not dephasing, for which we would also require conjugate zero modes protecting $\sigma_1^{x,y}$ as well. On the other hand, it is well known that one can use the Majorana zero mode localised on the edge of Kitaev chain for limited quantum computation [32]. The operations rely on braiding the zero modes and exploiting their anyonic properties, a feature of the topological order entirely absent in the spin picture. Nevertheless, for the rest of this thesis we will focus on the spin picture, and later will discuss how we might obtain the conjugate zero modes necessary for constructing a full qubit enjoying this edge protection.

3
Almost strong edge zero modes

The transverse-field Ising model is a free fermion system. One might therefore believe that the strong edge zero mode's existence relies on the absence of interactions. In fact, Fendley [14] proved that an exact strong edge zero mode also exists in the XYZ spin chain

$$H_{\mathrm{XYZ}} = \sum_{j=1}^{L-1} \left[J_x \sigma_j^x \sigma_{j+1}^x + J_y \sigma_j^y \sigma_{j+1}^y + J_z \sigma_j^z \sigma_{j+1}^z \right]. \tag{3.1}$$

He did this by constructing perturbatively a formula for the strong zero mode which is valid at all orders, much as we explained for the transverse-field Ising model, and showing that the normalisation converged to

$$\mathcal{N}_{\mathrm{XYZ}} = \sqrt{J_x^2 - J_z^2}\sqrt{J_y^2 - J_z^2}\,. \tag{3.2}$$

Technically we must also prove that the error $[H, \Psi]$ vanishes in the thermodynamic limit. This was not discussed in [14], but has now been proved. We will discuss this point further in section 8.1.

The XYZ model has interactions, but crucially it is still integrable. Is it possible to find a strong edge zero mode in a non-integrable system with interactions?

3.1 ADHH Theorem

The answer is yes, but only if we relax our criteria for the error. Rather than having the error decrease exponentially with system size, $|\mathcal{E}| < e^{-\alpha L}$, we shall instead bound

it by a factor exponentially small in the ratio n^* of a small to large coupling, so that $|\mathcal{E}| < e^{-cn^*}$. This means that as we approach semi-infinite limit the coherence time will *saturate* at some long but finite time. We will describe such strong edge zero modes as 'almost' strong edge zero modes as opposed to the 'exact' strong edge zero modes in the transverse-field Ising model and XYZ.

The existence of such almost strong edge zero modes, and rigorous bounds on their error, is provided by a theorem proved by Abanin, De Roeck, Huveneers and Ho (henceforth ADHH) [17]. This theorem applies to Hermitian Hamiltonians of the form

$$\hat{H} = -J\hat{N} + \hat{Y}, \tag{3.3}$$

where $\hat{N}$ is a sum of finite-range commuting terms, such that $\hat{N}$ has integer eigenvalues, i.e. $e^{2\pi i\hat{N}} = 1$. The proof in Ref. [17] assumes that each term in $\hat{N}$ acts only on a single site, but in Appendix A of [20] it was shown that assumption could be relaxed to terms with finite support. We define a parameter Y that is essentially the largest operator norm of any local term in $\hat{Y}$; more explicit forms are given in specific examples below. The theorem says that for Y/J sufficiently small, there exists a local unitary transformation $\mathcal{U}$ such that

$$\mathcal{U}\hat{H}\mathcal{U}^\dagger = -J\hat{N} + \hat{D} + \hat{V} \tag{3.4}$$

where $[\hat{N}, \hat{D}] = 0$ and $\|\hat{V}\| = O(e^{-cn_*})$ where

$$n_* = \left\lceil \frac{J/Y}{[1+\log(J/Y)]^3} \right\rceil \tag{3.5}$$

and c is a constant. Since we focus on the $J \gg Y$ limit, we often drop the 1 in the denominator of Eq. (3.5) for the sake of uncuttering the equations. As a result, the dynamics of the system conserves $\hat{N}$ until a time $t_* \propto e^{cn_*}$. A more precise statement of the ADHH theorem can be found in Ref. [17].

For our purposes, the essential point of the ADHH theorem is that such Hamiltonians have an emergent approximate $U(1)$ symmetry generated by $\hat{N}$. The symmetry violations come from terms in the transformed Hamiltonian that are nearly *exponentially small* in the large-J limit. Heuristically, the transformation to the form (3.4) means that it is very difficult for the terms in $\hat{Y}$ to cause transitions between different eigenspaces of

$\hat{N}$: in order to conserve energy, many excitations of $\hat{Y}$ must be created or annihilated. Such a process occurs slowly, so violation of the approximate $U(1)$ symmetry takes a very long time.

The key idea is that, when an almost strong zero mode exists, this emergent symmetry forbids the flipping of the edge spin in the transformed Hamiltonian. For example, suppose $\hat{N}$ is given by the transverse-field Ising model ordering term $\hat{N}_{\text{Ising}} = \sum_i \sigma_i^z \sigma_{i+1}^z$. Then the emergent $U(1)$ represents conservation of domain walls in the transformed Hamiltonian. Crucially, it is not possible to flip a single edge spin without creating or destroying a domain wall. For example, consider the process

$$\uparrow\downarrow\downarrow\cdots \qquad \Leftarrow \qquad \downarrow\downarrow\downarrow\cdots . \tag{3.6}$$

Here we have flipped the edge spin by moving a single domain wall all the way to the edge, but in doing so destroyed the domain wall, taking us to a different eigensector of $\hat{N}$, which is forbidden by ADHH.

Formally $\hat{D}$ cannot contain terms with only one of $\sigma_{1,L}^{x,y}$. This means that, excluding finite-size effects, σ_1^z is conserved up to time t_* in the transformed Hamiltonian. If we transform back, the almost strong zero mode is given by

$$\Psi = \mathcal{U}^\dagger \sigma_1^z \mathcal{U}.$$

Because $\mathcal{U}$ is a sum of local terms, Ψ is still edge localised.

3.1.1 Transverse-field Ising model with interactions

As a concrete example of the interactions to add into the $\hat{Y}$ term, let us consider the Hamiltonian

$$H = H_{\text{Ising}} - \Gamma_2 \sum_{j=1}^{L-1} \sigma_j^x \sigma_{j+1}^x - J_2 \sum_{j=1}^{L-2} \sigma_j^z \sigma_{j+2}^z \, . \tag{3.7}$$

In the fermionic picture, the new terms are the simplest four-fermion interactions, but as opposed to the XYZ chain, either interaction breaks the integrability. Both perturbing operators have dimension 4 at the Ising critical point, and so are irrelevant in the renormalization-group sense. We thus expect that for small enough J_2 and Γ_2,

the coherence time of the edge spin should remain infinite for all eigenstates s whose energy density is the same as that of the ground state, since if all the couplings other than J are small, the model is still ordered.

However, due to the existence of the almost strong zero mode, we should expect the coherence time to remain long, but finite, even at infinite temperature. Using exact diagonalisation to find all the eigenstates and eigenvalues, example decays of the autocorrelator are plotted in figure 3.1 for various system sizes for a Hamiltonian with $J_2 = 0$. We see that the coherence time is indeed long and furthermore there is saturation: the curves for $L = 12$ and $L = 14$ are virtually identical.

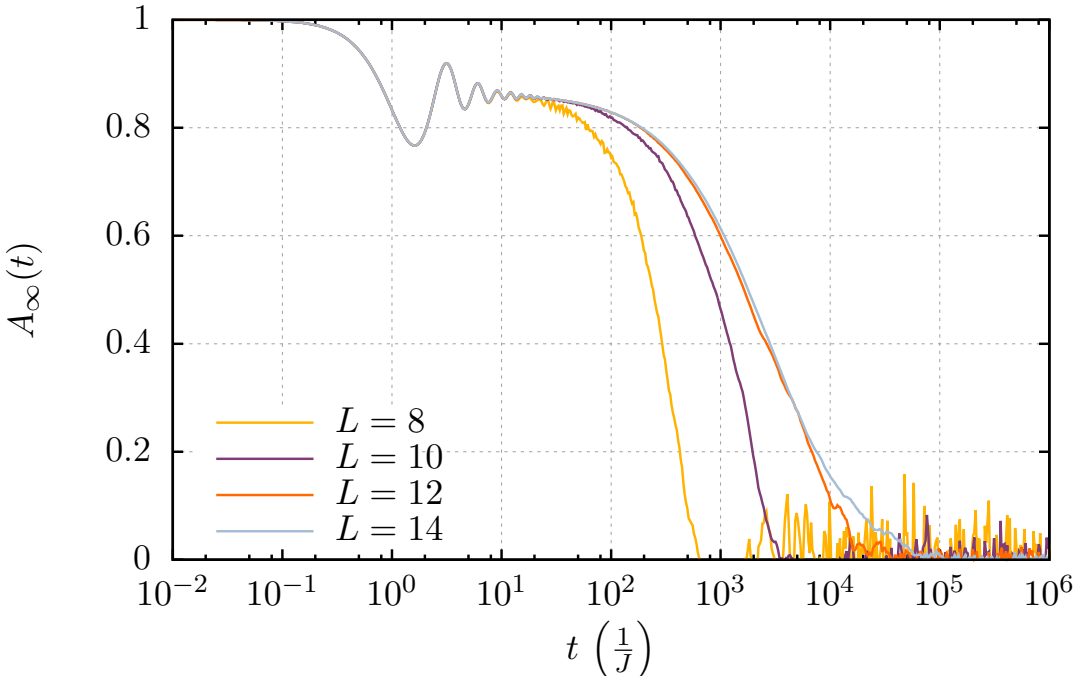

Figure 3.1: $A_\infty(t)$ for transverse-field Ising with $\Gamma = \Gamma_2 = 0.25$ from exact diagonalization. Notice the curve saturates with L.

In fact, the decay times are consistent with an exponential dependence on the ratio of scales J/Y until the lifetime becomes so long that finite-size effects become important, where $Y = \Gamma_2 / f(\Gamma/\Gamma_2)$ for some function $f(x)$. As may be seen from figure 3.2, the data collapses onto this form. Here the decay times have been estimated from an exponential fit to plots of $A_\infty(t)$ calculated from exact diagonalisation, such as in 3.1, and whenever a decay time plot is shown below it is calculated using this method. Notice the short

coherence time of a bulk spin in contrast to the edge spin, even at such comparatively small system sizes. A similar fit for the case when J_2 is the interaction term rather than Γ_2 is shown for system sizes up to $L = 20$ in 3.3.

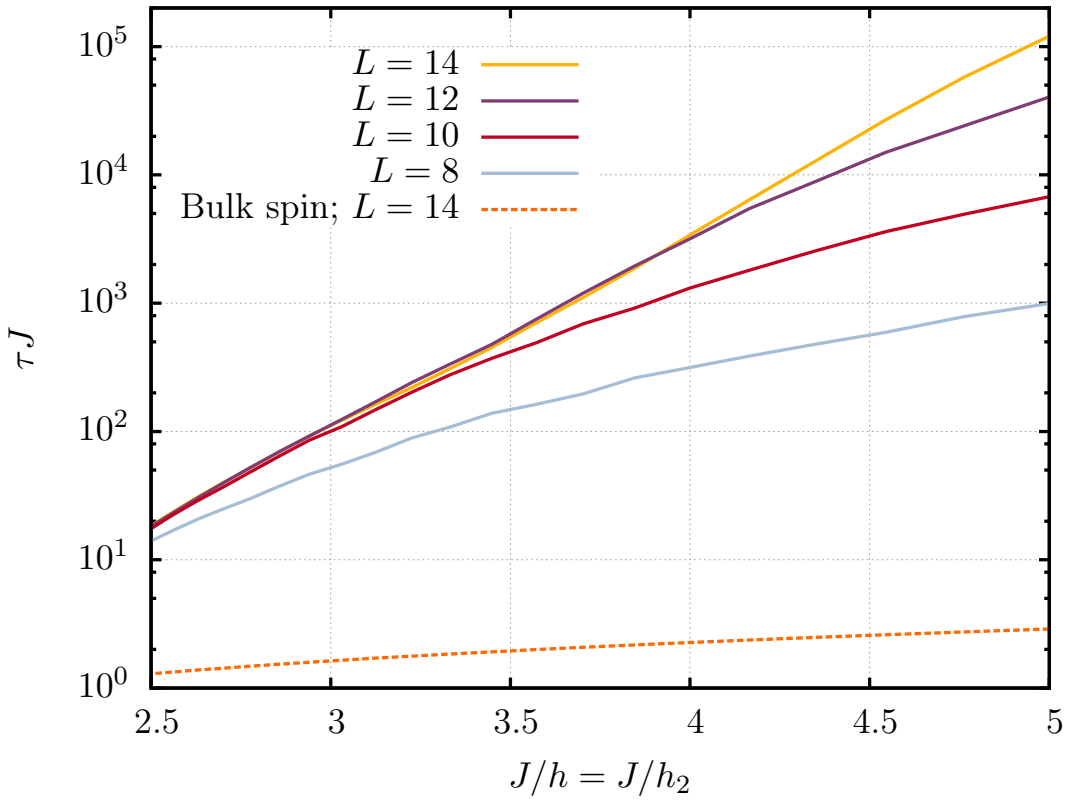

Figure 3.2: The decay time (on a logarithmic scale) of the edge spin at $T = \infty$ for $L = 8 - 14$ sites, as a function of Γ and Γ_2, as obtained by exact diagonalization. The data collapses onto the form $\ln \tau J = J/\Gamma_2 \, f(\Gamma/\Gamma_2) +$ constant, as expected, with deviations due to finite-size effects when the lifetime is long. The decay time of the spin at the centre of the $L = 14$ chain (dashed line) is not protected by the almost strong zero mode and is much shorter.

3.2 Explicit construction of the almost strong zero mode

While in this case then ADHH guarantees the existence of these almost strong zero modes, it does not provide an explicit construction, as we detailed for the transverse-field Ising model's exact strong zero mode in the section above. In fact we can use the same perturbative construction to construct the almost strong edge zero mode. Formally,

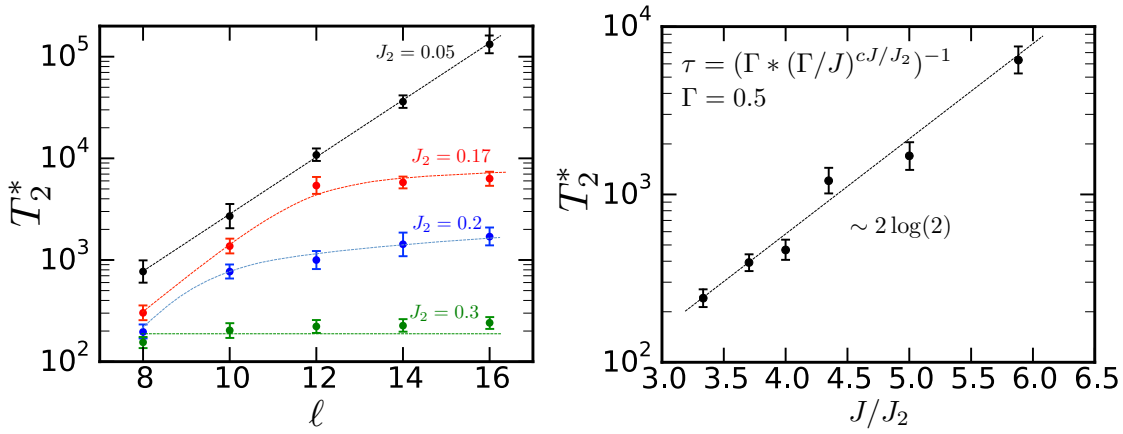

Figure 3.3: A fit of the decay times τ of the edge spin autocorrelator, saturated in system size, to the predicted form e^{cJ/J_2}. This was calculated using exact diagonalisation for system up to 20 sites long. [Numerics by Norm Yao, [21]]

we define the strong zero mode as

$$\Psi_N = \mathcal{N} \sum_{j=0}^{N} \Psi^{(j)} \tag{3.8}$$

where $\Psi^{(j)}$ is order j in $r = Y/J$, by assumption a small quantity. For Ψ_N to be a strong zero mode up to order N we desire

$$[H, \Psi_N] = \mathcal{E}_{N+1}, \text{ where } |\mathcal{E}_{N+1}| \propto O\left(r^{N+1}\right)$$
$$\Psi_N^2 = \mathbb{1} + O\left(r^{N+1}\right).$$

Our zeroth-order ansatz must thus commute with $\hat{N}$ – generally we will start with the edge spin σ_1^z. In order for Ψ_1 to commute with H to second order in r, we must a $\Psi^{(1)}$ to cancel $\Psi^{(0)}$'s non-zero commutator with $\hat{Y}$. This yields an iterative equation for the strong zero mode

$$[J\hat{N}, \Psi^{(j+1)}] = -[\hat{Y}, \Psi^{(j)}]. \tag{3.9}$$

This is linear inhomogenous equation for $\Psi^{(j+1)}$. The superoperator $\mathcal{V}(A) = [\hat{N}, A]$ is rank deficient, so there is no guarantee that there is a solution. Furthemore the null space, the set of operators commuting with $\hat{N}$, is exponentially large. For example, for $\hat{N}_{\text{Ising}}$ the null space includes any function of the σ_j^z. This means that even if a $\Psi^{(j+1)}$ can be found, it is not unique: any operator in this null space may be added onto $\Psi^{(j+1)}$

without changing its commutator with $\hat{N}$. This is important because the choice of $\Psi^{(j+1)}$ determines whether the equation for $\Psi^{(j+2)}$ will have a solution.

In fact, the correct choice is to use the ambiguity to satisfy the second condition we set out for a strong zero mode, that it should square to the identity, order by order as well. Motivated by our discussion of the unitary transform of ADHH above, we can bake this normalisation condition into our iterative procedure by solving for a unitary matrix with which to transform the edge spin, rather than calculating Ψ_N directly

$$\Psi_N = \mathcal{U}_N^\dagger \sigma_1^z \mathcal{U}_N \,, \tag{3.10}$$

and we write

$$\mathcal{U}_N = \exp\left(i \sum_{j=0}^{N} U^{(j)} \right), \tag{3.11}$$

where $U^{(j)}$ is Hermitian and of order r^j. The iterative equation to solve becomes

$$[J\hat{N}, [U^{(j+1)}, \gamma_1^A]] = i[H, e^{-i\sum_{n=0}^{j} U^{(n)}} \sigma_1^z e^{i\sum_{n=0}^{j} U^{(n)}}] \,. \tag{3.12}$$

Of course the $\mathcal{U}_N$ constructed in this manner will only contain terms which do not commute with σ_1^z. It is thus not the full unitary transform shown to exist by the ADHH theorem, and the correspondingly transformed Hamiltonian would not display the full emergent U(1) symmetry in the bulk. Nevertheless this 'boundary' unitary transform is sufficient to show conservation of the edge spin, which is all we require for our purposes.

For transverse-field Ising we calculated the exact expression for the strong zero mode to all orders (2.9). We can use this expression to calculate the boundary unitary transform exactly as well, by solving equation (3.10) for $\mathcal{U}$. We find

$$\mathcal{U} = \cos\frac{\theta}{2} + \cos\theta \sin\frac{\theta}{2}\, \sigma_1^z \sum_{j=2}^{\infty} \left(\frac{\Gamma}{J}\right)^{j-2} \left(\prod_{k=1}^{j-1} \sigma_k^x \right) \sigma_j^z \,, \tag{3.13}$$

where $\sin\theta = \Gamma/J$.

This is most easily verified in the Majorana fermion picture using the Jordan-Wigner transformation (2.4). σ_1^z becomes simply a_1, while $\mathcal{U}$ is given by

$$\mathcal{U} = \cos\frac{\theta}{2} + \cos\theta \sin\frac{\theta}{2}\, a_1 \sum_{j=2}^{\infty} \left(\frac{\Gamma}{J}\right)^{j-2} a_j \,. \tag{3.14}$$

Notice that any bilinear in Majorana fermions of the form $a_i a_j$ for $i \neq j$ is anti-Hermitian, so taking the Hermitian conjugate of $\mathcal{U}$ involves merely changing the sign of such bilinear terms. Furthermore, we shall need the relations $\{a_1 a_j a_1, a_1 a_k\} = 2a_1\delta_{jk}$ and $[a_1, a_1 a_j] = 2a_j$, which follow trivially from the Majorana fermion algebra (2.5). Substituting these results into the right hand side of equation (3.10), we obtain the desired formula

$$\begin{aligned}\mathcal{U}^\dagger a_1 \mathcal{U} &= a_1\left[\cos^2\frac{\theta}{2} - \cos^2\theta\sin^2\frac{\theta}{2}\sum_{j=2}\left(\frac{\Gamma}{J}\right)^{2(j-2)}\right] + 2\cos\theta\sin\frac{\theta}{2}\cos\frac{\theta}{2}\sum_{j=2}\left(\frac{\Gamma}{J}\right)^{j-2} a_j \\ &= \cos\theta\sum_{j=1}^{\infty}\left(\frac{\Gamma}{J}\right)^{j-1} a_j \\ &= \Psi\ ,\end{aligned}$$

where we have made use of the standard trigonometric identities, and recognised that $\cos\theta = \sqrt{1-(\Gamma/J)^2} = \mathcal{N}$, as given in equation (2.10).

3.2.1 Computer-aided algebra

Unfortunately, for non-integrable systems no such simple formula for the boundary unitary or strong zero mode can be found for all orders. However, we can still find analytical expressions up to large orders by using computer-aided algebra. These are in general considerably more complicated than the simple free fermion expressions, as one would expect.

For example, consider the transverse-field Ising Hamiltonian with interactions (3.7) in the case with $J_2 = 0$. The Γ_2 coupling is a disordering term like the transverse field Γ, and does not commute with J. In fact, if $\Gamma = 0$ as well, then (3.7) reduces to the XYZ chain with $J_y = 0$ and $\Gamma_2 = J_x$. The first correction must be the sum of those known analytically in Ising and XYZ

$$\Psi^{(1)} = \frac{\Gamma}{J}\sigma_1^x\sigma_2^z - \frac{\Gamma_2}{J}\sigma_1^y\sigma_2^y\sigma_3^z\ . \tag{3.15}$$

However, now $[H, \Psi^{(0)} + \Psi^{(1)}]$ is considerably more complicated than in the Ising or XYZ cases, containing five operators proportional to $\Gamma\Gamma_2$, in addition to the two we

would have obtained with only the Γ or Γ_2 couplings. It is, however, still possible to find a $\Psi^{(2)}$ that cancels all these terms. It is

$$\Psi^{(2)} = -\frac{\Gamma\Gamma_2}{J^2}\left(\sigma_1^x\sigma_2^y\sigma_3^y\sigma_4^z - \sigma_1^x\sigma_3^z - \sigma_2^x\sigma_3^z + \sigma_1^y\sigma_2^y\sigma_3^x\sigma_4^z\right) + \frac{\Gamma^2}{J^2}\sigma_1^x\sigma_2^x\sigma_3^z + \frac{\Gamma_2^2}{J^2}\sigma_1^y\sigma_2^y\sigma_3^y\sigma_4^y\sigma_5^z \,. \tag{3.16}$$

Alternatively, the boundary unitary to second order is given by

$$\mathcal{U}_2 = \exp(\frac{1}{2}[\Gamma\sigma_1^y\sigma_2^z + \Gamma_2\sigma_1^x\sigma_2^y\sigma_3^z + \Gamma^2\sigma_1^y\sigma_2^x\sigma_3^z + \Gamma\Gamma_2\sigma_1^y(\sigma_3^z - \sigma_2^y\sigma_3^y\sigma_4^z) - \Gamma_2^2\sigma_1^x\sigma_2^y\sigma_3^y\sigma_4^y\sigma_5^z]).$$

With the help of a Python program to do the algebra, we have implemented this procedure successfully to 11^{th} order when $\Gamma_2 = 0$ and 9^{th} order when Γ_2 is included, with or without J_2. The fact that this iteration is possible is highly non-trivial; as mentioned above, if one starts iterating instead with σ_j^z with $j \neq 1$ or L, the procedure breaks down instantly. Although starting at the edge works, the number of terms explodes dramatically compared to the integrable cases. For example, at 9th order with Γ_2 and J_2, there are 424,586 terms in the expansion, as compared to 10 terms at the same order for transverse-field Ising. The exponential growth order-by-order is plotted in figure 3.4. Notice the J_2 commutes with σ_1^z, so it has no effect at first order and produces fewer terms.

The limiting factor in the calculation is the solution of the iterative equation (3.12). This is an inhomogenous matrix equation of the form

$$A\vec{x} = \vec{b}.$$

where A and vector $\vec{b}$ are known and $\vec{x}$ is to be solved for. Here A is in fact a superoperator acting on linear combinations, or 'vectors', of operators. Our choice of operators at each site is the identity matrix or one of three Pauli matrices; thus the dimension of the vector space is 4^L. Fortunately in practice we can instead restrict ourselves to a smaller subspace. Our program constructs such a subspace by taking each operator in $\vec{b}$ and acting on it repeatedly with A until no new operators are produced. The set of operators which appear under this process then provide a basis for a sufficient subspace to find a solution if it

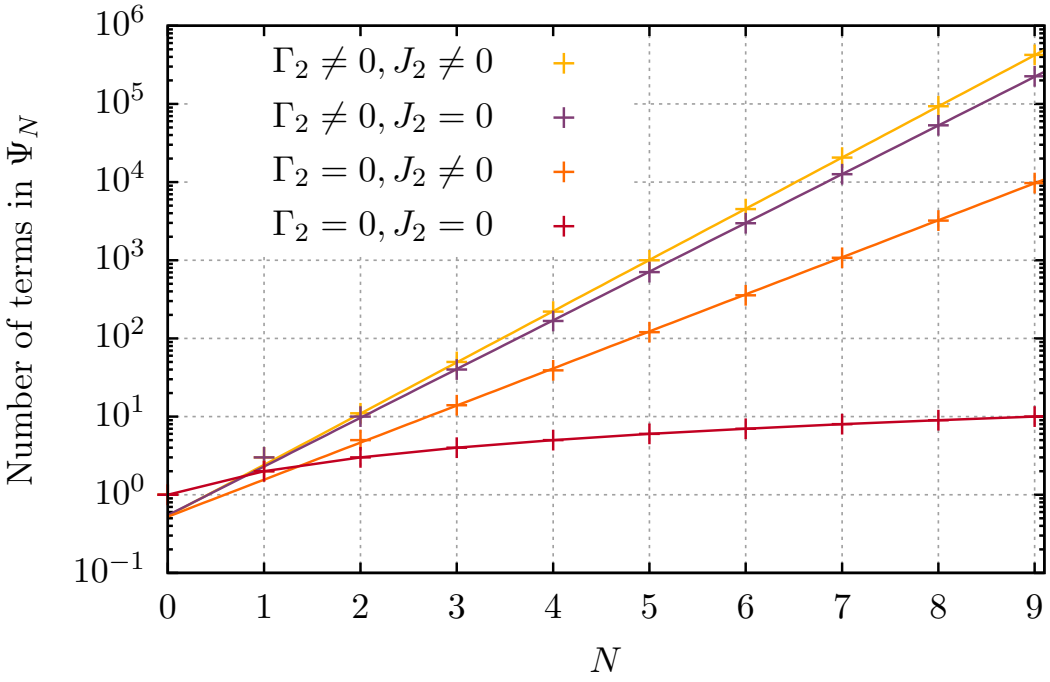

Figure 3.4: The number of terms in the perturbative construction of the strong zero mode at order N, for various types of interactions added to transverse-field Ising model. The solid lines are exponential fits to the data, except for the non-interacting case, which is linear. This suggests that as soon as interactions are turned on the number of terms in the strong zero mode grows exponentially.

exists. A graph of the subspace size is presented in figure 3.5, showing that although it does grow exponentially fast, it does so at a much slower rate than the full space.

Furthermore, even in this subspace, A is an extremely sparse and *block-diagonal* matrix. Exploiting this allows us to split up the equation into multiple smaller equations, saving memory and time. Ultimately, solving such inhomogeneous matrix equations symbolically is still the roadblock for going to higher orders in the expansion. CAS solve such systems efficiently using Gaussian elimination with pivoting, for example [33]. Pivoting requires confirmation that matrix elements do not vanish. Determining whether a symbolic expression is identically zero is a challenging problem in computer algebra, known as the 'constant problem' [34]. Either the expression has to be fully 'simplified' to see if it vanishes – a very computationally inefficient process – or heuristics have to be applied (for example, explicitly evaluating the expression over a carefully chosen range of numbers). We found that many CAS would stall at solving even comparatively small symbolic matrix equations of order 10 width. Consequently, our Python code written in

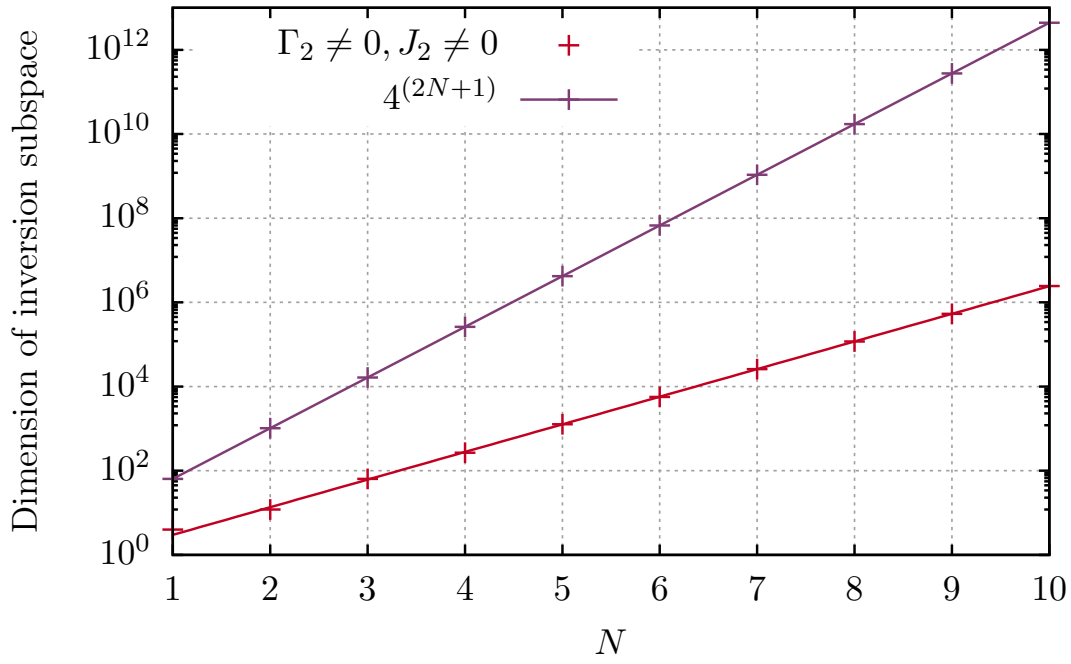

Figure 3.5: The dimension of the subspace over which equation (3.12) must be inverted at each order N in order to solve the strong zero mode expansion when both Γ_2 and J_2 are included; the solid line is an exponential fit. From the fit it grows as $\sim 2.13^{2N}$, which is considerably smaller than the full space size, 4^{2N+1}, where $2N+1$ is the support of the longest possible term at perturbation order N.

SymPy can call as its matrix-solving backend multiple CAS: SymPy [35], Mathematica [36], Matlab [37] and GiNaC[38]. GiNaC proved to be the fastest and most stable.

3.2.2 Asymptotic Series and the error of the expansion

Other than these purely technical limitations, there appears to be nothing to stop us from calculating this perturbatively to all orders. However, we know from our discussion above that with inteactions we expect an *almost*, not exact, strong zero mode. To understand why our series fails we must consider the error $[H, \Psi_n] = \mathcal{E}_n$. By construction we have guaranteed that this is suppressed by a factor r^{n+1}. However, the explosion of terms in our perturbative construction ultimately defeats this exponential. Thus there exists an order n_* at which we must truncate our expansion: it is an asymptotic series.

More formally, we define n_* as the lowest value such that

$$|\mathcal{E}_{n_*+1}| > |\mathcal{E}_{n_*}| \,, \tag{3.17}$$

where we use the trace norm $|\mathcal{E}_n|^2 \equiv \mathrm{Tr}(\mathcal{E}_n^\dagger \mathcal{E}_n)$. Under this definition, $n_* \to \infty$ for transverse-field Ising.

Using the explict expressions for $\Psi^{(n)}$ allows us to compute the error $\mathcal{E}_n$ to the same order. We find that when $J_2 = 0$, the maximum errors occur roughly at $\Gamma_2 = \Gamma$, not surprisingly as the strong zero mode is exact for $\Gamma\Gamma_2 = 0$. We thus plot $\mathcal{E}_n$ for various $\Gamma = \Gamma_2$ in figure 3.6; the lines are there to make the trends clear. The truncation point n_*

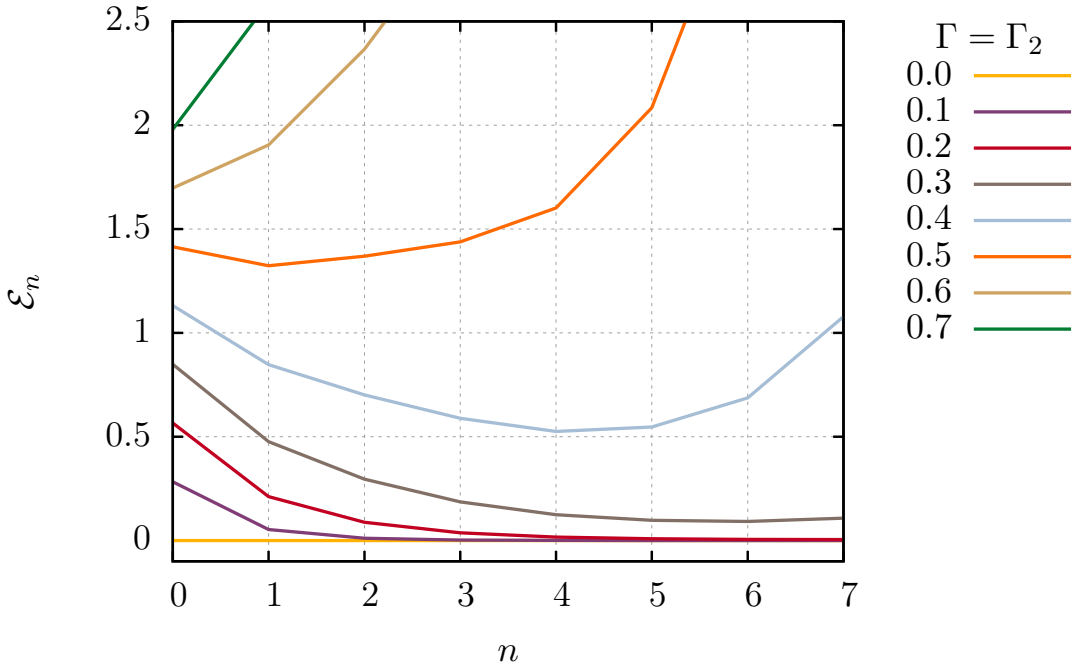

Figure 3.6: The error $|\mathcal{E}_n|$ of the almost strong zero mode Ψ_n as a function of truncation order n.

for given couplings is simply the minimum of the corresponding curve as a function of n. For example, when $\Gamma = \Gamma_2 \approx 0.25$ the expansion must be truncated at $n_* = 7$.

As an alternative way of presenting this data, we plot the curves $|\mathcal{E}_n| = |\mathcal{E}_{n+1}|$ as a function of Γ and Γ_2 in figure 3.7. We label each curve by the smaller value of n in the equality. Let us also define the interior of a curve as the area contained by the curve and the axes passing through the origin. Then from figure 3.7 one can read off the value of n_* at a given point (Γ_2, Γ) by finding the curve with the largest n which still has that point in its interior. Because some of the curves intersect, we must also provide the caveat that there must be no curves with lesser n which have that point in their exterior.

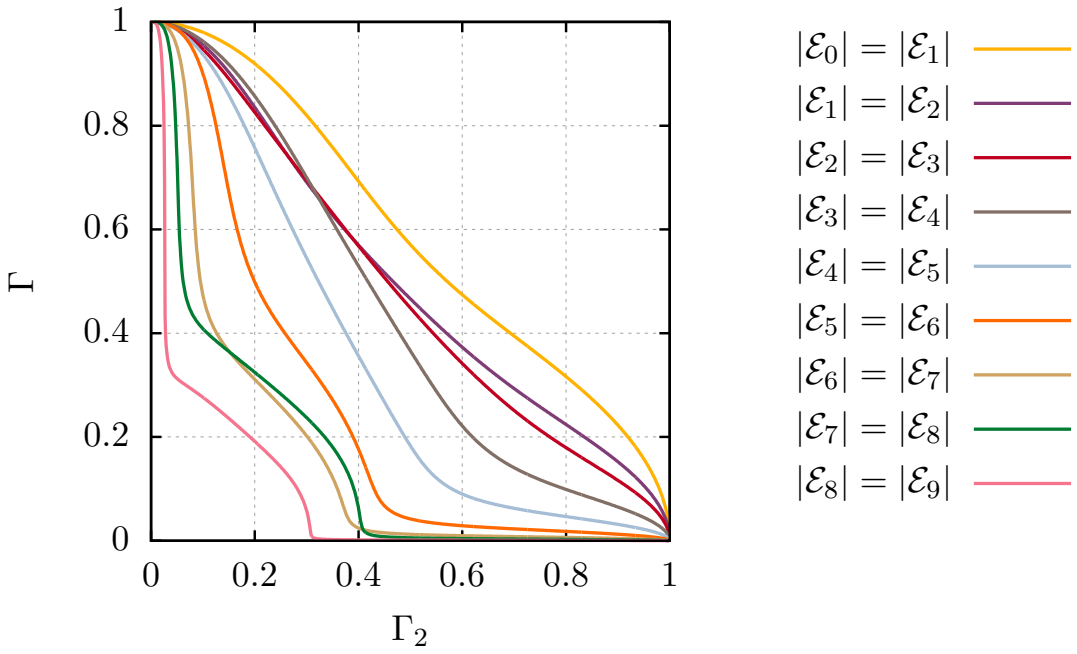

Figure 3.7: The solutions to the equations $|\mathcal{E}_n| = |\mathcal{E}_{n+1}|$ at which the errors of the almost strong zero mode at different truncation orders are equal, as a function of the couplings Γ and Γ_2. From these curves it is possible to read off the optimal truncation n_*.

We see that there is a dramatic effect on n_* as soon as two couplings are added and the system becomes interacting, as we would expect. There is, however, still a significant region in (Γ_2, Γ) space in which high orders in perturbation theory can be reached, as suggested by the ADHH theorem.

3.3 Failure of the almost strong zero mode

The ADHH theorem gives us two simple conditions which are sufficient for an almost strong zero mode to exist

1. A Hamiltonian of the form $J\hat{N} + \hat{Y}$ where $\hat{N}$ has integer eigenvalues and $J \gg |Y|$.

2. Any operation that flips a single edge spin does not commute with $\hat{N}$.

The first condition ensures we can apply ADHH, while the second ensures that the resulting $U(1)$ symmetry protects the edge spin.

If we start with an almost strong zero mode, we can obviously falsify the first condition by simply turning up the strength of any of the couplings in $\hat{Y}$. From the point of view the explicit expansion, we see that there is no enhancement in the edge coherence time once $n_* = 0$. This is because once $|\mathcal{E}_0| \leq |\mathcal{E}_1|$, adding extra terms to the bare σ_1^z only makes the commutator with the Hamiltonian worse.

We also require the almost strong zero mode to be localised at the edge. A test of this is the normalisation. This is the coefficient $\mathcal{N}$ of σ_1^z in Ψ, which is precisely the measure of the overlap between the almost strong zero mode and the edge spin.

For transverse-field Ising without interactions, we see from the exact strong zero mode (2.9) and its normalisation (2.10) that both the error and the normalisation fail when $\Gamma \geq J$. Thus the exact strong zero mode dies at the same values of the couplings as the ground state phase transition from the long-range-ordered, symmetry-broken phase to the paramagnetic phase. This should not be surprising because this phase transition is when the more well-known topological zero mode in the ground-state breaks down as well.

The interactions Γ_2 and J_2 in (3.7) are irrelevant operators in the context of this phase transition, so for *low energy densities* the topological zero mode will certainly remain as $L \to \infty$ in the ordered phase, with the phase transition providing an upper bound to the regime the almost strong zero mode.

We can see at what interaction strength the normalisation and error of the almost strong zero mode fail, and compare this to the phase transition. To fourth order the normalisation is given by

$$\begin{aligned}\mathcal{N}^{-2} = 1 + \Gamma^2 + \Gamma_2^2 + \Gamma^4 + 3\Gamma^2 J_2^2 - 8\Gamma_1\Gamma^2 J_2 \\ + 4\Gamma_2^2\Gamma^2 + 6\Gamma_2^2 J_2^2 + \Gamma_2^4 + \dots ,\end{aligned}$$

where $J = 1$.

The coefficients increase further at higher orders. The normalisation as a function of $\Gamma = \Gamma_2$ and $J_2 = 0$ for various truncations n_* is plotted in figure 3.8. We also plot the two-point correlator in the ground state, which shows the usual quantum phase transition occurs at $\Gamma = \Gamma_2 \sim 0.4$.

We can also look at the errors. Explicitly, we have

$$|\mathcal{E}_0|^2 = 4\left(\Gamma^2 + \Gamma_2^2\right)$$
$$|\mathcal{E}_1|^2 = 4\left(\Gamma^4 + 5\Gamma^2\Gamma_2^2 + \Gamma_2^4\right)$$

These are equal when $\Gamma = \Gamma_2 = \sqrt{2/7} \approx 0.53$.

We see that it is plausible that the effects of the almost strong zero mode survive throughout the ordered phase. However, the qualitative difference with the exact case is that there will be no sharp transition in behaviour at high energy densities due to the death of the almost strong zero mode at the phase transition, as we will discuss further below.

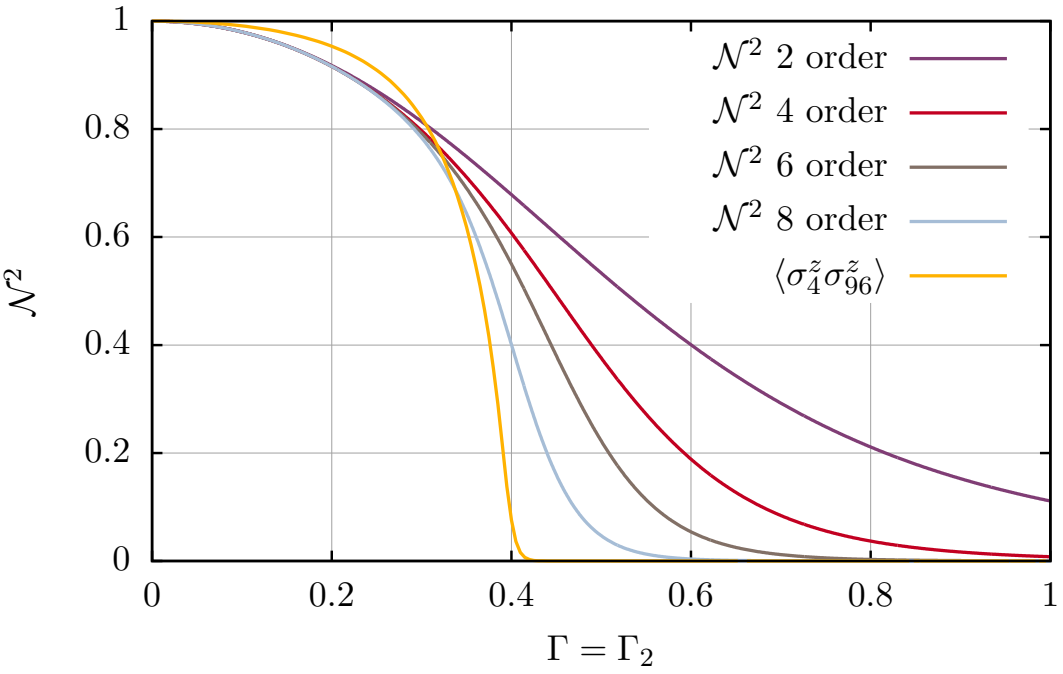

Figure 3.8: The normalisation $\mathcal{N}$ for $\Gamma = \Gamma_2$ and $J_2 = 0$ plotted at different truncation orders, compared with the two-point correlator in the ground state from DMRG with $L = 100$.

3.3.1 Resonances

The second condition for an almost strong zero mode is that the emergent $U(1)$ symmetry must protect the edge spin. This can fail trivially if $\hat{N}$ does not commute with σ_1^z or is single site. More interestingly, notice that for the Hamiltonian (3.7) the next-nearest-neighbour J_2 couplings commutes with σ_1^z and the nearest-neighbour J coupling.

Unlike Γ_2 then there is no reason why the almost strong zero mode should vanish if J_2 is similar magnitude to Γ_2.

Indeed, as is clear from figure 3.9, at small J_2, the behaviour is similar to that for small Γ_2; however, for larger values, the behaviour is completely different. The edge coherence time does *not* gradually decrease as J_2 increases. For example, at $J_2 = .5J$, the plateau is short-lived, whereas at $J_2 = .7J$ the decay time is similar to that at $J_2 = .3J$, in the billions of time steps. At $J_2 = J$, the decay is quick.

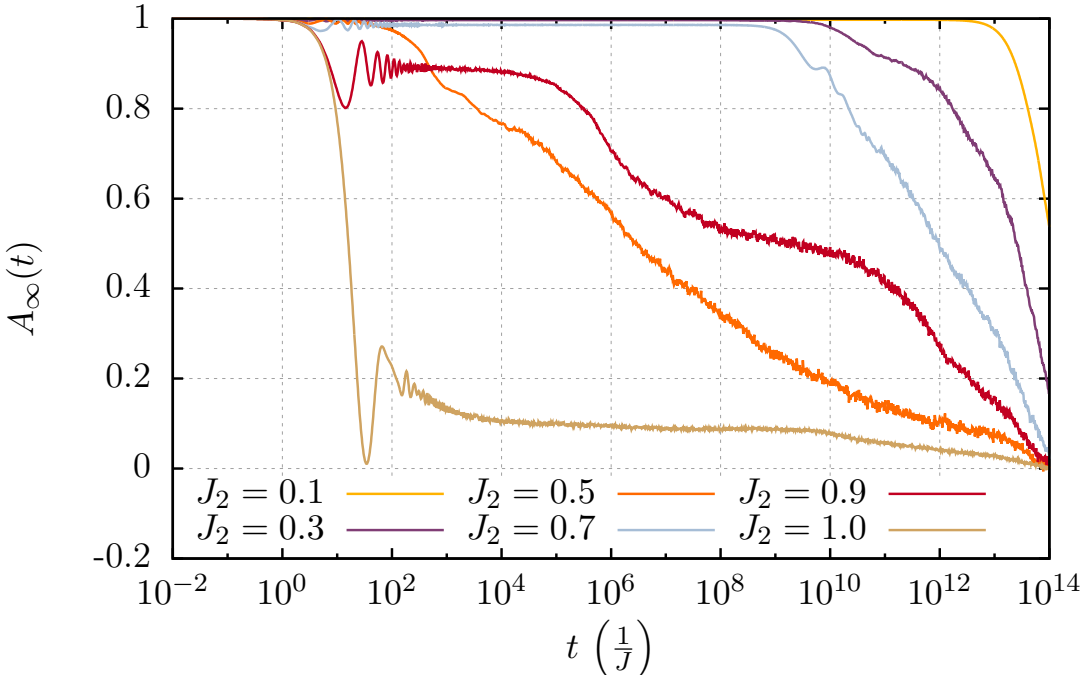

Figure 3.9: $A_\infty(t)$ for perturbed Ising from exact diagonalization on a log axis for time for $L = 14$, $\Gamma = 0.05$, $\Gamma_2 = 0$. Notice the non-monotonicity in J_2.

If J and J_2 are of the same magnitude then in order to apply the ADHH theorem, we must include both terms in $\hat{N}$. This presents a potential problem, since the theorem requires integer eigenvalues of $\hat{N}$. However, if we take rational $J_2/J = p/q$ for coprime integers p and q, then

$$\hat{N}_{nn} = \sum_j (q\sigma_j^z\sigma_{j+1}^z + p\sigma_j^z\sigma_{j+2}^z)\ , \tag{3.18}$$

still has integer eigenvalues. The Hamiltonian becomes $\hat{H}_{nn} = -(J/q)\hat{N}_{nn} + \hat{Y}_{nn}$.

We may now use the ADHH theorem to obtain an approximate conservation law for $\hat{N}_{nn}$. However, $\hat{N}_{nn}$ no longer counts domain-wall number; instead it is the sum of

the number of broken nearest and next-nearest neighbor bonds, weighted appropriately by q and p. This means it is possible to flip the edge spin while conserving $\hat{N}_{nn}$ by converting broken bonds of one type to the other.

Equivalently, terms will appear in $\hat{D}_{nn}$ which do not commute with the edge spin σ_1^z. For example if $J = J_2$, so that $p = q = 1$, then $\sigma_1^x(\sigma_2^z - \sigma_3^z)$ commutes with $\hat{N}_{nn}$ but flips the edge spin, ruining the conservation of the almost strong zero mode.

Physically, these operators describe processes which can flip the edge spin for no cost in energy. Heuristically, if such 'easy' edge spin flips exist they destroy the boundary coherence because they are not suppressed by an energy denominator in perturbation theory. For the $J = J_2$ case considered above, consider the process which swaps between these two spin configurations, identical but for the edge spin

$$\uparrow\uparrow\downarrow\cdots \qquad \Leftrightarrow \qquad \downarrow\uparrow\downarrow\cdots . \tag{3.19}$$

The energy contribution from the three spins on the left is $2(J + J_2)$, while on the right it is $2(2J)$, so when $J = J_2$ the edge-spin can be flipped for no energy cost.

Such easy edge spin flips was first described in [22] in the case of parafermions, and its effects on the energy level splitting of eigenstates was considered perturbatively in [23]. We call these special values resonances by analogy with similar behaviour in other quantum systems [39].

3.3.2 Poles in the strong zero mode expansion

We have just seen that even when ADHH can be applied to a Hamiltonian, terms can appear in terms $\hat{D}$ that flip the edge spin, meaning that the emergent $U(1)$ symmetry does not guarantee an almost strong zero mode. We should expect that the explicit perturbative strong zero mode expansion described in section 3.2 should also break down when there is a resonance.

Setting $\Gamma_2 = 0$ for convenience at present, we can calculate Ψ for the Hamiltonian (3.7) exactly as described in section 3.2, except that we treat both the J_2 and J terms as large, so that $\hat{N} = \hat{N}_{nn}$.

The zeroth-order term remains $\Psi^{(0)} = \sigma_1^z$, since it still commutes with both of the ordering terms. We then find $\Psi^{(1)}$ by inverting equation (3.9) with $\hat{N} = \hat{N}_{nn}$

$$\Psi^{(1)} = \frac{\Gamma}{J^2 - J_2^2}\sigma_1^x\Big(J\sigma_2^z - J_2\sigma_3^z\Big) \,. \tag{3.20}$$

The important difference is of course the inverse factor of $(J^2 - J_2^2)$. This pole means the expansion collapses for $J_2 = \pm J$ at first order in Γ.

Poles in the strong zero mode expansion correspond to processes which flip the edge spin but conserve $\hat{N}$. The operators which the poles multiply are related to those we would expect to find in $\hat{D}$ which flip the edge spin. Moreover, they illuminate the degenerate configurations related by flipping spins at and near the edge. For example, both terms in $\Psi^{(1)}$ contain σ_1^x, while the other two involve σ_2^z and σ_3^z. This suggest we look at configurations with domain walls between spins on these sites. One is thus led very quickly to the configurations illustrated in (3.19) when $J_2 = J$, and to the similar ones occurring when $J_2 = -J$.

Continuing the perturbative expansion, we find at second order in Γ we find

$$\begin{aligned}\Psi^{(2)} = {} & \frac{JJ_2\Gamma^2}{(J^2 - J_2^2)^2}\sigma_1^z\sigma_2^z\sigma_3^z \\ & + \frac{\Gamma^2}{(J^2 - J_2^2)^2(9J^2 - J_2^2)}\sigma_1^x\sigma_3^x\Big[2J^2J_2^2\sigma_2^z\sigma_4^z\sigma_5^z + 2J^2J_2^2\sigma_1^z\sigma_3^z\sigma_5^z - 6J^3J_2\sigma_1^z\sigma_3^z\sigma_4^z \\ & \quad + 2J^2J_2^2\sigma_1^z\sigma_2^z\sigma_3^z\sigma_4^z\sigma_5^z - JJ_2\left(J_2^2 - 3J^2\right)(\sigma_2^z + \sigma_4^z - \sigma_1^z\sigma_2^z\sigma_3^z) + J_2^2\left(J_2^2 - 7J^2\right)\sigma_5^z\Big] \\ & + \frac{\Gamma^2}{(J^2 - J_2^2)(J^2 - 4J_2^2)}\sigma_1^x\sigma_2^x\left[-JJ_2\sigma_1^z\sigma_2^z\sigma_3^z - JJ_2\sigma_4^z + 2J_2^2\sigma_1^z\sigma_2^z\sigma_4^z + \left(J^2 - 2J_2^2\right)\sigma_3^z\right] \,.\end{aligned} \tag{3.21}$$

New poles at $J_2 = \pm\frac{J}{2}$ and $J_2 = \pm 3J$ are immediately apparent. The poles in the even nastier expression for $\Psi^{(3)}$ are at $J_2 = J/3$, $J_2 = 3J/2$ and $J_2 = 5J$. We also note that the $J_2 = J$ pole reappears at second order in Γ. This may be understood as higher-order processes involving two spin-flips which also convert a single J_2 domain wall to a single J domain wall. Generically once a pole has appeared at a given order in pertubation theory we would expect it to reappear at higher orders.

It is not difficult to find the corresponding processes that flip the boundary spin without changing the energy. The terms in $\Psi^{(2)}$ with a pole at $J_2 = 3J$ contain spin-flip terms $\sigma_1^x\sigma_3^x$, and otherwise sample up to the fifth lattice site. This indicates the

configurations that have the same energy when $J_2 = 3J$ are related by flipping the first and third spins. They are

$$\uparrow\uparrow\uparrow\uparrow\downarrow\cdots \quad \Leftrightarrow \quad \downarrow\uparrow\downarrow\uparrow\downarrow\cdots \qquad J_2 = 3J\,, \tag{3.22}$$

Likewise, the two configurations

$$\uparrow\downarrow\downarrow\uparrow\cdots \quad \Leftrightarrow \quad \downarrow\uparrow\downarrow\uparrow\cdots \qquad J_2 = \frac{J}{2}\,. \tag{3.23}$$

have energies $2(2J + 2J_2)$ and $2(3J)$ respectively, equal at $J_2 = J/2$. They are related by flipping the first two spins, with the corresponding pole terms in $\Psi^{(2)}$ indeed containing $\sigma_1^x\sigma_2^x$.

The order in the expansion at which a pole occurs is the same as the number of times terms in $\hat{Y}$ need to be applied to go between the degenerate configurations. For example, swapping the first two spins to switch between configurations in (3.23) requires two applications of the Γ transverse-field coupling term, so it appears at second order. But if $\Gamma_2 \neq 0$, then this process would only require a single application of $\sigma_1^x\sigma_2^x$, so the pole would occur at first order, with a coefficient proportional to $\Gamma_2/(J^2 - 4J_2^2)$ appearing in $\Psi^{(1)}$. By contrast, if we then set $\Gamma = 0$, the pole at $J = J_2$ disappears at first order, because the setup for the degenerate configuration in equation (3.6) requires that *only* the edge spin be flipped, which cannot be achieved with only a single application of Γ_2.

The order at which a pole appears is important, because we can always truncate the expansion before a pole is reached. This truncation is equivalent to the one we performed above for the almost strong zero mode because of the explosion of terms. A pole at order $(n_p + 1)$ for a certain value of the couplings in $\hat{N}$ thus forces the truncation of the strong zero mode at order n_p, so that the error term is order $(n_p + 1)$, regardless of the magnitude of the terms in $\hat{Y}$.

When, and at what order, will poles appear for given values of p and q? One way to investigate this is to explicitly construct the easy edge-spin flip processes. For example, set $q = 1$ so that $J_2 = pJ$. If p is odd, we have

$$\underbrace{\uparrow\uparrow\uparrow\uparrow\cdots\uparrow\uparrow}_{p+1 \text{ up spins}}\downarrow\cdots \quad \Leftrightarrow \quad \underbrace{\downarrow\uparrow\downarrow\uparrow\cdots\downarrow\uparrow}_{p+1 \text{ alternating spins}}\downarrow\cdots \tag{3.24}$$

These are related by the spin flips $\sigma_1^x \sigma_3^x \cdots \sigma_p^x$. This process creates p domain walls (broken J bonds), while decreasing the number of broken J_2 bonds by one by making the spins at sites $j = p$ and $p + 2$ the same. The resulting change in energy is $2(pJ - J_2)$, which indeed vanishes when $J_2 = pJ$. If we include only the transverse field in $\hat{Y}$, the resulting pole in the almost strong zero mode will thus appear at order $(p + 1)/2$.

Can we find a similar process for $q = 1$ and p even? In fact it is simple to prove that no such process exists, so that the almost strong zero mode is free from resonances. We will assume we are in the semi-infinite limit so that we do not have to consider flipping both edge spins. Let us define the change in eigenvalue of $\hat{N}$ when we flip a spin j in an eigenstate $|s\rangle$ as $2\Delta_j(s)$. Notice we have factor of two in front of the integer $\Delta_j(s)$ to account for the fact that healing or breaking a bond accounts for an eigenvalue change of *twice* the coupling. Equivalently the energy of the state changes by $2J\Delta_j(s)/q$. In order for a resonance to exist we must be able to flip the edge spin without changing the eigenvalue of $\hat{N}$; that is, there must exist some state s_c and a set of pairs of states and spin flip locations $\{|s_i\rangle, j_i\}$ where $j_i > 1$ such that

$$\Delta_1(s_c) = -\sum_i \Delta_{j_i}(s_i). \tag{3.25}$$

Now, notice that the edge spin is associated with one J and one J_2 bond. Thus the possible values of the change of eigenvalue are $\Delta_1(s) = \pm_s(p \pm_s q)$, where each $\pm_s$ can be different depending on the configuration of $|s\rangle$. Meanwhile, all bulk spins are associated with two J bonds and two J_2 bonds. Thus flipping a bulk spin either heals two or none of each type of bond. Explicitly $\Delta_{j>2}(s) = \pm_s(p \pm_s q) \pm_s (p \pm_s q)$. This means that $\Delta_{j>2}(s)$ is always even. On the other hand, the parity of $\Delta_1(s)$ is only even if the parity of p and q are the same. Naively it appears that equation (3.25) has no solution if p and q have different parity.

In fact there is an additional complication: we must consider the edge spin's neighbour at $j = 2$ as another special case, due to the fact we have a next-nearest-neighbor coupling. This is associated with two J bonds like a bulk spin, but only one J_2 bond. Thus $\Delta_2(s) = \pm_s(p \pm_s q) \pm_s q$. This is odd if and only if p is odd.

Thus equation (3.25) has no solutions, and therefore there are no resonances, if and only if p is even and q is odd.

As an example of this, if $p = 1$, so that $J_2 = J/q$, there should be resonances regardless of the parity of q. First consider a configuration with the maximum number of broken J_2 bonds within the first $3(q+1)/2$ spins

$$\underbrace{\uparrow\uparrow\downarrow\downarrow\uparrow\uparrow\downarrow\downarrow\cdots}_{3(q+1)/2 \text{ spins}}$$

For q odd, act on this with the flips $\sigma_1^x\sigma_4^x\cdots\sigma_{(3q-1)/2}^x$. This decreases the number of broken J_2 bonds by q, because flipping the first spin heals one J_2 bond, while the remaining $(q-1)/2$ flips heal two bonds each. This process increases the number of broken J bonds (i.e. the number of domain walls) by one, since flipping the first spin creates one domain wall, while the remaining flips do not change the number, but rather just move a domain wall. Thus for this process the change in energy is $2(J - qJ_2)$, indeed giving a resonance at $J_2 = J/q$ for odd q. Similarly, for q even, consider the configuration

$$\uparrow\underbrace{\downarrow\downarrow\uparrow\uparrow\downarrow\downarrow\uparrow\uparrow\cdots}_{3q/2 \text{ spins}}$$

which also has the maximum number of broken J_2 bonds. Here the combination of flips $\sigma_1^x\sigma_2^x\sigma_5^x\sigma_8^x\cdots\sigma_{3(q-2)/2}^x$ gives the same change in energy $2(J - qJ_2)$. Thus there are indeed resonances when $J_2 = J/q$ for all q.

Note these are not the unique processes yielding poles at $J_2 = J/q$. The preceding process for $q = 3$ occurs only in $\Psi^{(4)}$, whereas the pole at $J_2 = J/3$ in $\Psi^{(3)}$ involves $\sigma_1^x\sigma_3^x\sigma_4^x$. However, degeneracies giving resonances at $J_2 = J/q$ occur only for states whose energy grows with q as qJ. The reason is that one needs at least q broken J_2 bonds in one of the states to have this degeneracy, and this implies at least $q/2$ broken J bonds in that state. Thus the effects of the higher order poles occurring at J_2/J small only should affect highly excited states, i.e. those whose energy density relative to the ground state is nonzero. Equivalently, the larger q, the larger n_*, as we would expect from transferring the J_2 coupling from $\hat{N}$ to $\hat{Y}$ before applying the ADHH argument.

Resonances also make clear the difference between edge and bulk spins. In a system with a translationally invariant bulk it will always be possible to find $\Delta_j(s) = 0$ for j

farther away from the edge than the longest-range coupling of $\hat{N}$, by trivially exploiting the translational invariance. This means that bulk spins have first-order resonances and no associated almost strong zero modes.

One the other hand, when we have a next-nearest-neighbour coupling, σ_2^z is not such a bulk spin. In fact, we can easily modify the argument above given for the location of resonances for σ_1^z to σ_2^z. Consider the equivalent of equation (3.25) in this case

$$\Delta_2(s_c) = -\sum_i \Delta_{j_i}(s_i) \text{ for } j_i \neq 2. \tag{3.26}$$

If p is odd, then the left hand side of this equation is also odd. The only way the right hand side of equation can be odd is if $\Delta_1(s_i)$ is odd, which, given p is odd, would require q to be even.

Therefore, if p and q are odd, the almost strong zero mode starting at σ_2^z has no resonances. If this condition is not satisfied, then the almost strong edge zero modes still exists but suffers from resonances as for the one starting from the edge spin itself. The exception is at $2|J| = |J_2|$, where the processes like

$$\uparrow\uparrow\uparrow\downarrow\cdots \quad \Leftrightarrow \quad \uparrow\downarrow\uparrow\downarrow\cdots \qquad J_2 = 2J \tag{3.27}$$

kill the almost strong zero mode at first order, much like $J = J_2$ case for the edge spin.

The fact that there is an almost strong edge zero mode starting at σ_2^z is not particularly surprising when one considers that for $\Gamma_2 = 0$ and $J = 0$, H_{pert} splits into two uncoupled transverse-field Ising chains with corresponding exact strong zero modes starting at σ_1^z and σ_2^z.

Notice that the ground-state physics resulting from $J_2 \neq 0$ in (3.7) is different from that coming from $\Gamma_2 \neq 0$. The latter is a disordering term like the transverse field, and so qualitatively does not change the physics of the ground state, as long as it is not made too large. It mainly makes its presence felt in excited-state behaviour. Conversely, $J_2 > 0$ favours aligning next-nearest-neighbor spins, while $J_2 < 0$ favours anti-aligning them. The latter interaction competes with the ordering favored by the J term, which no matter its sign, favours aligning spins two sites apart. Consequently at $J_2 = -J/2$ for $J_2 < 0$ there is a transition between ferromagnetic phase and a phase with antiferromagnetic

Limiting Factor	Cutoff Order
Finite Size	n_L, related to system size L and range of couplings.
Resonance	$(n_p + 1)$ = order of resonance.
Breakdown of perturbation theory	n_*, given by ADHH theorem, depends on J_0/J.

Table 3.1: A table summarising the possible limiting factors on the strong zero mode. The lowest value of n gives the cutoff order. If n_L is the only limiting factor even in the thermodynamic limit then the strong zero mode is exact.

structure where two up spins are followed by two down spins, called the $\langle 2 \rangle$ structure [40]. If the transverse field Γ is non-vanishing, these phases are not adjacent, but rather there is a transitional paramagnetic phase separating them [41]. There is also an equivalent set of transitions at $J_2 < 0, J < 0$ and $J_2 = J/2$.

Nevertheless, the almost strong zero mode at infinite temperature is blind to this complicated ground-state physics. The poles in the strong zero mode expansion are the unaffected by the signs of J and J_2. Even more fundamentally, the extent to which conditions for applying the ADHH theorem are satisfied are not changed at all by changing the signs of J and J_2. However, the behaviour at low temperatures will of course be dramatically affected, which we will discuss in more detail in the section on finite temperature in section 4.7.

3.3.3 The effect of resonances

As we have discussed, a resonance of order $(n_p + 1)$ effectively forces an upper bound on the order of the error of the strong zero mode. Thus if $n_p < n_*$, the autocoherence time of the edge spin will saturate at a value less than where there are no resonances. For a resonance of higher order the decay time will be longer. If $n_p > n_*$, or if the system is small enough the finite size limits the decay time more than the resonance, then the effect of the resonance will not be observed. The possible limiting factors on the strong zero mode are summarised in table 3.1. We will discuss the finite-size effects in more detail below.

We can see the resonances clearly in figure 3.10. The saturation of the decay time due to the resonances at $J_2 = J$ and $J_2 = J/2$ are particularly apparent. We notice that the resonances have some width as a function of J_2/J, rather than being delta-function

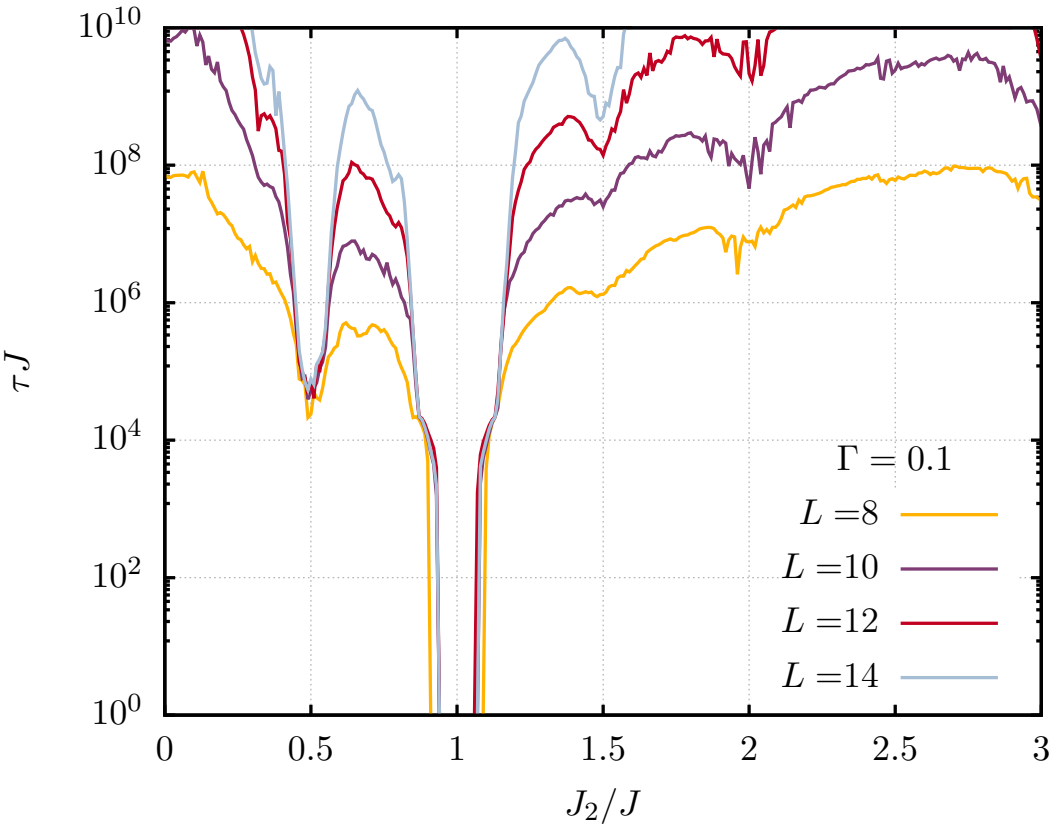

Figure 3.10: The decay time (on a logarithmic scale) of the edge spin at $T = \infty$ for $L = 8 - 14$ sites, as obtained by exact diagonalization, for $\Gamma = 0.1$. The non-monotonicity of the decay time as a function of J_2/J due to the resonances is clear.

peaks about given rational values. This width grows with Γ, as can be seen in figure 3.11, but crucially does not grow with system size. That the resonances have width should be expected, because close to the resonances at ratios of J_2/J with very large p and q, the effective gap J/q for the ADHH theorem is very small, so that $n_* \approx n_p$. We will discuss this width, and its dependence of system size and the perturbing coupling in more detail in section 5.2.

Interestingly, as is particularly apparent in figure 3.11, for small J_2, the decay time is almost independent of J_2. Of course the difference between zero and non-vanishing J_2 will be exceptionally important in the thermodynamic limit, as it means the difference between an exact and almost strong zero mode. Nevertheless, consider the strong zero mode expansion for small J_2, so that we place J_2 in the perturbing $\hat{Y}$ term. Because the next-nearest-neighbor coupling commutes with the zeroth-order ansatz σ_1^z, it has no effect

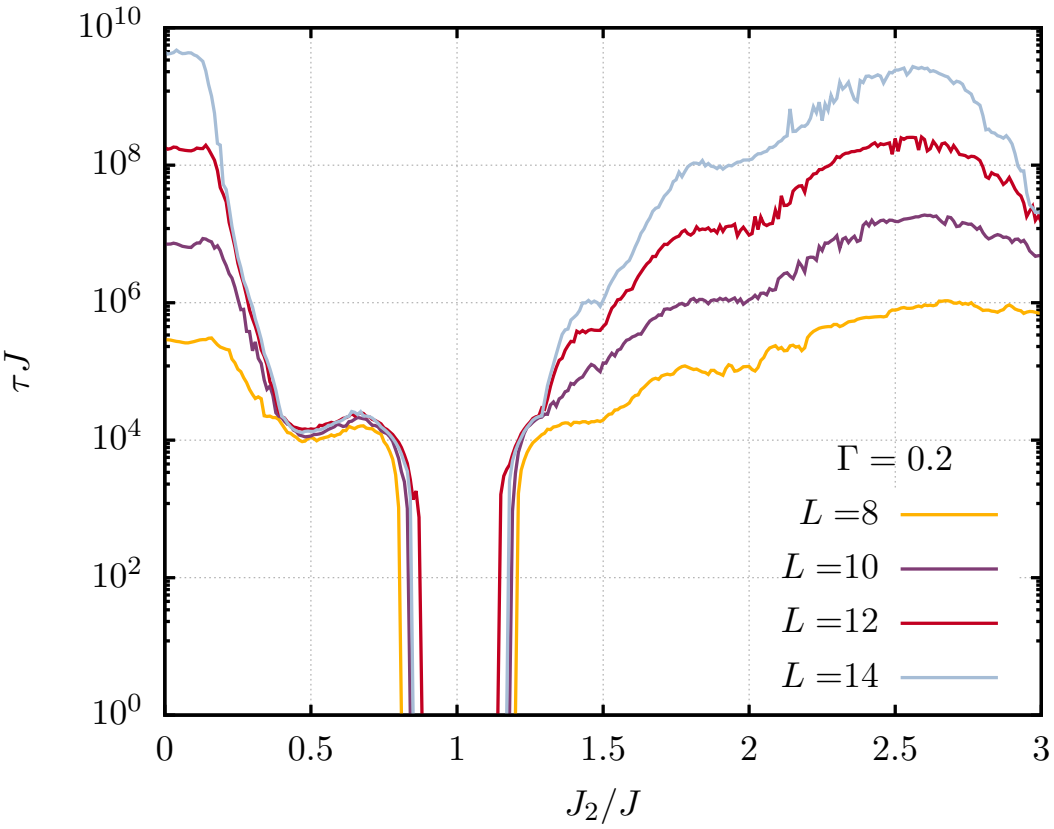

Figure 3.11: The decay time (on a logarithmic scale) of the edge spin at $T = \infty$ for $L = 8 - 14$ sites, as obtained by exact diagonalization, for $\Gamma = 0.2$. The falloff in decay time as a function of J_2/J around each resonance is much wider than in figure 3.10 with a smaller Γ. The resonance at $J_2 = 3J$ is also more prominent.

at first order in the expansion, and instead only appears in terms of order $J_2\Gamma/J^2$ at second order. If $\Gamma \gg J_2$, this will be even smaller than terms which are second order in Γ. Thus the strong zero mode should indeed be insensitive to changes in small, but non-zero, J_2.

We can also see from figure 3.10 that there is no resonance at $J_2 = 2J$, at least for the system sizes we can test, as the decay time continues to exponentially increase. We test further even ratio values by plotting J/J_2 instead in figure 3.12. Again we see no resonances for even values of p and odd values of q. As opposed to small J_2, we see that at small J the system seems to saturate in decay time even at small system sizes. This is because for zero J the spin chain splits into two independent chains of even and odd spins, and there are two exact strong zero modes. As soon as J is turned on it couples the two chains. Thus, even though it commutes with σ_1^z like J_2, it limits the decay time when small as it allows the edge spin to interact with even spins.

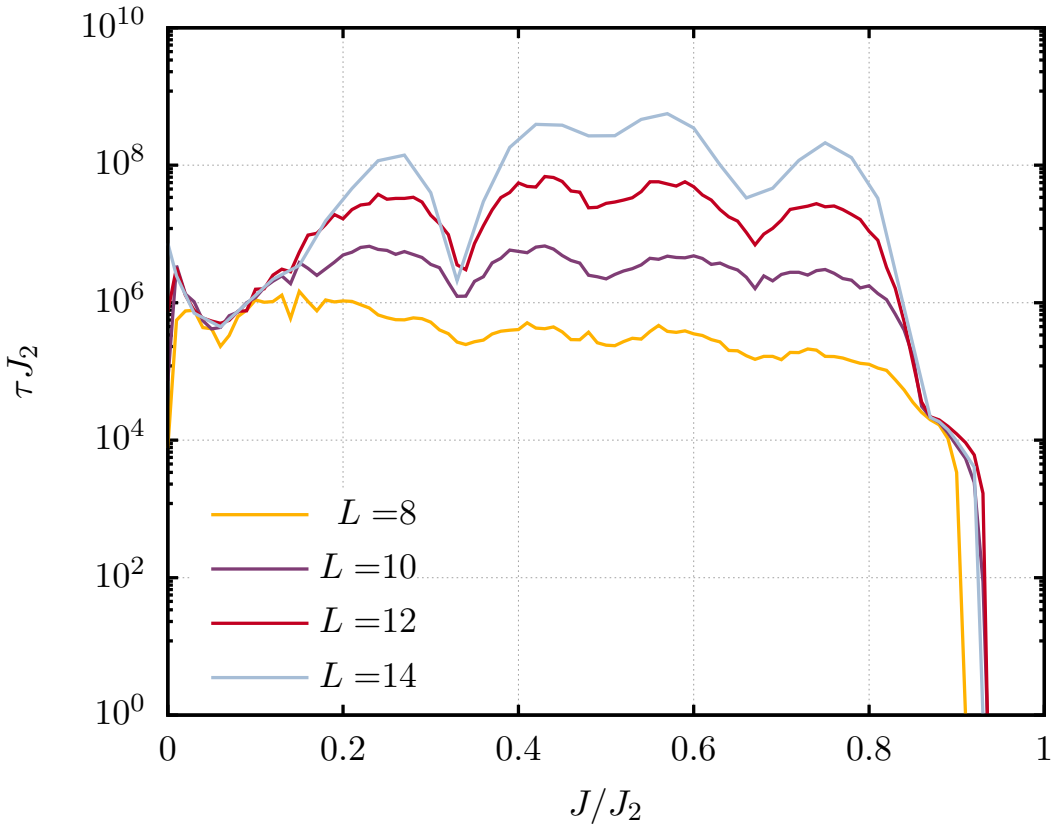

Figure 3.12: The decay time (on a logarithmic scale) of the edge spin at $T = \infty$ for $L = 8 - 14$ sites, as obtained by exact diagonalization, for $\Gamma = 0.1$, plotted against J/J_2 rather than J_2/J. The resonances at $J = J_2$, $J = J_2/3$ and $J = 2J_2/3$ are clearly visible, but there are no poles at $pJ = J_2$ for even p.

Another observation made in section 3.3.2 was that because J_2 is a next-nearest-neighbor coupling, σ_2^z is an edge spin and should have enhanced autocoherence time, particularly when p and q are both odd so there are no resonances. This is shown in figure 3.13.

3.3.4 Integer eigenvalues and resonances

One of the conditions we need to apply ADHH to a system is that $\hat{N}$ have integer eigenvalues. If this is not the case, then as $L \to \infty$ we can find different eigenvalues of $\hat{N}$ which are arbitrarily close together. This means that no matter how large we make J, terms in $\hat{Y}$ will always be able to easily take states from different eigenspaces of $\hat{N}$, and there will be no emergent $U(1)$.

For the bulk of the system this is very different from the cases we considered for

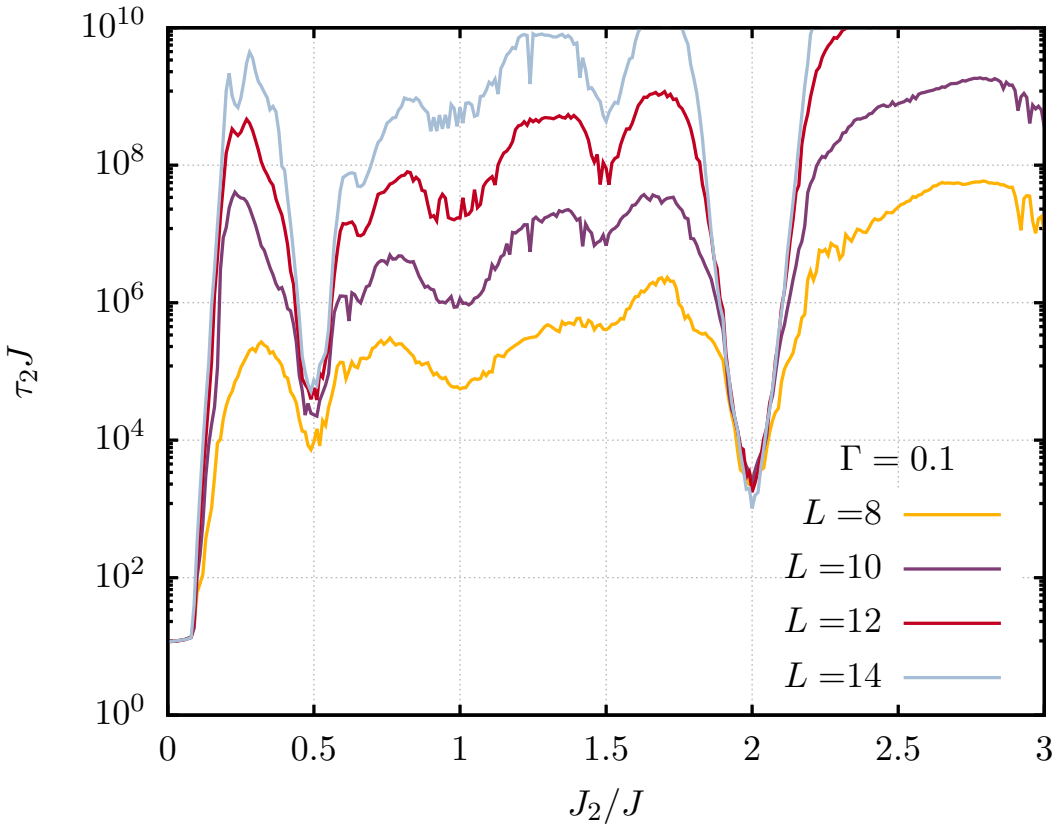

Figure 3.13: The decay time (on a logarithmic scale) for σ_2^z, the spin next to the edge, at $T = \infty$ for $L = 8 - 14$ sites, as obtained by exact diagonalization, for $\Gamma = 0.1$, plotted against J_2/J. Because the J_2 interaction is next-nearest-neighbour, σ_2^z also has enhanced coherence time, except at resonances. We see that there are no resonances at $p/q = J_2/J$ for both p and q odd, as we expect.

resonances above, in which $\hat{N}$ *did* have integer eigenvalues and there *was* an emergent $U(1)$ symmetry. However, from the point of view of the almost strong zero mode, the effects are the equivalent: there are easy edge spin flip processes which flip the edge spin for no cost in energy, destroying the edge coherence.

Of course there is no reason why we cannot use the explicit perturbative expansion of the almost strong zero mode when $\hat{N}$ does not have integer eigenvalues. When we calculated the first and second-order expressions (3.20) and (3.21) we did not specify rational J_2/J. However, the large terms in the expansion due to nearby resonances will affect the error of the strong almost zero mode and force us to truncate the almost strong zero mode at an earlier n_* than the ADHH lower bound. This explains why the pole have width in the decay time plot above from the point of view of the perturbative expansion.

4

Systems with strong edge zero modes

We have discussed the general conditions for almost strong zero modes in section 3.3 and possible reasons these can fail to be met. In this chapter we discuss classes of systems which do or do not have strong zero modes, including those at finite size and temperature, and the effects of the difference between the almost strong zero mode and the edge spin.

4.1 Integrability and strong zero modes

There are only two systems proved to have exact strong zero modes: transverse-field Ising [12, 22] and the XYZ spin chain [14]. Both of these systems are integrable, and transverse-field Ising is also free. It seems natural to assume that only integrable systems can possess exact strong zero modes. This is because having an exact strong zero mode implies $n_* \to \infty$ for the ADHH transformation. This means that the emergent $U(1)$ symmetry becomes exact. In integrable systems this exact $U(1)$ symmetry can be explained as particle number conservation [7, 42]. We will comment more on the possible deeper connection between integrability and exact strong zero modes in section 8.1.

Nevertheless, the converse is not true, and there are of course integrable systems which do not satisfy the conditions for a strong zero mode. We have already seen the free fermion transverse-field Ising model lacks a strong zero mode when $\Gamma \geq J$ because the single site transverse-field term does not protect the edge spin. Similarly, the XYZ

chain does not possess as strong zero mode when at least two of the couplings from the Hamiltonian (3.1) are the same, and the different one, if it exists, is smaller.

This can be easily illustrated. Without loss of generality suppose $J_x = J_y > J_z$. In this case $\hat{N}$ is given by

$$\hat{N}_{\mathrm{XX}} = \sum_{j=1}^{L-1} \left[\sigma_j^x \sigma_{j+1}^x + \sigma_j^y \sigma_{j+1}^y\right], \tag{4.1}$$

as opposed to $\hat{N}_{\mathrm{Ising}} = \sum_i \sigma_i^z \sigma_{i+1}^z$ if J_z were greater. We see that the failure of the strong edge zero mode is even more trivial than for transverse-field Ising as the edge spin simply cannot commute with the two conjugate nearest-neighbour couplings in $\hat{N}_{\mathrm{XX}}$. Moreover, $\hat{N}_{\mathrm{XX}}$ does not have integer eigenvalues. Thus the XXZ model for $J_x < J_z$, and similarly, the XXX Heisenberg point, have no strong edge zero modes.

Another well-known integrable model with no strong edge zero mode is the Hubbard model. This model describes spin-half fermions hopping on the chain with a single site Coulomb interaction [43]:

$$H_{\mathrm{Hubbard}} = -\sum_{j=1,\sigma}^{L-1} t\left(f_{j,\sigma}^\dagger f_{j+1,\sigma} + f_{j+1,\sigma}^\dagger f_{j,\sigma}\right) + \sum_{j=1,\sigma}^{L} U n_{j,\uparrow} n_{j,\downarrow} \tag{4.2}$$

Here $f_{j,\sigma}^\dagger$ is the usual fermion creation operator on site j with spin σ, and the number operator $n_{j,\uparrow} = f_{j,\sigma}^\dagger f_{j,\sigma}$. Regardless of the relative strengths of the couplings t and U, this model does not have an edge mode. The interaction term U is single site and so does not protect the edge fermion, while the hopping t term suffers from the same problem as $\hat{N}_{\mathrm{XX}}$; namely, that it has non-integer eigenvalues and does not commute with the edge fermion. This is unsurprising because $\hat{N}_{\mathrm{XX}}$ turns into the hopping terms under a Jordan-Wigner transformation.

4.2 Energy gap

One might notice that Hubbard and XXZ models share another feature: they are both gapless in the regime where there is no strong zero mode. Similarly, we know that a gap in the spectrum is important for protecting a *topological* zero mode. However, we stress that by definition a *strong* zero mode affects all states, not just those at low energy

density. Fundamentally, it is not the presence or absence of a gap that is important, but rather whether $\hat{N}$ has integer eigenvalues. Of course, if $\hat{N}$ is gapless this will generally not be the case.

4.3 Symmetry

Consider the two possible parameter regimes of the XXZ model. When there is a strong zero mode, $\hat{N}_{\text{Ising}}$ has a global $\mathbb{Z}_2$ symmetry under flipping all the spins. On the other hand $\hat{N}_{\text{XX}}$ remains invariant under a $U(1)$ rotation of spins about the z-axis, and has no strong zero mode. Similarly, Hubbard has a much larger symmetry group than $\mathbb{Z}_2$ and has no strong zero mode.

Although there is no precise statement to be made here, in general $\hat{N}$ obeying a larger set of symmetries will make it less likely a strong zero mode exists. The more symmetries the greater the chance of a resonance, and indeed also the less likely that $\hat{N}$ will have integer eigenvalues.

In fact, Fendley [22] identified this problem when he calculated the strong zero mode for the chiral Potts, or clock, model. The chiral Potts model can be thought of as generalisation of the Ising model where the 'spins' can take on more than two values: rather than just $\uparrow$ or $\downarrow$, they can take Q values $A, B, C \ldots$. The $\mathbb{Z}_2$ spin flip symmetry of Ising becomes the symmetric group Z_Q, where a spin flip becomes a clock shift one forward or back: B to C, or B to A, and so on. The equivalent of Majorana fermions for the clock model are called 'parafermions', but we will not discuss there further here.

The simplest concrete example $Q = 3$ is given by the Hamiltonian

$$H_3 = -J \sum_{j=1}^{L-1} \left(\sigma_j \sigma_{j+1}^\dagger e^{i\theta} + \text{h.c.} \right) - f \sum_{j=1}^{L} \left(\tau_j e^{i\phi} + \text{h.c.} \right) , \tag{4.3}$$

where the 'clock' operators σ_i are equivalent to σ_i^z in transverse-field Ising, but its eigenvalues are $1, \omega, \omega^2$, where $\omega = (1)^{\frac{1}{3}}$, rather than just ± 1. τ_i is the shift operator equivalent to σ_i^x which cycles through clock values. They are defined by the algebra:

$$\sigma^3 = \tau^3 = 1 , \qquad \sigma^\dagger = \sigma$$

$$\sigma\tau = \omega\tau\sigma , \qquad \tau^\dagger = \tau$$

The equivalent of $\hat{N}_{\text{Ising}}$ for the clock model in this case is the part of the Hamiltonian in (4.3) proportional to J, while the term proportional to f is the perturbation $\hat{Y}$.

Returning to the general Q case, the eigenvalue of $\hat{N}_{\text{Clock}}$ does not measure only domain-wall number, but also type. For example, for $Q = 3$, the 'in-order' broken bonds of type AB, BC, CA carry a different energy to the 'out-of-order' type BA, CB, AC, due to the $e^{i\theta}$ term breaking the symmetry. In general there will be $(Q-1)$ different types of domain walls, which we label with positive integer q. The domain-wall free states of form AA will still have the same energy as each other, due to the $\mathbb{Z}_Q$ symmetry.

In order for us to apply ADHH, $\hat{N}_{\text{Clock}}$ must have integer eigenvalues. This can be achieved if the energies of the domain walls are evenly spaced; that is, if the energy of domain-wall type q is

$$E_q = E_0 + n_q \epsilon \,, \tag{4.4}$$

where $n_q \in \mathbb{Z}$, E_0 is the energy of the domain-wall free states, and ϵ is arbitrary. We will always take the index of n_q modulo Q, and if all the n_q have a common factor we will absorb this into ϵ.

Even with this restriction to integer eigenvalues, a particularly degenerate case is immediately apparent: if n_q is the same for all q, all of the domain walls have the same energy. In this case the $\mathbb{Z}_Q$ symmetry is promoted to the full symmetric group S_Q, as we are no longer required to permute 'clock' values cyclically. For example, AB and CB have the same energy. This is disastrous for a putative strong zero mode, because it allows us to change the edge 'clock' without changing the eigenvalue of $\hat{N}_{\text{Clock}}$, for example via the process

$$ABBBB\cdots \quad \Leftrightarrow \quad CBBBB\cdots \qquad n_q = c \forall q \,.$$

This is a particularly clear example where increasing the symmetry causes the strong zero mode to fail at first order due to a resonance. In fact this was the first example of these sort of resonances to be identified [22], and its effects on the energy level splitting of eigenstates was described in [23].

We can identify points that are resonance-free by the same simple arguments used for the next-nearest-neighbour Ising case in section 3.3.2. At the edge, shifting a clock value converts a single domain wall of one type to another, so that the change in eigenvalue of $\hat{N}_{\text{Clock}}$ is proportional to $\Delta_1(s) = n_{q\pm1} - n_q$, where the addition of q indices is always taken modulo Q, and for convenience the domain-wall-free state is given by $n_0 = 0$. Meanwhile in the bulk, we must also consider the effect of the shift on the other bond, so that $\Delta_{j>1}(s) = n_{q\pm1} - n_q + n_{p\mp1} - n_p$. Thus the equation for resonances, equivalent to equation (3.25), is given by

$$n_{q'\pm1} - n_{q'} = \sum_{q,p} N_{q,p} \left(n_{q\pm1} - n_q + n_{p\mp1} - n_p \right) \ . \tag{4.5}$$

If this equation has a solution for any arbitrary q' and integers $N_{q,p}$, then we have a resonance.

For example, for transverse-field Ising, $Q = 2$, and this simplifies to $n_1 = 2N_{1,0}n_1$ which has no solutions, because the left and right hand sides have different parities. This means there are no resonances, as we would expect.

This example illuminates the method needed to prove the cases when there are no solutions for $Q > 2$: find when the two sides of the equations must have different values modulo Q. For example, for $Q = 3$, the simplest clock model case, the possible left hand sides of equation (4.5) are n_1, n_2, $n_1 - n_2$, while the terms to be summed in the right hand side are $n_1 + n_2$, $2n_1 - n_2$ and $2n_2 - n_1$. If

$$(n_1 + n_2) \mod 3 = 0, \tag{4.6}$$

then the right hand side will always be $(0 \mod 3)$, while unless $n_1 = n_2 = 0$ the left hand side will not. This identifies the resonance-free points of the $Q = 3$ clock model.

This set of resonance-free points was identified by Moran *et al.* in [24] under the name 'anti-resonant' points. They used a different but ultimately equivalent method more natural in their context of finding degenerate bands of the unperturbed clock Hamiltonian, rather than almost strong zero modes. It should be noted, however, that the 'resonances' in that paper, which the authors prove to be dense in θ, are not the same as our resonances above,

but rather are a consequence of a parameter regime in which $\hat{N}_{\text{Clock}}$ has non-integer eigenvalues (see the discussion above in section 3.3.4).

We can convert from the n_q to the θ parameter of the Hamiltonian (4.3) by noticing that the energy of the domain-wall type q in the unperturbed model $f = 0$ is given by direct substitution by:

$$-2J\cos(\theta + \frac{2q\pi}{3}) \tag{4.7}$$

By comparing this with the definition of n_q (4.4), we find

$$\theta = \arctan\left(\frac{\sqrt{3}n_1 - n_2}{n_1 + n_2}\right) . \tag{4.8}$$

We can then compare our predictions with numerics. In figure 4.1 the decay time of the edge clock is plotted against θ. The simplest resonance-free point, $n_1 = 2$,$n_2 = 1$ at $\theta = \pi/6$ is indeed resonance-free, while the trivial first-order resonance at $n_1 = n_2$ is also apparent at $\theta = 0$ and $\pi/3$. Second-order resonances are visible at $n_1 = 3$, $n_2 = 2$ and $n_1 = 3$, $n_2 = 1$.

Even when there are no resonances, we have an almost strong zero mode, so the decay time should eventually saturate at the ADHH bound. However, for certain values of the couplings the clock model becomes integrable (or even 'superintegrable') [22, 44] and where these points coincide with (4.6) one might expect the almost strong zero mode to become exact, although there is no proof of this.

Another case where too much symmetry can be problematic is if we attempt to find almost strong zero modes in higher dimensions. For example, we can take the first step to two dimensions by considering the quasi-1D case of two coupled transverse-field Ising chains

$$\begin{aligned} H'_{\text{SPT}} = J_1 \sum_{j=1}^{M-1} \sigma^z_{2j}\sigma^z_{2j+2} + \Gamma \sum_{j=1}^{L} \sigma^x_{2j} \\ + J_2 \sum_{j=1}^{M-2} \sigma^z_{2j+1}\sigma^z_{2j+3} + \Gamma \sum_{j=1}^{L-1} \sigma^x_{2j+1} \\ + \Gamma_2 \sum_{i=1}^{L-1} \sigma^x_i \sigma^x_{i+1}. \end{aligned} \tag{4.9}$$

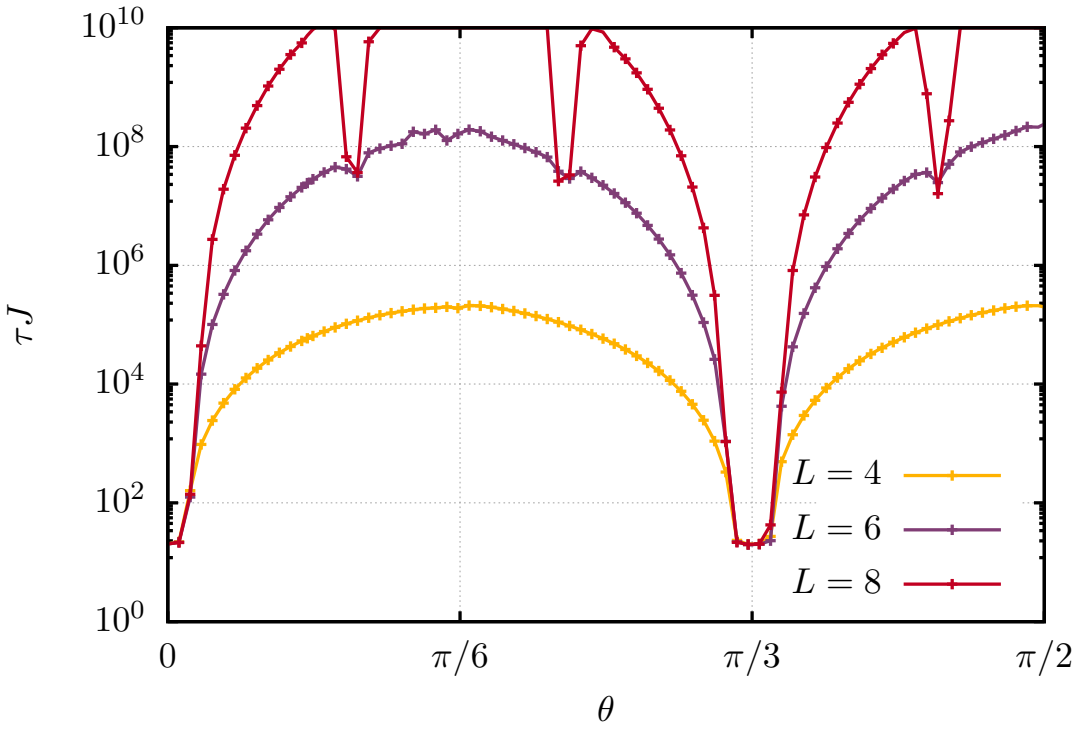

Figure 4.1: The decay time (on a logarithmic scale) of the edge clock in the chiral Potts model at $T = \infty$ for $L = 4 - 8$ sites, as obtained by exact diagonalization, for $f = 0.05$. The lines are to guide the eye. The first-order resonances at $\theta = 0, \pi/3$ are clearly visible, as are the second-order resonances at $\theta = \arctan(\frac{\sqrt{3}}{5}), \arctan(\frac{\sqrt{3}}{2})$. The point $\pi/6$ is resonance free, as we would expect.

If $J_1 = J_2$ it is clear that there will be a first-order resonance caused by hopping a domain wall from the edge of one chain to the edge of the other. In order to avoid this we must break the $\mathbb{Z}_2$ symmetry between the chains by making J_1 different from J_2. We will discuss this ladder in more detail in section 6.2, and higher dimensions in section 8.1.

One might also wonder whether too little symmetry might be a problem for the almost strong zero mode. In particular, all the models we have studied so far have at least a $\mathbb{Z}_2$ spin-flip symmetry. There is nothing in our arguments which relies on this, however, and we can, for example, add a small longitudinal magnetic field $B \sum_i \sigma_1^z$ to $\hat{Y}$ without destroying the almost strong zero mode, although there will be a resonance order q for $B = J/q$. This relies on $B \ll J$ – when B is of the same magnitude or larger than J we will no longer be able to apply the ADHH theorem due to the single-site nature of the field. I am carrying out numerical work to systematically test these claims.

All of our models so far also share translational invariance in the bulk: that is, if

we replaced the open boundary conditions with periodic they would be invariant under translations of multiples of the unit cell. In section 5.3 we will describe the effects of breaking this symmetry by adding disorder. We shall find that strong disorder generically helps the almost strong zero mode rather than hinders it, while in contrast weak disorder turns exact strong zero modes into almost strong zero modes.

4.4 Long-range couplings

The original proof of the ADHH theorem in [17] required that $\hat{N}$ be the sum of operators supported on a single site. In Appendix B of reference [20], Else proved that this could be extended to the sum of operators with finite support. A major problem to extending the theorem to long-range couplings is that the proof of the theorem relies on the so-called Lieb-Robinson bound. This provides a strict upper bound on the speed of the spread of information in quantum systems with short-range couplings [45]. Recently, Lieb-Robinson bounds for long-range systems have been reported [46, 47]. Suppose the sum of the norm of all long-range operators with support greater than or equal to R acting on any single site decays as a power-law $\frac{1}{R^\alpha}$, for $\alpha > d$, the dimension. Then Else *et al.* [47] have shown that at any fixed time, the spatial decay of quantum information follows arbitrarily closely to $\frac{1}{r^\alpha}$. For our purposes, this could be used extend the proof of the ADHH theorem for spin chains as long as $\alpha > 1$, although the resultant bounds on the error and the locality of the unitary transform would have to be changed.

Even suitably modified, there are further problems with ADHH for systems with long-range couplings. In a semi-infinite system a truly long-range coupling which decays as a power law will not have integer eigenvalues. A solution is to truncate $\hat{N}$ to be only terms with some chosen finite support, and place the even longer-ranged terms into $\hat{Y}$. This of course increases the magnitude of the perturbing terms and forces the drop-off to be sharp enough so that we still obtain an n_* large enough for there to be a difference between bulk and edge spins.

This brings up a further problem: even if we can apply an ADHH-like theorem to systems with long-range couplings, we must account for the possibility of resonances

between terms of different range. In fact, our analysis of resonances above for next-nearest-neighbour terms is a first step towards doing this, but we would also need to consider the effect of adding longer range J_3, J_4 terms and so on. We will treat an explicit example numerically in the context of an actual experimental system in section 7.1.

4.5 The edge spin and the strong zero mode

In a semi-infinite system, an exact strong zero mode commutes with the Hamiltonian and thus the autocorrelation time $\langle \Psi(0)\Psi(t)\rangle = 1$ for all times and temperatures. We have shown above that for an almost strong zero mode this is true for a time exponentially long in a small coupling.

However, physically we are not interested in the behaviour of the strong zero mode itself but rather the edge spin. What are the consequences of the existence of the strong zero mode for the autocorrelation of the edge spin?

Recall that the strong zero mode was given by a unitary transform of the edge spin $\Psi = \mathcal{U}^\dagger \sigma_1^z \mathcal{U}$.. This was because the transformed Hamiltonian $H' = \mathcal{U} H \mathcal{U}^\dagger$ conserved the edge spin: it had no terms involving σ_1^x or σ_1^y, up to exponentially small corrections. Rather than view this as an active transformation we may of course also view it as a change of basis $\sigma_i^a \to \sigma_i'^a$ where $\sigma_1'^a = \mathcal{U}\sigma_i^a\mathcal{U}^\dagger$. Using this notation $\Psi = \sigma_1'^z$.

Now typically we will start with σ_1^z as our zeroth-order estimate for Ψ. This means that $\Psi = \mathcal{N}\sigma_1^z + \dots$ where $\mathcal{N}$ is the normalisation. Crucially the remainder does not contain any further terms where the only Pauli operator is σ_1^z. Given that Pauli matrices are traceless, it follows that the trace inner product is $\mathrm{Tr}(\sigma_1^z\Psi) = \mathcal{N}$. We can use this to inverse transform σ_1^z and write it in terms of the $\sigma_i'^a$, because unitary transforms preserve the trace inner product. We have

$$\sigma_1^z = \mathcal{N}\sigma_1'^z + R \tag{4.10}$$

where the remainder R is orthogonal under the trace inner product to $\sigma_1'^z$, and must square to $(1-\mathcal{N}^2)$ to preserve normalisation. For example in transverse-field Ising

without interactions

$$\sigma_1^z = \mathcal{N}_{\text{Ising}} \left(\sigma_1'^z - \sum_{j=1}^{L} \left(\frac{\Gamma}{J} \right)^j \sigma_j'^z \prod_{k=1}^{j-1} \sigma_k'^x \right); \tag{4.11}$$

that is, the same as for Ψ in equation (2.9) but with a change of sign for the 'tail' of the operator into the bulk.

Assuming $\sigma_1'^z$ commutes exactly with the Hamiltonian and so is constant, the autocorrelation time at infinite temperature is given by

$$\langle \sigma_1^z(0)\sigma_1^z(t) \rangle = \mathcal{N}^2 + \langle R(0)R(t) \rangle \ . \tag{4.12}$$

Notice the expectation at infinite temperature involves taking the trace, so we have exploited orthogonality to cancel cross terms.

This places a lower bound on the value of the autocorrelator of $2\mathcal{N}^2 - 1$ because of the magnitude of R. Moreover, we expect the remainder term $\langle R(0)R(t) \rangle$ to decay to zero quickly. The commutator $[H', R]$ will be first order in the perturbing terms such as Γ, because these contributions would cancel with the commutator with the edge spin if R were in the strong zero mode. Comparing this to the commutator $[H, \sigma_1'^z]$ which is of order L in Γ (see equation (2.11)), we see that $\langle R(0)R(t) \rangle$ should decay much faster than $\langle \Psi(0)\Psi(t) \rangle$ does. Physically, from equation (4.11) R is the just the sum of *bulk* domain walls in transverse-field Ising. Unlike at the edge, there is no emergent conservation law forbidding the domain walls from moving freely around the bulk, even if their total number must be conserved, thus it is natural that R should quickly dephase. Once we add in interactions, R will simply include interactions between the domain walls, making dephasing even faster.

Thus we expect for times much shorter than any full decay of the strong zero mode to see the strong zero mode partially decay to a plateau of height $\mathcal{N}^2$. This is qualitatively visible already in figures 3.1 and 3.9, where a fast decay to a plateau can be seen. The height of the plateau from exact diagonalisation at $L = 14$ is plotted against the normalisation for transverse-field Ising in figure 4.2 and for XYZ in figure 4.3 against the analytical results for $\mathcal{N}^2$. We can also compare the plateau values of the almost strong zero mode when the Γ_2 term is added to Ising with $\mathcal{N}_*^2$. We do this for various n_* in

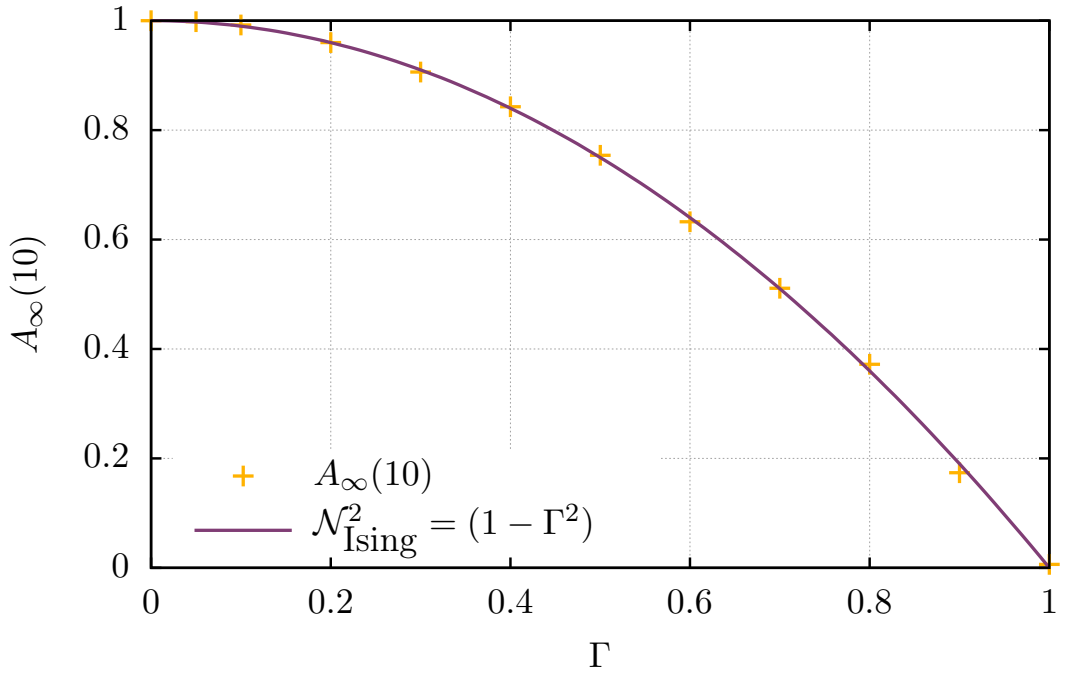

Figure 4.2: $A_\infty(10)$ for the transverse-field Ising model from exact diagonalization as a function of Γ for $J = 1$ and $L = 14$, compared with the analytic estimate $\mathcal{N}^2_{\mathrm{Ising}}$ from equation (2.9).

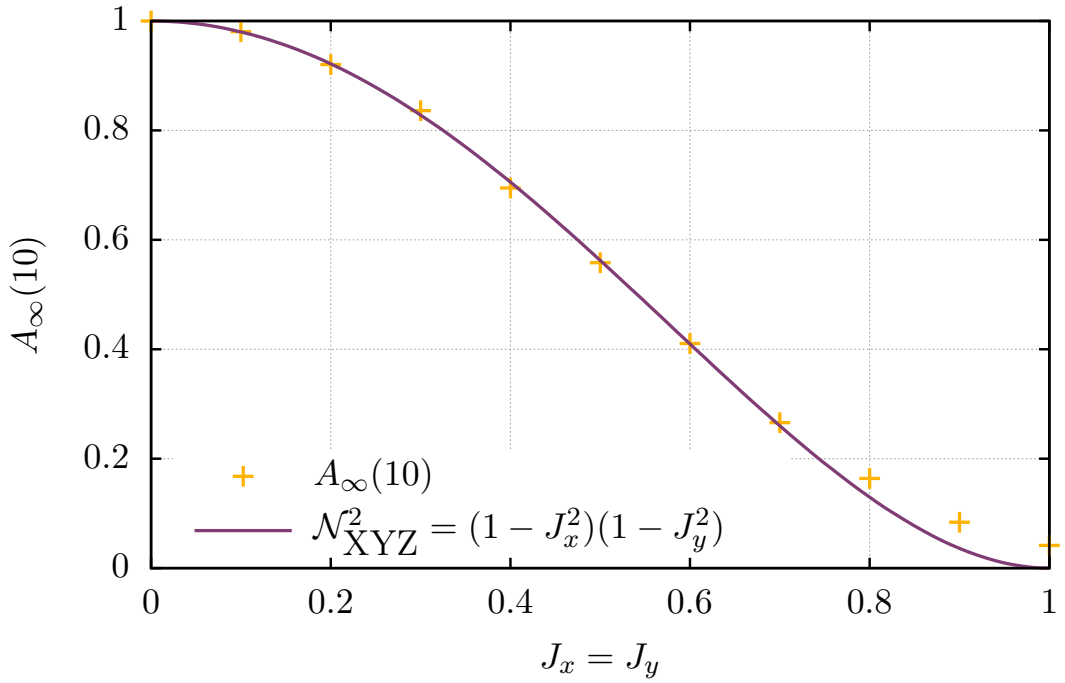

Figure 4.3: $A_\infty(10)$ for XYZ from exact diagonalization as a function of $J_x = J_y$ for $J_z = 1$ and $L = 14$, compared with the analytic estimate from $\mathcal{N}^2_{\mathrm{XYZ}}$, see equation (3.2).

figure 4.4, and find that the estimate is accurate until the perturbing term becomes large. This is anyway the point at which the almost strong zero starts to break down. Even for exact strong zero modes, the larger the interaction terms the greater the finite-size effects.

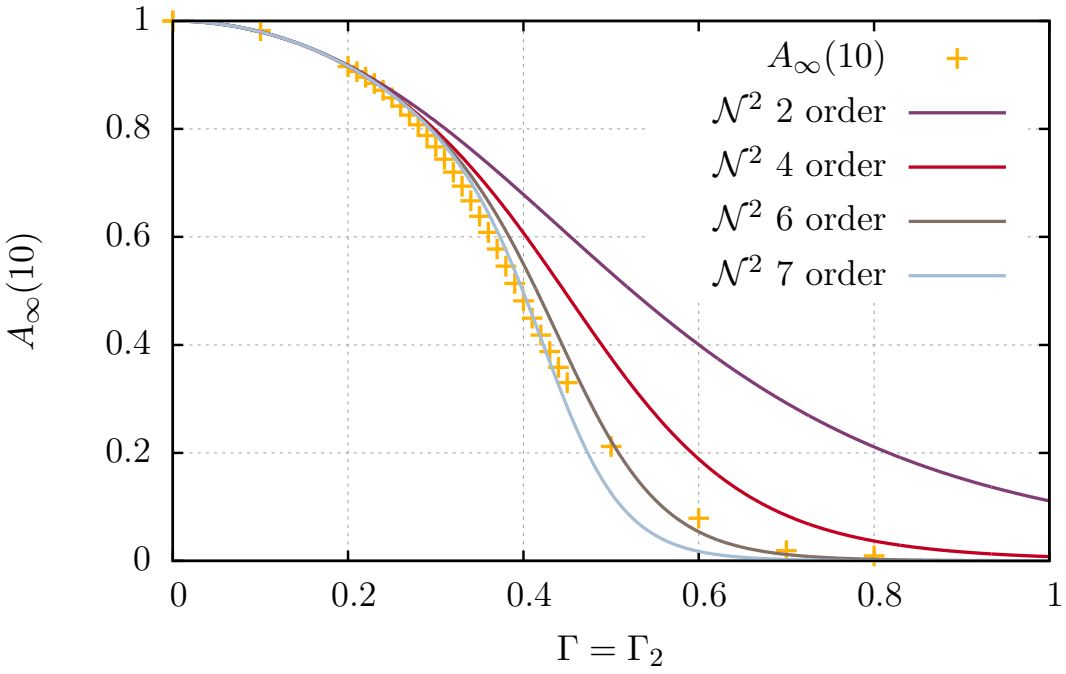

Figure 4.4: $A_\infty(10)$, the plateau height, for $L = 14$ and $J_2 = 0$ from exact diagonalization, compared with the estimate.

We can also measure the autocorrelation time of not just the edge spin but add in further terms from the Ψ. If we do this then the plateau height should increase by the appropriate amount related to the magnitude of the terms we added in, up to staying at one if we measured the full Ψ. It should not, however, affect the length of time before the plateau ultimately decays. This is shown in figure 4.5 where we add the first-order term given by equation (3.15) to the zeroth-order estimate σ_1^z, normalising to first order. The plateau height is increased but ultimately the autocorrelation takes the same time to fully decay. The amplitude of the fast frequency oscillations about the plateau at early times also significantly decreases.

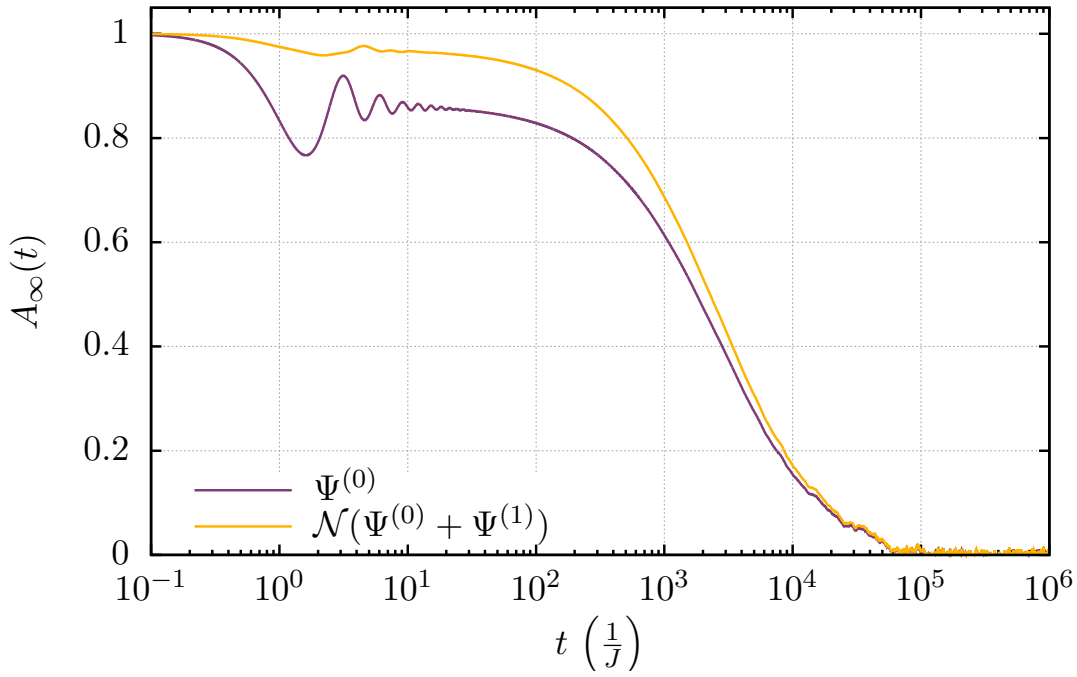

Figure 4.5: $A_\infty(t)$ for the edge spin $\Psi^{(0)} = \sigma_1^z$ and the same with the first-order term in the expansion added from equation (3.15), normalised to first order. The plateau height is increased but the decay time remains the same.

4.6 Finite systems

When the system is not semi-infinite, we are forced to truncate the strong zero mode expansion, whether it is an exact or almost strong zero mode. For exact strong zero modes, this means that the commutator between the strong zero mode and the Hamiltonian does not vanish, but is exponentially small with the length of the system, and therefore Ψ is not constant. This can be seen in figure 2.1. The coherent oscillations are a special feature of the transverse-field Ising model due to its free fermion nature. Notice that the error given in (2.11) has a particularly simple form: it consists of a single term. In fact this term is the product of the spin flip symmetry $\mathcal{F}$ with the edge spin on the other end σ_L^z. But we know that this edge spin is just the zeroth-order estimate for the strong edge zero mode living on the other end, Ψ_R. More precisely we can write the equivalent of equation (4.10)

$$\sigma_L^z = \mathcal{N}\Psi_R + R_R\ , \tag{4.13}$$

where the remainder R_R is orthogonal to Ψ_R. Now by symmetry the error of Ψ_R will just be proportional to our original edge spin multiplied by $\mathcal{F}$ again. Thus using

equations (4.10) and (4.13) we find

$$\frac{\mathrm{d}^2}{\mathrm{d}t^2}\Psi = -[H,[H,\Psi]] = -4\mathcal{N}_{\text{Ising}}^4\Gamma^2\left(\frac{\Gamma}{J}\right)^{2(L-1)}\Psi + \dots \tag{4.14}$$

where the remainder is proportional to R and $\mathcal{F}[H, R_R]$. As we discussed in the previous section, the size of the normalisation limits their possible magnitude. Futhermore, they are trace orthogonal to Ψ. This means that we can neglect these terms and we find the coherent oscillations observed in figure 2.1. Reading off from equation (4.14), their frequency f in units of J is given by $\mathcal{N}_{\text{Ising}}^2\left(\frac{\Gamma}{J}\right)^{(L)}/\pi$. Here $\mathcal{N}_{\text{Ising}}$ is given by equation (2.10), the full L-dependent expression, which we denote $\mathcal{N}_L$, rather than its asymptotic value.

This analytic expression for the frequency is plotted against results from exact diagonalisation on a log-log axes and natural axes in figures 4.6 and 4.7 respectively. The frequency is obtained from a parabolic interpolation of the peak of a discrete fourier transform of the oscillations. We see that the agreement is excellent except for Γ close to the transition, where it is worse for smaller system sizes. It seems likely that this is due to the proximity to the finite-size crossover to the paramagnetic phase.

The oscillations do not appear as soon as we add interactions, even for an exact strong zero mode in an integrable system. For the only other known example of an exact strong zero mode, the XYZ chain, we plot $A_\infty(t)$ from exact diagonalization in figure 4.8. We see that the autocorrelator decays to zero, but like the onset of oscillations in Ising, the time which it takes to decay increases exponentially with length. This occurs because the commutator $[H, \Psi]$, the error, decreases exponentially with length, because the longer the system the higher order in perturbation theory we can go in the strong zero mode expansion. In particular if $\hat{N}$ is nearest neighbour, and there are nearest-neighbour interaction terms in $\hat{Y}$, as in XYZ, then the strong zero mode expansion order n requires at least a system of size $L = 2n + 1$. On the other hand if there are only single site terms in $\hat{Y}$ then $L = n + 1$ suffices. The effect of finite size is of course not quite the same as finite order cutoff in perturbation theory. A particularly obvious example is if there are both single and nearest-neighbour terms in $\hat{Y}$: then it is possible to continue to iterate over the single site terms to higher orders in perturbation theory than the two site terms. This will reduce the error of the almost strong zero mode compared to simply

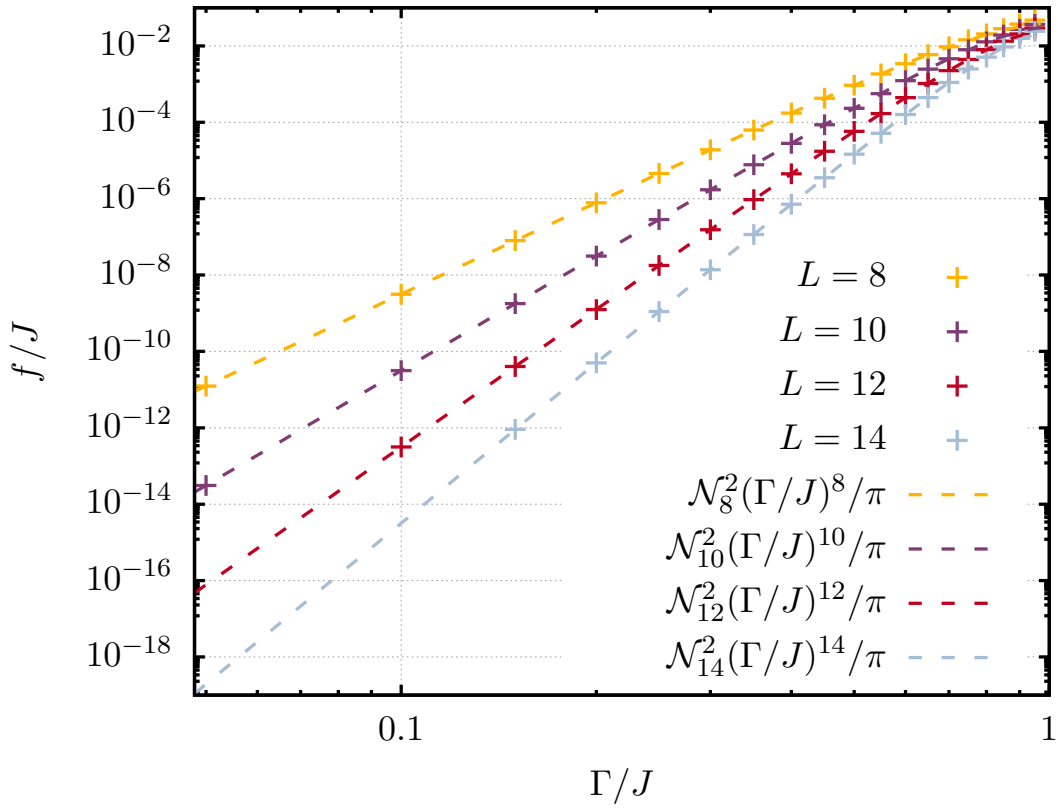

Figure 4.6: The frequency f of the oscillations of the autocorrelation of the edge spin in transverse-field Ising from exact diagonalisation plotted against the analytic predictions at various system sizes on log-log axes. The agreement to the power law prediction in the transverse-field Γ is excellent.

halting the process as soon as the expansion reaches the end of the chain, but it will not change its order in perturbation theory, because there will be contributions from the two site terms which cannot be improved due to the finite size.

A more subtle ambiguity in treating the effects of finite size on the strong zero mode expansion involves treatment of the normalisation. If we calculate the strong zero mode to some order n_c directly, and then multiply by the normalisation, there will be terms in the expansion with order greater than the cutoff. On the other hand if we calculate the boundary unitary instead then the resulting strong zero mode expansion will only have terms of order less than or equal to the cutoff. Regardless, both terms will be normalised to that order in perturbation theory and have error terms the same order of magnitude.

Thus even with these ambiguities, we see that the leading contribution to the error will decrease exponentially as we increase the length, as long as the length does not allow

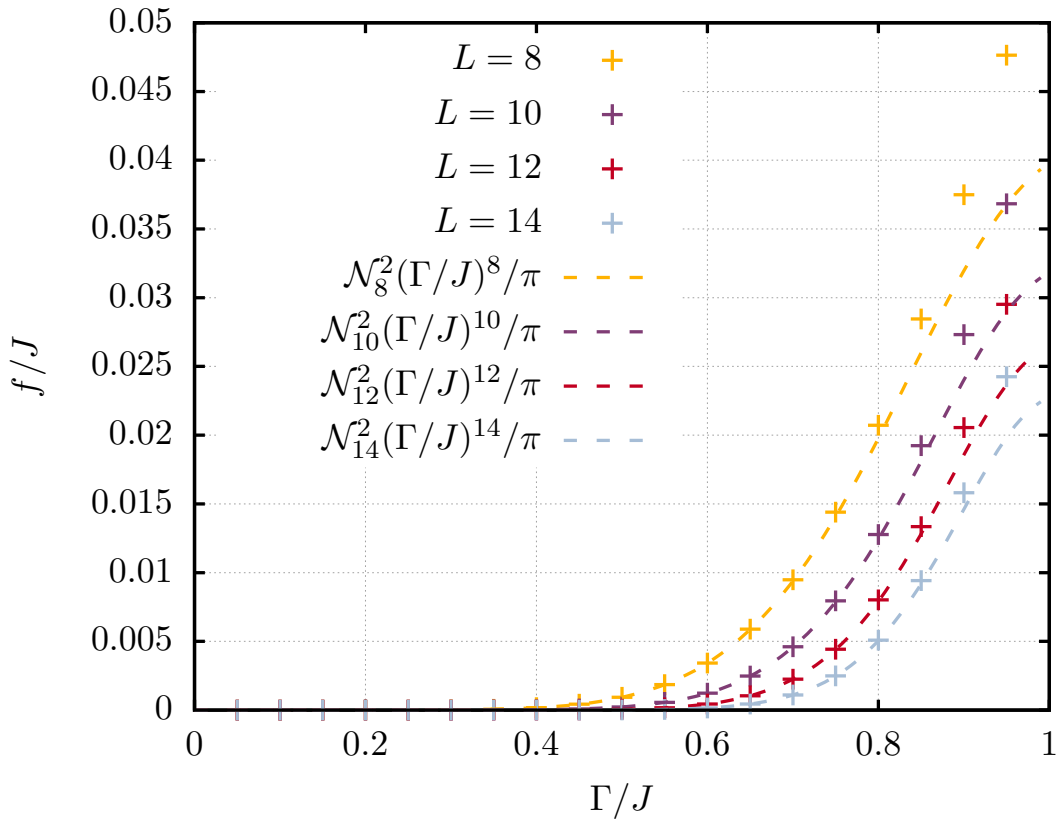

Figure 4.7: The frequency f of the oscillations of the autocorrelation of the edge spin in transverse-field Ising from exact diagonalisation plotted against the analytic predictions at various system sizes on natural axes. We see that there starts to be deviations at large Γ, particularly for the smaller system sizes, which we interpret as being due to the finite-size crossover to the paramagnetic phase.

us to come close to reaching the saturated cutoff n_*. At these lengths the autocorrelator of the edge spin will behave as it did for the XYZ chain: decaying to zero, but with a time increasing exponentially with length. As n_* is approached, the increase in time with length will diminish until it saturates once this system is large enough to accommodate the full strong zero mode expansion up to n_*. This behaviour can be seen in figure 3.2.

An illuminating way of illustrating that the finite size has no effect once saturation is reached is to ask what happens when we change the boundary conditions at the other end of the chain. For example, we can fix the value of the edge spin at the other end. Now, recall that the reason for the long coherence time of the edge spin in the first place is that it is protected by the ADHH theorem if changing the value of *only one* edge spin changes the eigenvalue of $\hat{N}$. The reason we have to put in the single edge-spin caveat

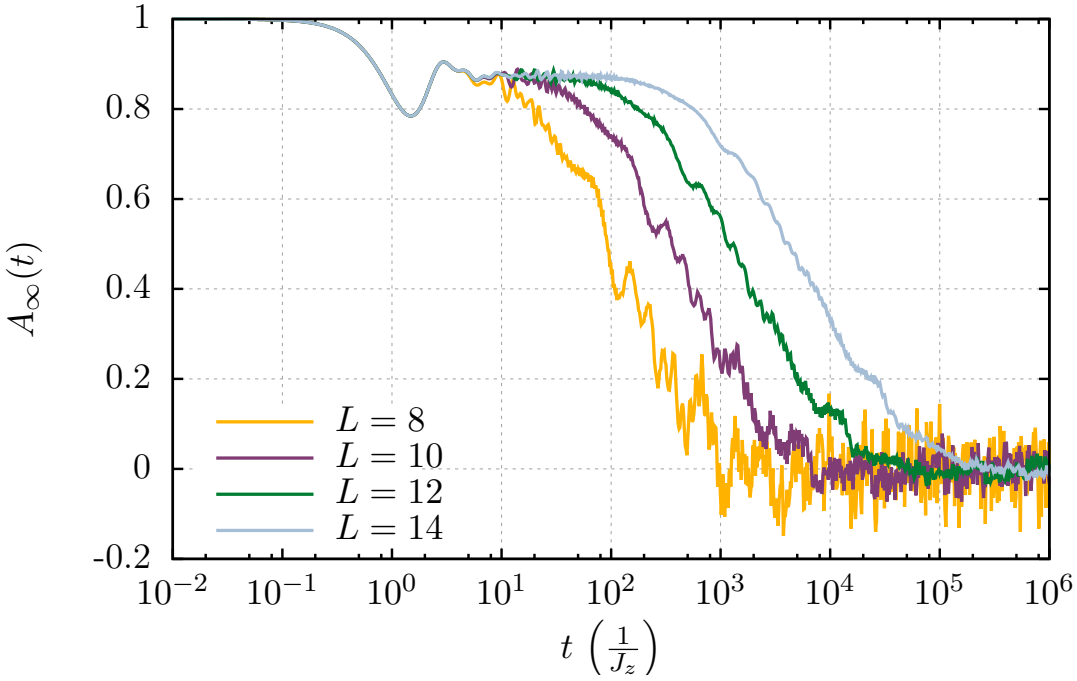

Figure 4.8: $A_\infty(t)$ for XYZ from exact diagonalization on a log axis for time for $L = 14$, $J_x = 0.2$, $J_y = 0.3$, $J_z = 1$.

is that we can always flip both edge spins and keep $\hat{N}$ constant. For example, let us use the language of the resonances section and assume $\hat{N} = \hat{N}_{\text{Ising}}$. Then we know that flipping an edge spin causes an odd parity change Δ_1, Δ_L, but bulk spins yield an even parity change $\Delta_{1<j<L}$. But if we can flip both edge spins we can cause an even change in parity whilst flipping edge spins – that is, we have a resonance. Thus in finite size there is effectively always at least one resonance at the order proportional to the length of the change – more precisely, at the order in perturbation theory needed for the expansion to reach the other end of the chain. This is another perspective on why the autocorrelation time is not infinite, even with an exact strong zero mode.

However, if we now fix one of the edge spins, this resonance can no longer occur. In this case, if the strong zero mode is exact, or if the system size is not large enough to observe saturation, then the autocorrelator of the strong zero mode will not decay. If we measure the autocorrelator of the edge spin instead, then of course the fast decay to the plateau will still occur, but the plateau itself will not. On the other hand, if we are at system sizes larger than saturation, then the decay is not due to finite size, but

rather due to the fact we have hit the time limit for what the emergent symmetry provided by ADHH can protect. Thus the behaviour will be unchanged by fixing the edge spin. This is shown in the solid lines in figure 4.9, compared to the behaviour with typical boundary conditions equivalent to figure 2.1.

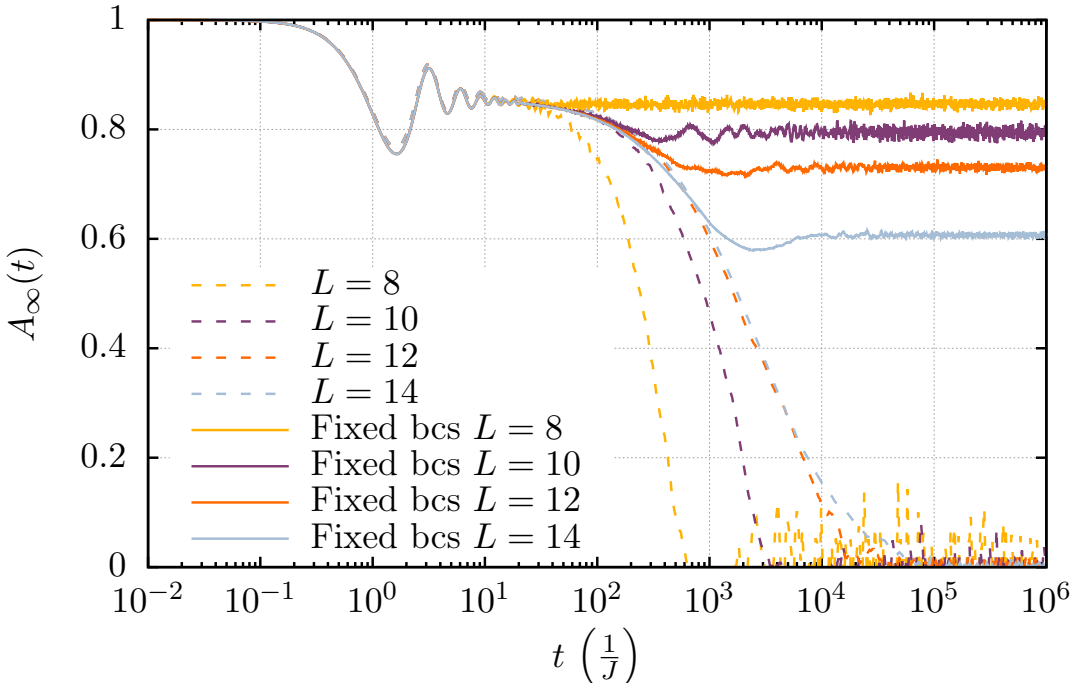

Figure 4.9: $A_\infty(t)$ from exact diagonalization for the transverse-field Ising model on a log axis for time for $\Gamma = 0.3$. The solid lines show the behaviour when the value of σ^z_L is fixed, compared to the dashed lines when it is not. We see that the long-time value of the autocorrelator only starts to decay once saturation at $L = 12$ to 14 is reached and the ADHH bound start to have an effect, whereas finite size does not cause the autocorrelator to decay.

4.6.1 Near the edge

Throughout this thesis we have been comparing the edge spin behaviour to bulk spins, crucially, for example, in figure 3.2. Of course, for the relatively small system sizes we can test, all the spins could be considered close to the edge. Furthermore, we know that the strong zero mode is not solely confined to the edge spin but has a tail into the bulk, although this should be exponentially suppressed. We therefore check the specific behaviour of the decay of the autocorrelator for each spin as we go into the bulk. This is shown in figure 4.10 for $L = 14$. The extreme enhancement of the edge spin compared to the rest is immediately apparent. Even at this length the middle spin is unaffected by

the edge zero mode. The second spin still has some long-lived components, presumably due to overlap with the first-order correction to the strong zero mode.

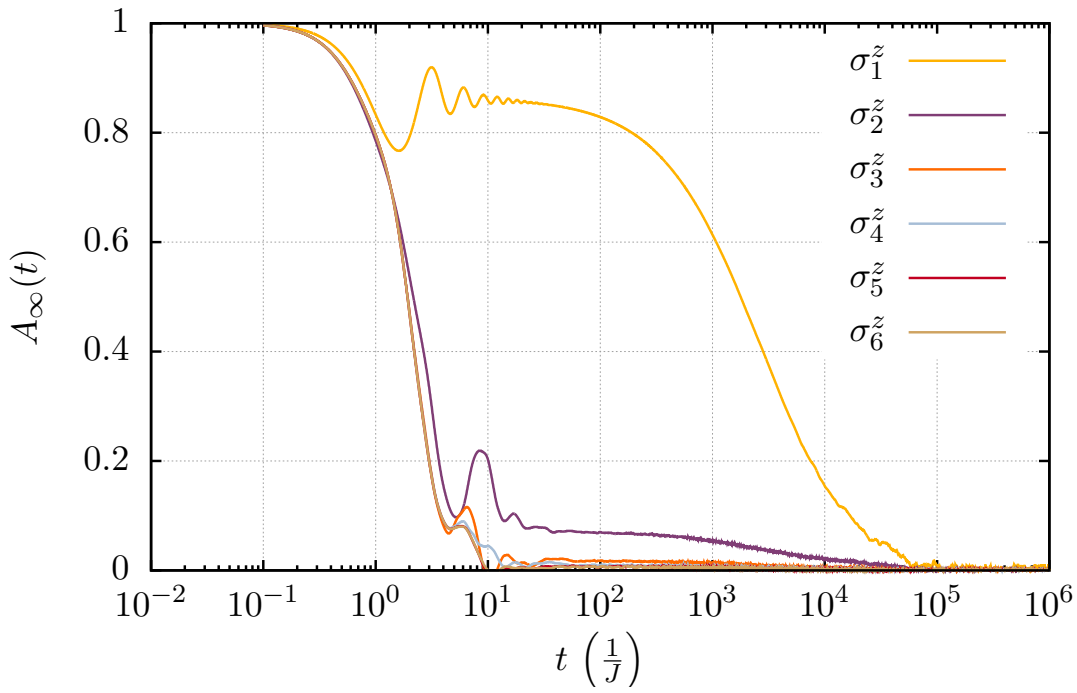

Figure 4.10: The autocorrelation of spins from the edge to the bulk $A_\infty(t)$ from exact diagonalization for the transverse-field Ising model on a log axis for time for $\Gamma = \Gamma_2 = 0.25$ and $L = 14$. The enhancement of the edge compared to the bulk is immediately visible.

4.7 Finite temperature

In section 2.1, we discussed the meaning of infinite temperature, and the fundamental difference between high and low energy density states. We have since only considered the behaviour at infinite temperature. What happens when we lower the temperature?

In the opposite limit, zero temperature, the answer is manifest. For all strong zero modes there is a corresponding 'weak' zero mode, which is only valid for the ground state. This is true because the conditions for a weak zero mode are a subset of those for a strong zero mode. In particular, for a weak zero mode we only need a gap in the unperturbed Hamiltonian, rather than an integer spectrum, which can be viewed as requiring a 'gap' at every energy level, rather than just above the ground state. All such weak zero modes are exact in the sense that they have they have an exponentially long coherence time

with system size, regardless of whether the system is integrable or not. This stability of the weak zero mode to arbitrary perturbations which do not close the gap was shown in Kitaev's original paper on the Majorana zero mode [12].

For the transverse-field Ising model with or without interactions, the presence of the weak zero mode causes the ground level to be degenerate, with two states in the even and odd sectors of the $\mathbb{Z}_2$. This ground-level degeneracy is associated with spontaneously global symmetry breaking for spins and topological order for fermions. Regardless, at finite size, interaction between the two weak zero modes lifts this degeneracy with a splitting exponentially small in their separation. This leads to the autocorrelator oscillating in the ground state, rather than decaying to zero, exactly as we observed for the entire spectrum in the non-interacting case in section 4.6. We will explain explicitly the link between weakly lifted degeneracy and oscillations in Chapter 5.

If the temperature is finite, then we must appeal to the strong zero mode rather than the weak zero mode. Unless the strong zero mode is exact, its autocorrelation time will be finite. Thus as the temperature is increased, we should expect the autocorrelator to transition from oscillating at late times to decaying to zero. This is shown in figure 4.11. Note that if the Hamiltonian is of our typical ADHH form, given by equation (3.3), then the gap above the ground state is given by $\Delta_g \sim J$ with corrections of order Y, the magnitude of the interactions. As the temperature is increased above the gap the influence of the ground state on the autocorrelator in the mixed finite temperature state should become negligible. The root mean square of the oscillator at late times as a function of temperature is plotted in figure 4.12, and indeed we see that the amplitude of the oscillations decays extremely rapidly above the gap.

A surprising feature of figure 4.11 is that the decay time appears to *increase* with temperature, as can be most easily seen by comparing the autocorrelator at $T = 2J$ and $10J$. In fact, this is a finite-size phenomenon. The period of the oscillations increases exponentially with system size, see section 4.6, while the decay time of the plateau saturates with system size, reaching a fixed upper bound. However, at the small system sizes we can reach with exact diagonalisation, the period of the oscillations are in fact *less* than the decay time. This means at higher temperatures where less weight is given

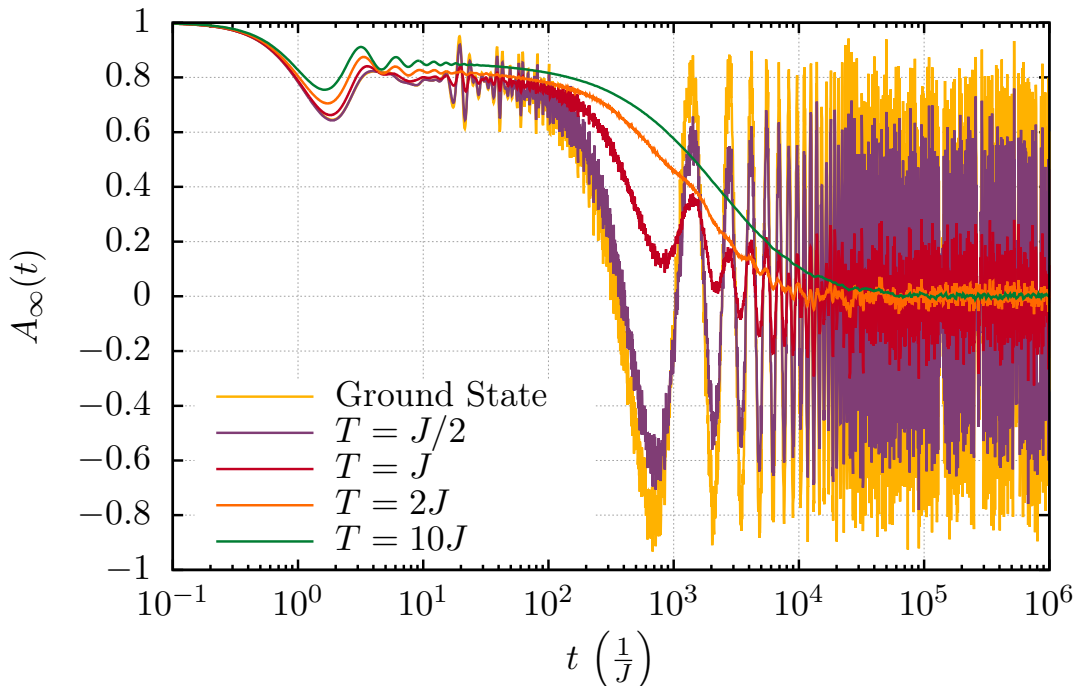

Figure 4.11: The autocorrelator of the edge spin at infinite temperature $A_\infty(t)$ for the transverse-field Ising model at size $L = 14$ with $\Gamma = \Gamma_2 = 0.25$ plotted for different temperatures from exact diagonalisation. At low temperatures oscillations are observed which decrease in amplitude as the temperature increases, transitioning to the plateau followed by a decay to zero familiar from infinite temperature, c.f. figure 3.1.

to the ground state and these oscillations, the coherence time is longer. Of course, for larger system size the oscillations will have greater period, and the relation increasing the temperature will decrease the coherence time.

Generally, if the temperature is below the gap, we should expect the coherence time to be enhanced, because higher energy excitations are exponentially suppressed. We might expect the autocorrelation time will be increased by a factor proportional to $e^{\Delta/T}$, in addition to the factor of e^{cn_*} from the almost strong zero mode present even at infinite temperature. However, we require excitations from the $\hat{Y}$ term to flip the edge spin by changing the eigenvalue of $\hat{N}$, rather than excitations of the unperturbed Hamiltonian – if this were not the case we would have a resonance. The effective gap Δ in the thermal prefactor of the autocorrelation time is therefore larger than Δ_g. In order to transition between different eigensectors of $\hat{N}$, one needs approximately J/Y applications of $\hat{Y}$, so we find $\Delta \sim \Delta_g J/Y \sim \Delta n_*$. It is natural that n_* should appear here, as ultimately the bound in ADHH comes from exactly these sorts of transition. A more rigorous proof

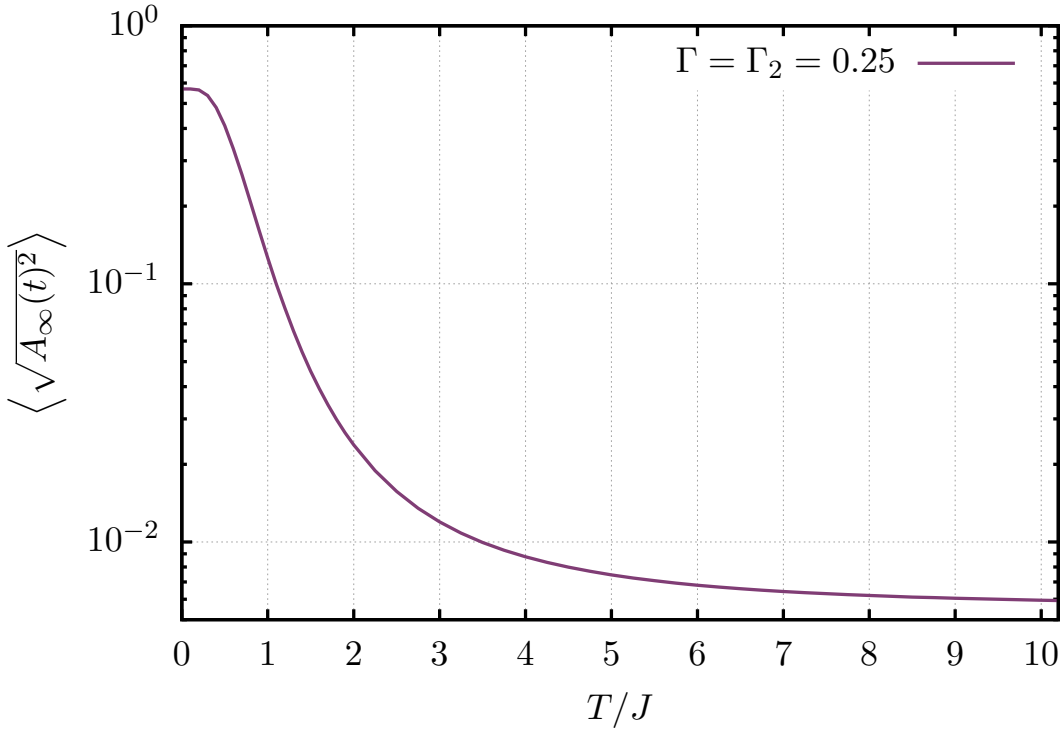

Figure 4.12: The root-mean-square of the autocorrelator of the edge spin at infinite temperature $A_\infty(t)$ calculated for times $t > 10^5 J$ as a function of temperature, for the transverse-field Ising model at size $L = 14$ with $\Gamma = \Gamma_2 = 0.25$ from exact diagonalisation. We see that the amplitude of the oscillations in figure 4.11 sharply drop once the temperature is greater than the gap $\Delta_g \sim J$.

of the energy bandwidths involved in this transition between two different eigensectors of $\hat{N}$ is given by Chetan Nayak in Appendix C of reference [20].

Unfortunately, it has so far been impossible to test the predicted $e^{\Delta/T}$ enhancement numerically, because it has proven difficult to find a method which can handle a sufficient temperature range *and* sufficient system sizes *and* sufficiently long times. Furthermore, even at small system sizes, the behaviour shown in figure 4.11 casts doubt on the straightforward multiplication of the thermal prefactor $e^{\Delta/T}$ and almost strong zero mode prefactor e^{cn_*} to find the total enhancement of the coherence time presented in [20]. Rather, it appears possible that these two factors set timescales for different types of long-lived behaviour, and that their protection does not stack.

Finite temperature also affects how resonances manifest. We have seen that physically resonances can be understood as converting different types of bonds at the edge, flipping the edge spin for no energy cost. This requires specific configurations of spins such as

shown in (3.24), which only occur at energies high enough in the spectrum. The higher order the resonance, the higher energy the excited states needed to achieve it will be. Of course, the occupation of these states will be suppressed at finite temperature. If we are at a significantly lower temperature than the energy required for the processes to resonantly flip the edge spin, we will not observe the resonance at all. A graph showing the effects of temperature on resonances at first and second order for $J_2 = J$ and $\pm J/2$ for $J > 0$ is shown in figure 4.13. The enhancement of the decay time as the temperature is lowered is striking, except for the resonance at $J_2 = -J/2$, where the opposite relation is observed. This is not only surprising of its own accord, but also because at infinite temperature the almost strong zero mode was entirely invariant under changing the relative signs of J and J_2.

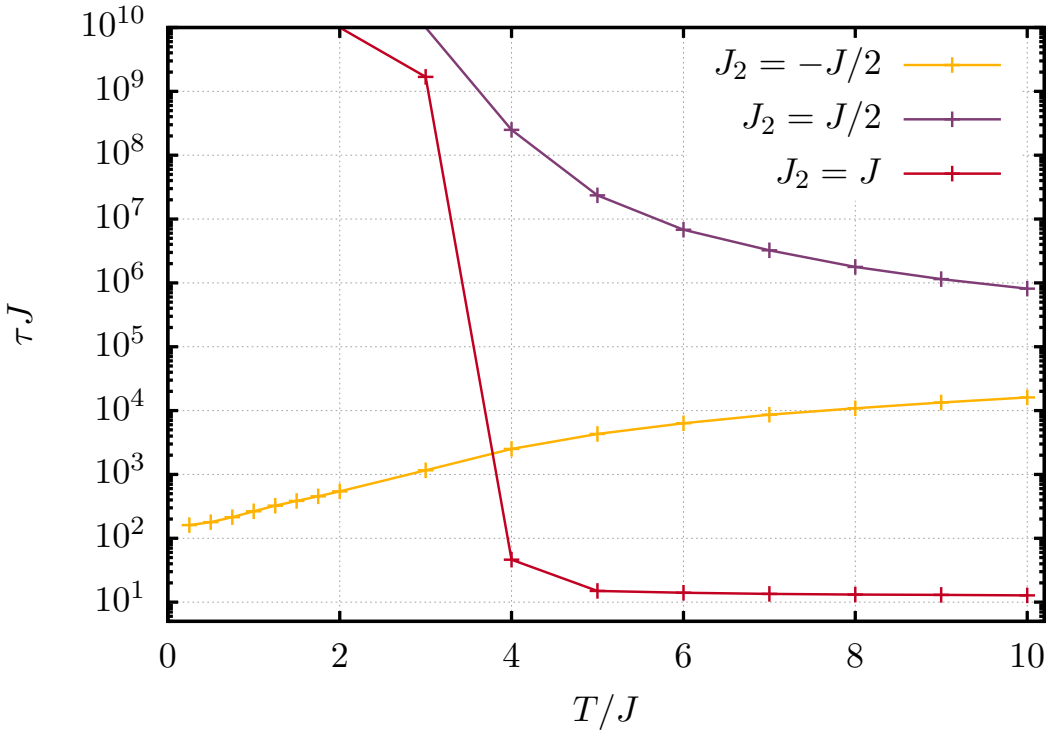

Figure 4.13: The decay time of the autocorrelator of the edge spin as a function of temperature from the edge from exact diagonalization of the transverse-field Ising model for $\Gamma = 0.1$, $\Gamma_2 = 0$ and $L = 14$, at the first-order pole $J_2 = J$ and second-order poles $J_2 = \pm J/2$. The lines are to guide the eye. The enhancement of the decay time at low temperatures is immediately visible, except for $J_2 = -J/2$ where the decay time *decreases* with temperature, due to a paramagnetic ground state, as explained in the main text below.

To understand this behaviour, recall that, as discussed in section 3.3.2, there is a

phase transition at $J_2 = -J/2$ for $J_2 < 0$ and $\Gamma = 0$ between a ferromagnetic phase and a phase with the antiferromagnetic $\langle 2 \rangle$ structure [40]. Crucially if the transverse field does not vanish there is an additional transitional paramagnetic phase between the two [41]. Heuristically, this comes about because the J and J_2 couplings are competing for different types of order, and at precisely $J_2 = -J/2$ they match in strength and cancel each other out, leaving the transverse field to dominate – even if it is much smaller in magnitude. The transverse field is a single site term and thus does not protect the edge over the bulk, so there is no edge enhancement of the coherence time in the ground state. However, as we have already argued in section 3.3.2, at infinite temperature the almost strong zero mode *does* exist at $J_2 = -J/2$, albeit with a second-order resonance. This still leads to a significant enhancement in the edge coherence time, even for $\Gamma = 0.1$ as in figure 4.13. Thus the coherence time must increase with temperature to account for the enhancement at infinite temperature, but not in the ground state. Unlike the behaviour in figure 4.11, we do not expect this to be a finite-size artefact.

5 Eigenstate spectrum and pairing

5.1 Exact strong zero mode pairing

We have discussed in detail how the existence of a strong zero mode gives rise to long coherence times for edge spins. Another famous consequence of the Majorana, or weak, zero mode, is the topological degeneracy of the ground state [12]. For exact strong zero modes, this degeneracy exists not just in the ground state, but in *every* state, all the way up the spectrum, as was mentioned in section 2.2. This occurs because the exact strong zero mode commutes with the Hamiltonian, but anticommutes with the parity symmetry $\mathcal{F}$ (2.1). Thus the strong zero mode maps an eigenstate of the Hamiltonian in the even parity sector to one with the same energy in the odd sector. Explicitly, eigenstates of H form "pairs" $|s_+\rangle$ and $|s_-\rangle$, with $E_{s_+} \approx E_{s_-}$ and $|s_\pm\rangle \approx \Psi|s_\mp\rangle$. Here $\approx$ means equal up to corrections vanishing exponentially fast as $L \to \infty$. In the case of the clock model with the $\mathbb{Z}_Q$ symmetry, the putative exact strong zero mode in the integrable parameter regime takes states from the q^{th} sector to the $(q+1)^{\text{th}}$ sector, so there are Q degenerate states at each energy level.

We can see the connection between this pairing and the infinite coherence time of the

edge spin by introducing a resolution of the identity into the autocorrelator:

$$\begin{aligned} A_s(t) &= \sum_r \left\langle s \left| e^{-iHt}\sigma_1^z e^{iHt} \right| r \right\rangle \langle r \,|\, \sigma_1^z \,|\, s\rangle \\ &= \sum_r |\, \langle s \,|\, \sigma_1^z \,|\, r\rangle \,|^2 e^{i(E_r - E_s)t} \,, \end{aligned} \tag{5.1}$$

where $|s\rangle$ and the $|r\rangle$ are eigenstates of H with energies E_s and E_r respectively. When $|s\rangle$ is a highly excited eigenstate, typically the matrix element $\langle s \,|\, \sigma_1^z \,|\, r\rangle$ is non-vanishing and small for many states r with many different energies E_r. The sum in (5.1), and the further sum over the $A_s(t)$ at finite temperature, then contains many incoherent oscillating factors which decay very rapidly in time. However, if there is a state r where both

1. $\langle r \,|\, \sigma_1^z \,|\, s\rangle$ is finite,

2. $E_r = E_s$,

then this state will provide a constant, non-vanishing contribution to the autocorrelation. The remainder terms still oscillate incoherently and decay rapidly. This means that the edge coherence time is infinite in the large-size limit. These special paired states are of course exactly the $|s_\pm\rangle$ for which $\langle s_- \,|\, \Psi \,|\, s_+\rangle = 1$ in the thermodynamic limit. Thus this argument is equivalent to that given for autocorrelator in equation (4.12): the constant term $\mathcal{N}^2$ is due to these special degenerate paired states, while the remainder terms which decay contribute to $\langle R(0)R(t)\rangle$.

Here we illustrate the pairing in a simple example, the special case $\Gamma = 0$ of the Ising chain. The eigenstates and eigenvalues of the Hamiltonian with $\Gamma = 0$ are given by specifying all the eigenvalues of the σ_j^z. The states $|+++\cdots++\rangle$ and $|---\cdots--\rangle$ are both ground states when $J > 0$. They are not eigenstates of spin-flip symmetry, but these are easily found:

$$\begin{aligned} |g_\pm\rangle &= \frac{1}{\sqrt{2}}(|+++\cdots++\rangle \pm |---\cdots--\rangle) \\ &= \frac{1 \pm \mathcal{F}}{\sqrt{2}}|+++\cdots++\rangle \,. \end{aligned}$$

All eigenstates of both the Hamiltonian and $\mathcal{F}$ can be written in the form

$$|s_\pm\rangle = \frac{1 \pm \mathcal{F}}{\sqrt{2}}|+\pm\pm\pm\ldots\rangle$$

for all 2^{L-1} choices of the $\pm$ signs. Since $[\mathcal{F}, H] = 0$ and $\mathcal{F}^2 = \mathbb{1}$, the energies obey $E_{s_+} = E_{s_-}$. One way of toggling between these degenerate states is simply to measure the edge spin. Because σ_1^z anticommutes with $\mathcal{F}$,

$$\langle s_\pm \,|\, \sigma_1^z \,|\, s_\mp \rangle = 1 \,.$$

Thus in this limit, $A_{s_\pm}(t) = 1$ for all t and $s_\pm$. This of course is not surprising, given there are no off-diagonal terms in the Hamiltonian. But it persists for Γ non-vanishing, and also occurs in at least the one other model with an exact strong zero mode, the XYZ spin chain, which has interactions.

If the system is finite size, we have instead $E_{s_-} \approx E_{s_+}$ up to the typical exponentially small corrections. This means that at infinite temperature the autocorrelator will decay, because the finite-size corrections will cause the contributions from the paired states to oscillate at a slightly different frequencies and ultimately decay. The exception to this would occur if the finite-size corrections were the same for every pair. In this case, instead of decaying the long-time behaviour would be oscillations. This is in fact what occurs for transverse-field Ising, as we have already discussed in section 4.6, because the commutator with the Hamiltonian is the other strong zero mode to first order in Γ. Hence we observe coherent oscillations in transverse-field Ising before the autocorrelator decays. This illustrates the fact that it is the *variance* in energy differences which drives the decay, a point we will return to below.

Now that we know that the long-time contributions to the autocorrelator come from the paired states, it is illuminating to measure properties of the pairing directly. For example, we should be able to find the plateau value of the autocorrelator, its asymptotic value in the thermodynamic limit, without performing any evolution in time as we did in section 4.5, but instead simply measuring matrix elements of σ_1^z in the eigenstate basis of H and $\mathcal{F}$. First we need to find the paired states. At finite size, $\Psi \,|s\rangle$ is not exactly an eigenstate. Furthermore, σ_1^z is not exactly Ψ and thus $\sigma_1^z \,|s\rangle$ is further from an eigenstate. Let us consider $|s_+\rangle$ in the even sector. In order to find its paired eigenstate $|s_-\rangle$, we compute the matrix element $\langle s_+ \,|\, \sigma_1^z \,|\, s' \rangle$ for all $|s'\rangle$ in the odd sector, and find

the one with the maximum magnitude. We will refer to this magnitude as the 'pairing' between the 'paired' eigenstates $|s_-\rangle$ and $|s_+\rangle$.

The mean of these paired matrix elements is then exactly the measure of overlap between σ_1^z and Ψ, excluding finite-size effects. Indeed by inserting a resolution of the identity we find

$$\begin{aligned}\mathcal{N} = \langle \sigma_1^z \Psi \rangle &= \frac{1}{2^L} \sum_{s,s'} \langle s \,|\, \sigma_1^z s' \rangle \, \langle s' \,|\, \Psi \,|\, s \rangle \\ &= \frac{1}{2^L} \sum_{s_+} \langle s_+ \,|\, \sigma_1^z \,|\, s_- \rangle \,. \end{aligned} \tag{5.2}$$

Here the first sum is over all eigenstates s and s', but we restrict it to a sum only over the even sector by noticing that $\langle s' \,|\, \Psi \,|\, s \rangle$ vanishes unless the two eigenstates are paired, in which case it is unity. Physically the normalisation squared represents the plateau value of the autocorrelator at infinite temperature, because the autocorrelator contains two copies of σ_1^z. Here we have continued to neglect finite-size corrections, which we will discuss in more detail below. The analytical normalisation squared for transverse-field Ising and XYZ is plotted against the prediction from the pairing on the right hand side of equation (5.2) calculated from exact diagonalisation in figures 5.1 and 5.2 respectively. We can see that the mean pairing is indeed converging to the normalisation as the system size increases.

5.2 Almost strong zero mode pairing

We have discussed how the ADHH bound n_* for almost strong zero modes, finite-size corrections n_L, and resonances at order $(n_p + 1)$ all have a similar effect on the autocorrelation: the minimum $n_{\min}$ determines the long decay time of the plateau. However, the fact that $n_{\min} \not\to \infty$ as $L \to \infty$ leads to a significant difference to how we must treat the pairing when considering almost strong zero modes compared to exact. This is because as $L \to \infty$ the number of eigenstates grows exponentially, and for our local Hamiltonians, the mean energy spacing between them thus shrinks exponentially. Let us label the almost strong zero mode truncated at $n_{\min}$ by $\Psi_{n_{\min}}$. When $n_{\min}$ stops increasing with L, the error $[H, \Psi_{n_{\min}}]$, even if small, will be finite. The pairing will

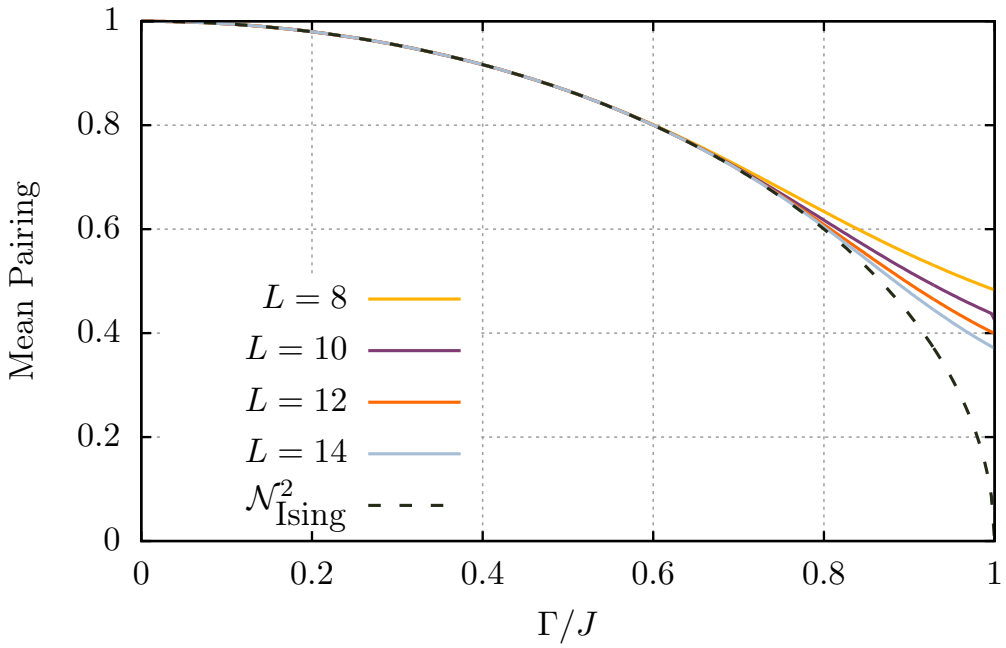

Figure 5.1: The mean of the maximum matrix element $\langle s_+ \,|\, \sigma^z_1 \,|\, s\rangle$ for each eigenstate $|s_+\rangle$ in the even sector, which we call the mean pairing, plotted from exact diagonalisation for transverse-field Ising. As L increases it converges towards the normalisation $\mathcal{N}^2_{\text{Ising}}$, see equation (2.9).

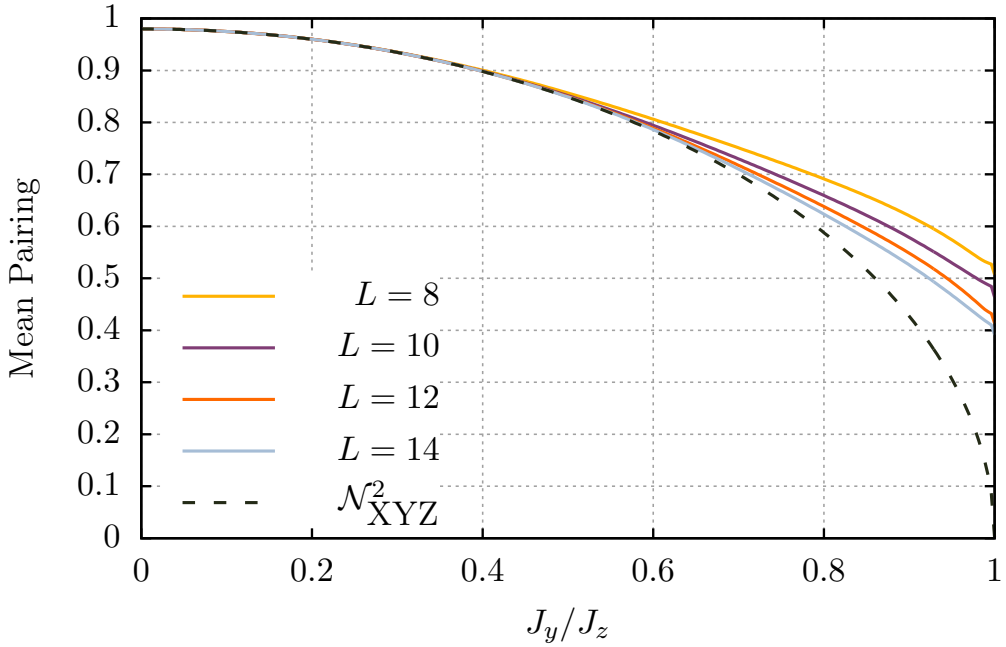

Figure 5.2: The mean of the maximum matrix element $\langle s_+ \,|\, \sigma^z_1 \,|\, s\rangle$ for each eigenstate $|s_+\rangle$ in the even sector, which we call the mean pairing, plotted from exact diagonalisation for the XYZ model with $J_x/J_z = 0.2$. As L increases it converges towards the normalisation $\mathcal{N}^2_{\text{XYZ}}$, see equation (3.2).

then necessarily vanish as L continues to increase, because the state $\Psi_{n_{\min}} |s\rangle$ will have overlap with an exponentially large number of eigenstates.

If we carried through the argument above relating the plateau value to the mean pairing, then the pairing vanishing would seem to imply that the plateau also vanishes as the system size increases. However, from our numerics and analytical work independent of paring in chapter 3, we know that this is not the case. Indeed, in figure 5.3, we plot both $A_\infty(t)$ and the contributions to it coming solely from the eigenstate pairs $|s_+\rangle$ and $|s_-\rangle$ for the Ising model with the interaction Γ_2. We see that for small Γ_2, and therefore $n_{\min}$

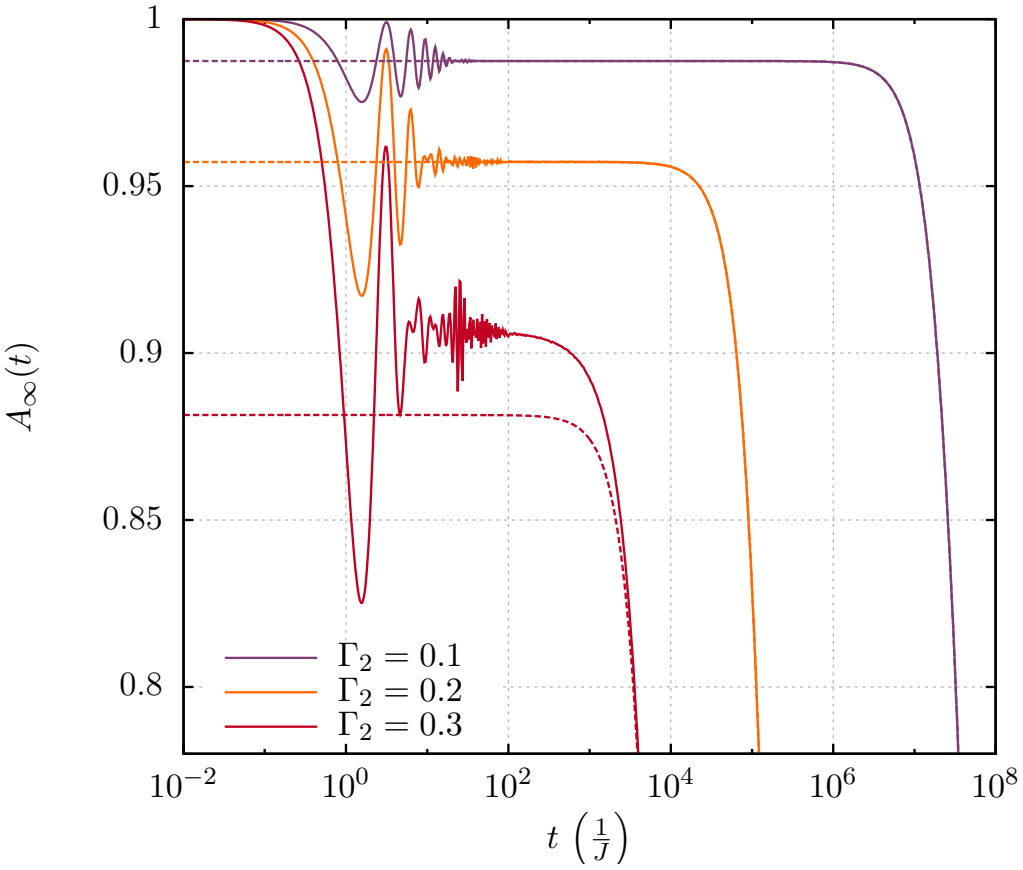

Figure 5.3: A comparison of $A_\infty(t)$ calculated using all contributions (solid line) and only those from paired eigenstates (dashed line) for $L = 14$.

limited by finite size, the two curves agree almost exactly at long times. The long-lived plateau is only made up of contributions from paired eigenstates. Increasing Γ_2 has several effects. It decreases $n_{\min}$, making the ADHH bound on the almost strong zero mode more important that of finite size. Thus it reduces the pairing – and as discussed

above, the greater the system size, the more eigenstates will fall within a given energy range, so the further the pairing will be reduced. It also decreases the normalisation $\mathcal{N}$, and thus the plateau value, in a way that is independent of L. Thus as we increase Γ_2, we should expect to see both the plateau height calculated from all the states and that calculated from just the paired eigenstates to fall, but for the plateau height calculated from the pairs to fall faster. Thus the contributions from the paired eigenstates contribute total a smaller fraction of the autocorrelator as the system size or interaction strength increases. The latter is exactly what we observe in figure 5.3, and I have also checked the former with exact diagonalisation.

Of the two most important consequences of the strong edge zero mode, the long autocorrelation time of the edge spin is thus more robust to the presence of interactions than the twofold degeneracy of all eigenstates. The decay time is reduced as the interaction strength increases, but remains long, albeit not infinite, while the degeneracy immediately breaks. Rather than itself being an eigenstate, the *partner* $|\psi_s\rangle$ for each eigenstate $|s\rangle$

$$|\psi_s\rangle \equiv \Psi_{n_{\min}} |s\rangle \tag{5.3}$$

is a linear combination of eigenstates, none of which have a macroscopic contribution in the thermodynamic limit. Importantly, the expected energy difference between the partner $|\psi_s\rangle$ and eigenstate is finite but small. In particular it is of order n_* in the interaction as it is given by

$$\langle s \,|\, (\Psi_{n_{\min}} H \Psi_{n_{\min}} - H) \,|\, s\rangle = \langle s \,|\, \Psi_{n_{\min}} \Psi_{n_{\min}} H - H + [H, \Psi_{n_{\min}}] \,|\, s\rangle = \langle s \,|\, \mathcal{E}_{n_{\min}} \,|\, s\rangle \,.$$

This bounded difference in energies is what protects the autocorrelation time of the edge spin.

Because $(\Psi_{n_{\min}})^2 \sim \mathbb{1}$, again up to order $n_{\min}$ corrections, $\langle \psi_r \,|\, \psi_s\rangle \sim \delta_{rs}$, so the partners $|\psi_s\rangle$ form a complete linearly independent set of states. We can then fix the argument that led to equation (5.2) relating the normalisation to the plateau value at infinite temperature to work for almost strong zero modes by using these partner states instead of paired eigenstates, by simply replacing one of the paired eigenstates with partner states instead.

We can explicitly treat the autocorrelator in the same manner. Inserting a resolution of the identity through partner states into the expansion for $A_s(t)$, analogously to (5.1), yields

$$\begin{aligned} A_s(t) &\sim \sum_r \langle s \,|\, \sigma_1^z \,|\, \psi_r \rangle \left\langle \psi_r \,\middle|\, e^{-iHt} \sigma_1^z e^{iHt} \,\middle|\, s \right\rangle \\ &\sim \sum_r |\, \langle s \,|\, \sigma_1^z \,|\, \psi_r \rangle \,|^2 e^{i\left(E_s - E_{\psi_r}\right)t} \,. \end{aligned} \tag{5.4}$$

Neglecting the finite error terms means we have neglected energy differences of order $|\mathcal{E}_{n_{\min}}|$, which will appear in the $(E_s - E_{\psi_r})$ factor in the argument of the exponential in equation (5.4). The consequence of using partners rather than paired eigenstates implies a long but not infinite coherence time, exactly as we would expect.

Is there some way in which we can measure the decay time from the properties of the eigenvalues, as we did for the plateau value, rather than directly evolving it in time? Recall from our discussion above that if all the energy differences were the same, the autocorrelator would oscillate rather than decay, as happens in transverse-field Ising to first order in Γ. This illustrates clearly the idea that it is not the energy differences of paired states that cause a decay to zero in $A_\infty(t)$, but rather their *variance*, as it is this variance which drives dephasing. For the almost strong zero mode ideally we would like to measure the partner states $|\psi_s\rangle$. However, this would require constructing the almost strong zero mode numerically. Alternatively, we can use the same method to find the paired eigenstates of the exact strong zero mode, namely finding the maximum matrix element $\langle s' \,|\, \sigma_1^z \,|\, s \rangle$ for each eigenstate $|s\rangle$. This finds the eigenstate with the dominant contribution to the partner state, assuming the normalisation is large enough that $\Psi_{n_{\min}}$ is still the dominant term in σ_1^z. We can then estimate the variance of the energy differences of the partner states to the eigenstates by measuring the variance of the paired eigenstates. We call this quantity the paired energy-difference variance (PEDV).

Formally, we calculate the PEDV with the following steps:

1. For each eigenstate in the even sector $|s_j\rangle$, find its paired eigenstate $|s'_j\rangle$ in the odd sector by maximising the matrix element $\left\langle s'_j \,\middle|\, \sigma_1^z \,\middle|\, s_j \right\rangle$.

2. Calculate the difference between the energy of the two paired eigenstates $\delta_j = E'_j - E_j$.

3. The PEDV is then given by the variance of all the energy differences: PEDV $=$ Var$(\{\delta_j\})$.

As well as indicating how consistently an almost strong zero mode starting with σ_1^z pairs the energy spectrum, the inverse of the PEDV gives an estimate of the timescale on which the decay from the plateau at $\mathcal{N}^2$ occurs at infinite temperature – the less the variance, the less the longer the different terms take to dephase. For an exact strong zero mode, the PEDV thus exponentially decreases with system size with the error of the strong zero mode. We can see this in figure 5.4 for the transverse-field Ising and figure 5.5 for the XYZ model. At $\Gamma = J$ or $J_y = J_z$, when the exact strong zero modes break down, there is a jump in the PEDV, and they saturate in system size. This makes the PEDV a particularly clear indicator of the transition between systems with and without strong zero modes.

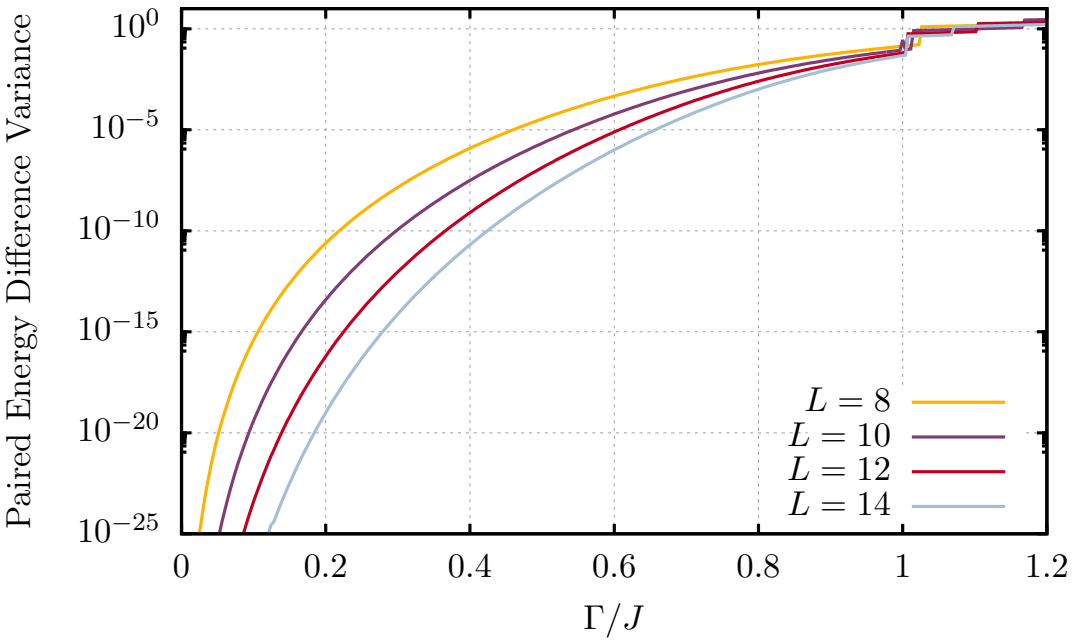

Figure 5.4: The PEDV (see text) from exact diagonalisation for the transverse-field Ising model as Γ is varied. For the regime when the exact strong zero mode exists it decreases exponentially with system size. The PEDV jumps at the transition $\Gamma = J$.

Unlike the mean pairing, the PEDV remains a useful quantity to calculate for the almost strong zero mode, even as we increase the system size. The PEDV does not vanishes for the almost strong zero mode as $L \to \infty$, but rather saturates at a finite, small value. This must be the case else the decay time would be infinite – but crucially also,

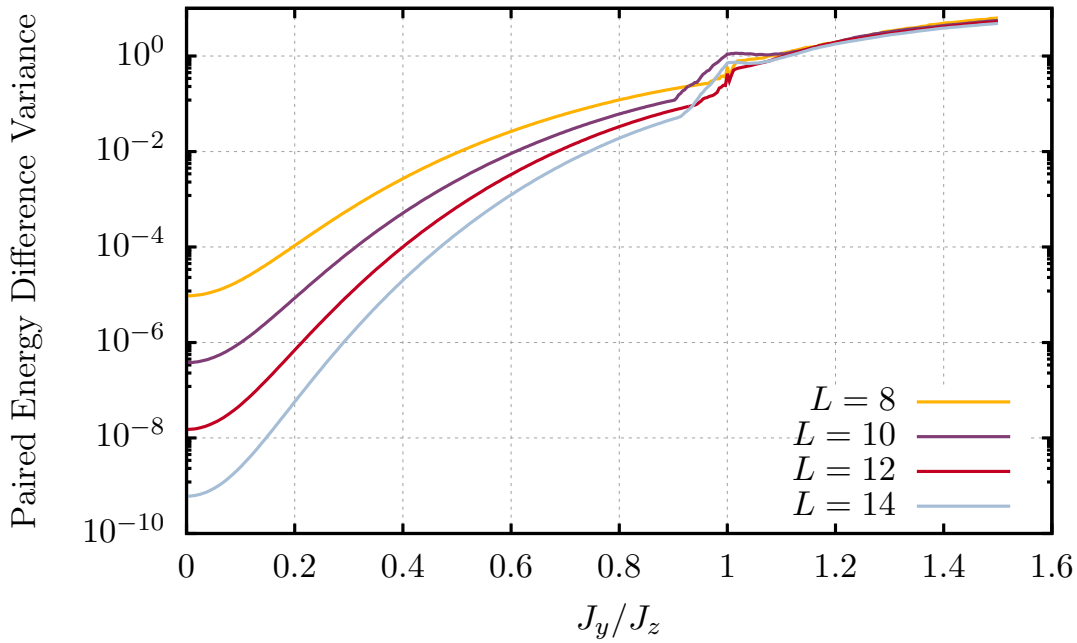

Figure 5.5: The PEDV (see text) from exact diagonalisation for the XYZ model with $J_x/J_z = 0.3$ as J_y is varied. For the regime when the exact strong zero mode exists it decreases exponentially with system size. The PEDV jumps at the transition $J_y = J_z$.

the PEDV does not increase as L increases, so the decay time remains long even in the thermodynamic limit. We see this in figure 5.6 for transverse-field Ising with Γ_2. The PEDV looks like XYZ and Ising for very small $\Gamma = \Gamma_2$, but starts to grow relatively faster with interaction strength for the larger system sizes as the ADHH bound is met. This is visible as kinks in the otherwise smooth curves of the PEDV, and ultimately causes saturation of the PEDV in system size. The jump in the PEDV for all system sizes at $\Gamma \approx 0.4$ is due to the phase transition, as in Ising and XYZ. We have already established this is the regime in which the phase transition occurs in figure 3.8 and associated discussion.

5.2.1 Resonances and Pairing

A resonance can replace the ADHH bound n_* with a much lower n_p. This should of course be immediately visible in the mean pairing, because for a given system size it will increase the spread of eigenstates in the partner state ψ_s. A good way to check this with exact diagonalization is to illustrate this is to choose a value of the interaction for which the almost strong zero mode has not achieved saturation with system size. The

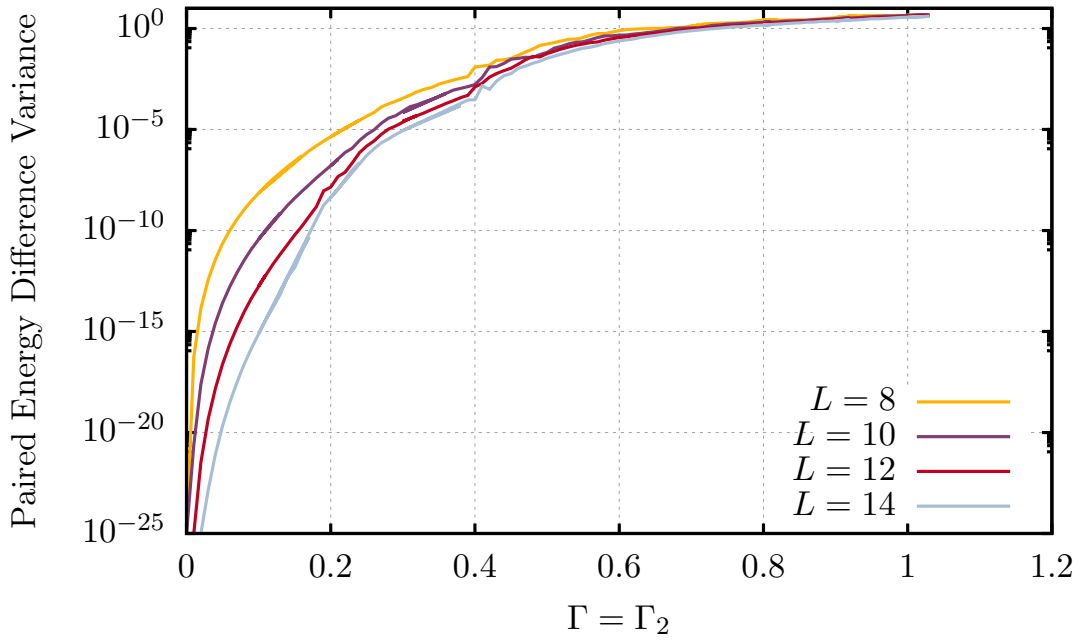

Figure 5.6: The PEDV (see text) from exact diagonalisation for the transverse-field Ising model with interactions as $\Gamma = \Gamma_2$ is varied. For small interaction strengths and system sizes the PEDV behaves like for an exact strong zero, c.f. figure 5.5. At intermediate system sizes the PEDV begins to saturate in system size; for example $L = 12$ to 14 at around $\Gamma = 0.2$. The jump in all system sizes at $\Gamma \approx 0.4$ is due to the phase transition, c.f. figure 3.8.

mean pairing should then be close to unity away from the resonances. In Figure 5.7, this is shown for the small value $\Gamma = 0.05$. The mean pairing away from the resonance is almost perfect. The decrease in pairing for the first-order pole is dramatic, while for the second-order pole the decrease with system size is rather slow. Note that this graph is also symmetric about $J_2 = 0$, indicating that this structure is independent of the different ground-state physics occurring when J_2 is antiferromagnetic, as we would expect.

The PEDV is a much more sensitive probe of the resonances than the pairing, and is plotted for the J_2 large case in Figure 5.8. The peaks in the energy differences measured by the PEDV occur precisely at the couplings with poles in the strong zero mode expansion. Not only are the first- and second-order poles visible but so are the third-order poles at $J = J/3$, $3J/2$ and at the larger system sizes even fourth-order poles at $J_2 = J/4$ and $3J/4$. The higher order the pole the lower the peak, indicating a longer decay time. Notice also the absence of poles at $J = 2J_2$, as we would expect.

If we set $\Gamma = 0$ and turn on Γ_2 as in figure 5.9, the positions and heights of the poles

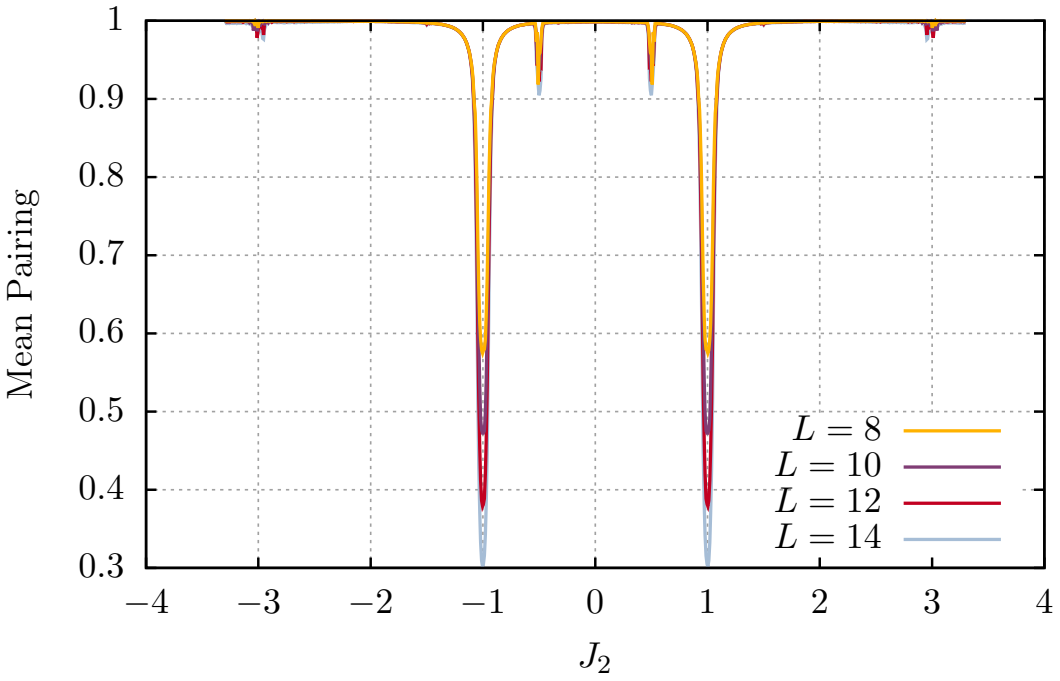

Figure 5.7: The mean of the maximum σ_1^z matrix elements between eigenstate pairs for $\Gamma = 0.05$. The resonances are clearly visible.

change, as the order at which the resonances appear changes. For example, the resonance at $J_2 = J/2$ becomes first order, because the process depicted in equation (3.23) requires only one application of the Γ_2, whereas it needed two with Γ. On the other hand the resonance at $J = J_2$ becomes higher order, because the process equation (3.23) cannot be carried out by flipping exactly two neighbouring spins. If we use both Γ and Γ_2, the order of the resonance is the lowest present in either, so that both $J/2$ and J resonances are first order, as we would expect, see figure 5.10.

Away from the peaks/poles the PEDV exponentially decreases with system size. Notice the log scale on the y axis: this structure in the PEDV traverses almost 30 orders of magnitude! This is the finite-size behavior of an exact strong zero mode, because we have not reached saturaton of the almost strong zero mode. As case without resonances described above, this will ultimately converge in system size even at points without resonances.

On the other hand, close to the poles even at these system sizes the PEDV appears to saturate with L. Importantly, the peaks are *not* increasing in height or width. The

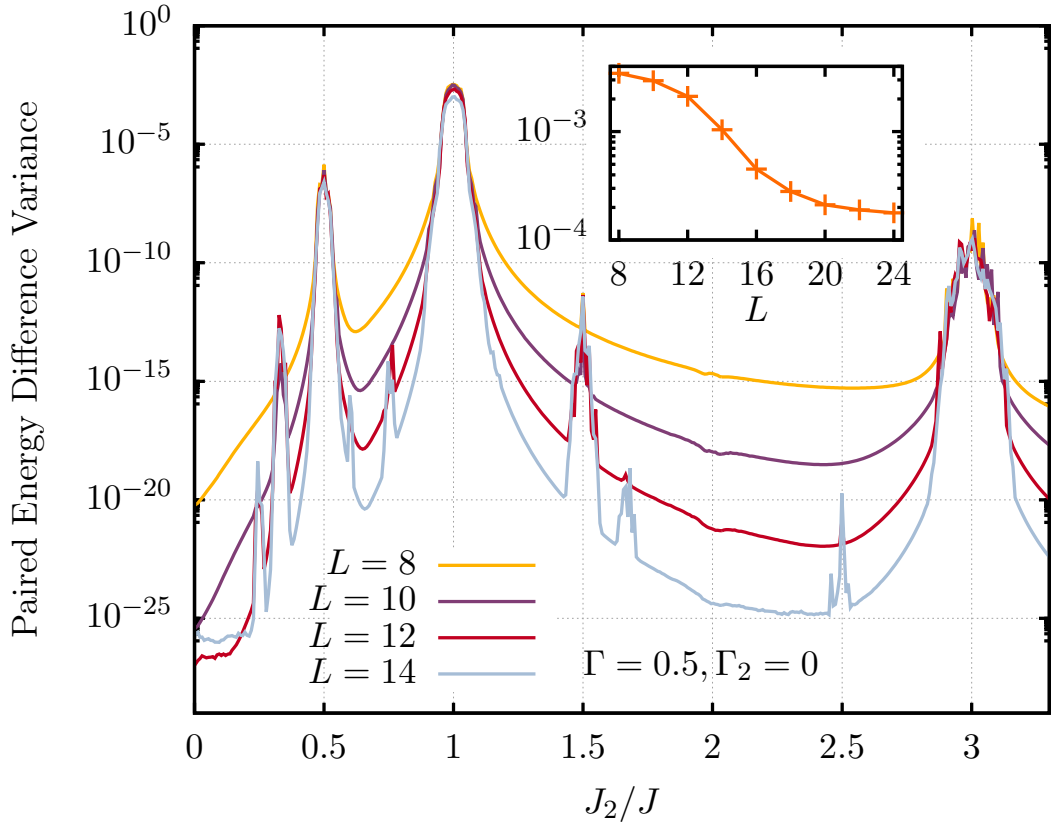

Figure 5.8: The PEDV (see text) calculated for $\Gamma = 0.05$ and $\Gamma = 0$ using exact diagonalisation. Many orders of resonances are visible, even at small system sizes. Inset: The height of the first-order peak in PEDV at $J_2 = J$ plotted against system size. The line is to guide the eye.

width of the peak affects how far away from a pole we must tune the couplings in order to avoid its effect. It is clear from figure 5.8 that the width converges with L – all the curves of different L intersect when they transition from finite-size behaviour (exponentially decreasing with L) to resonant behaviour. Moreover, the width depends on the couplings as

$$\text{width} \sim 2\frac{J_2}{J}\Gamma$$

as is clear from figure 5.11.

This behaviour may be explained heuristically by the following argument. The resonances are caused by easy edge-spin-flip processes that convert between between states with the same potential by exchanging J and J_2 bonds. When we plot the PEDV against J_2, we are implicitly testing edge-spin flip processes where we know the energy of the J_2 bonds we are sending in, but are affected by the energy uncertainty of produced

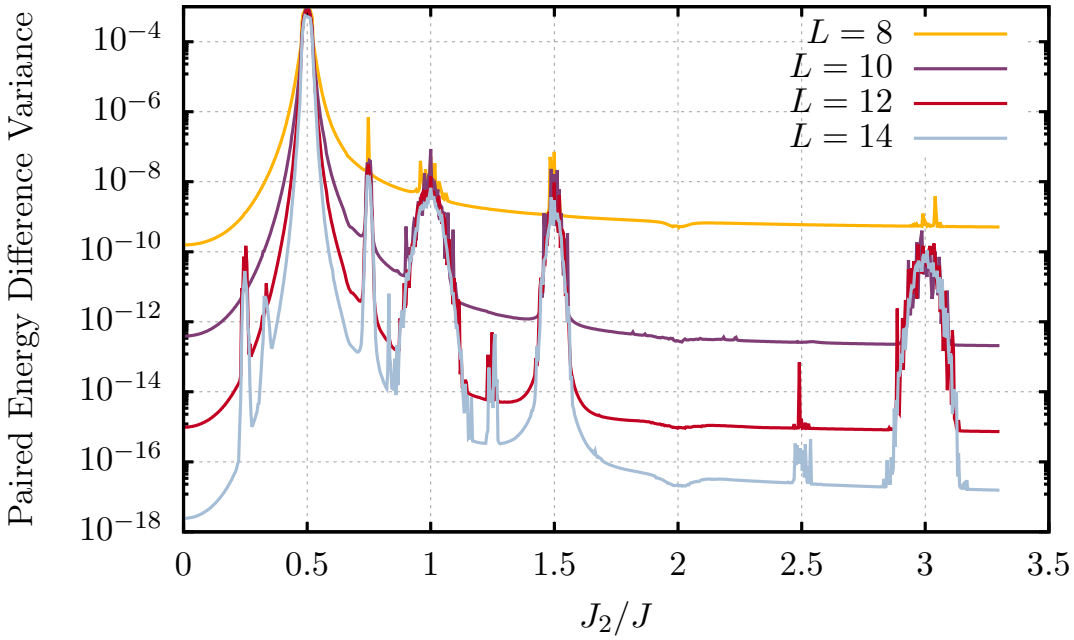

Figure 5.9: The PEDV (see text) calculated for $\Gamma = 0$ and $\Gamma_2 = 0.05$ using exact diagonalisation. Notice that the resonance at $J_2 = J/2$ is now first order, while that at $J_2 = J$ is not.

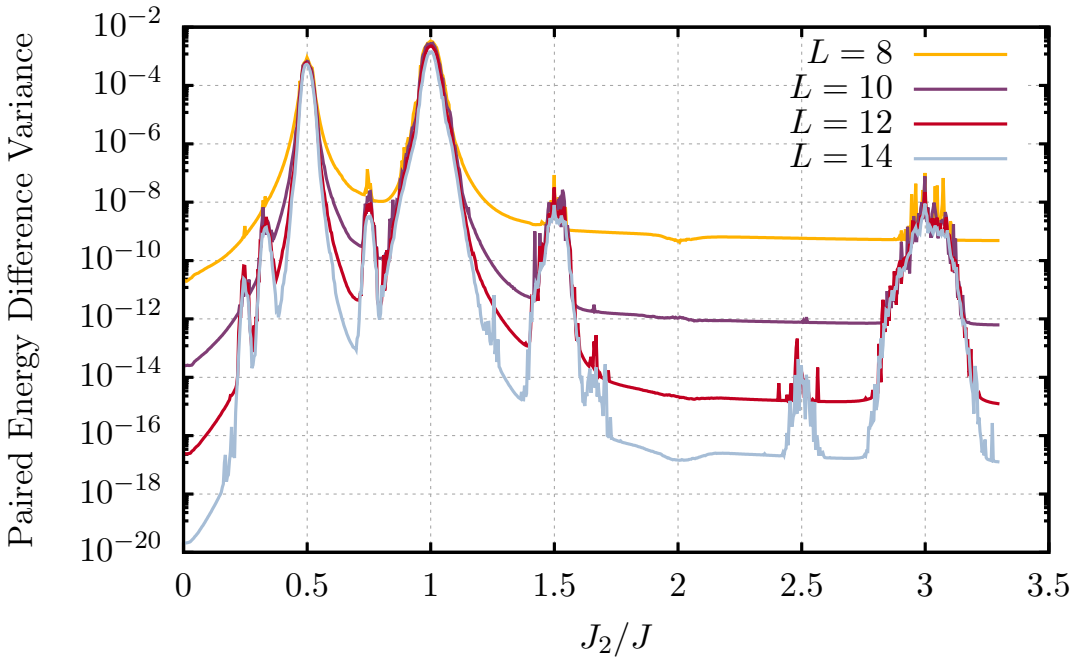

Figure 5.10: The PEDV (see text) calculated for $\Gamma = 0.05$ and $\Gamma_2 = 0.05$ using exact diagonalisation. Both the resonances at $J_2 = J/2$ and $J_2 = J$ are first order.

J bonds. Moreover, for non-zero Γ domain walls have a finite lifetime and therefore an energy uncertainty $\sim \Gamma$. So for example close to the $J_2 = 3J$ pole, the flip converts one J_2 bond to three J bonds, each with associated energy uncertainty Γ. We thus expect the half-width of the pole in J_2 to be 3Γ. Likewise, at $J_2 = J/2$ we convert two J_2 bonds to one J bond, so the half-width is reduced to $\Gamma/2$. In general we thus expect the half-width to be $\Gamma J_2/J$, as the data indicate. At large values of Γ the peaks widen and begin to merge, so the estimate for the width of the PEDV peaks breaks down.

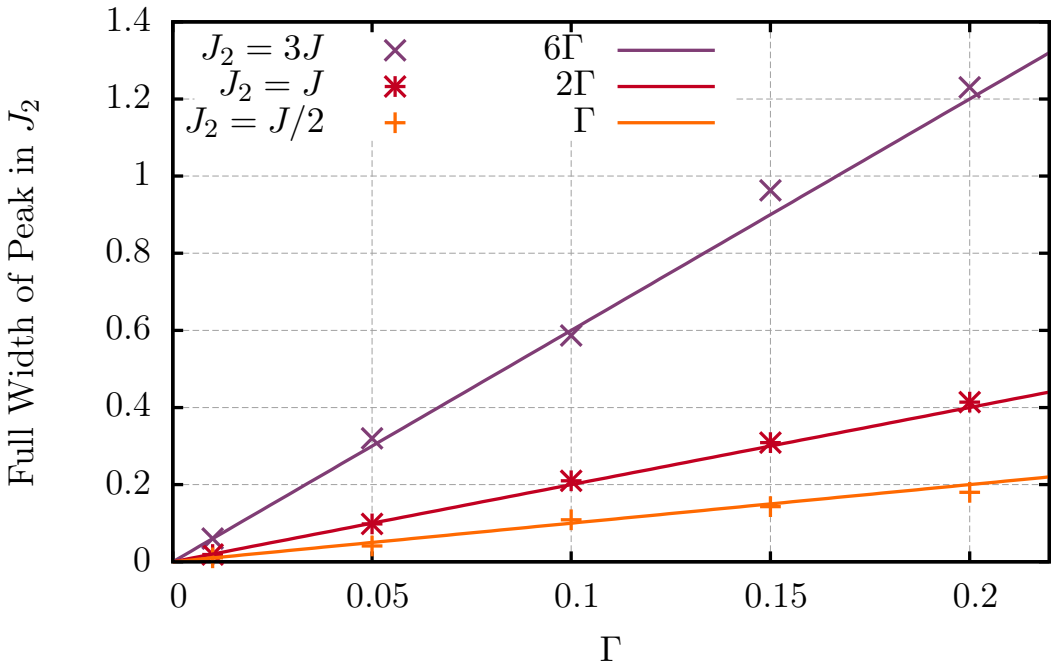

Figure 5.11: The width of the first- and second-order poles in the PEDV as a function of Γ from exact diagonalisation (points) and the theoretical prediction $2\Gamma J_2/J$ (lines).

Another way to test this heuristic argument is to plot the PEDV against J/J_2 and observe if the width changes appropriately for the same poles. This is shown in figure 5.12 where we see that, for example, the pole at $J_2 = 3J$ is correspondingly narrow compared to that in figure 5.12. Figure 5.12 is also a good test of the prediction that there are no resonances at $pJ = J_2$ for even p already examined in figure 3.12, as the PEDV is a cleaner probe than the decay time.

The fact that the PEDV curves for different L intersect suggest that the peak height also saturates with L. A closer look at the first-order pole at $J_2 = J$ in the inset of

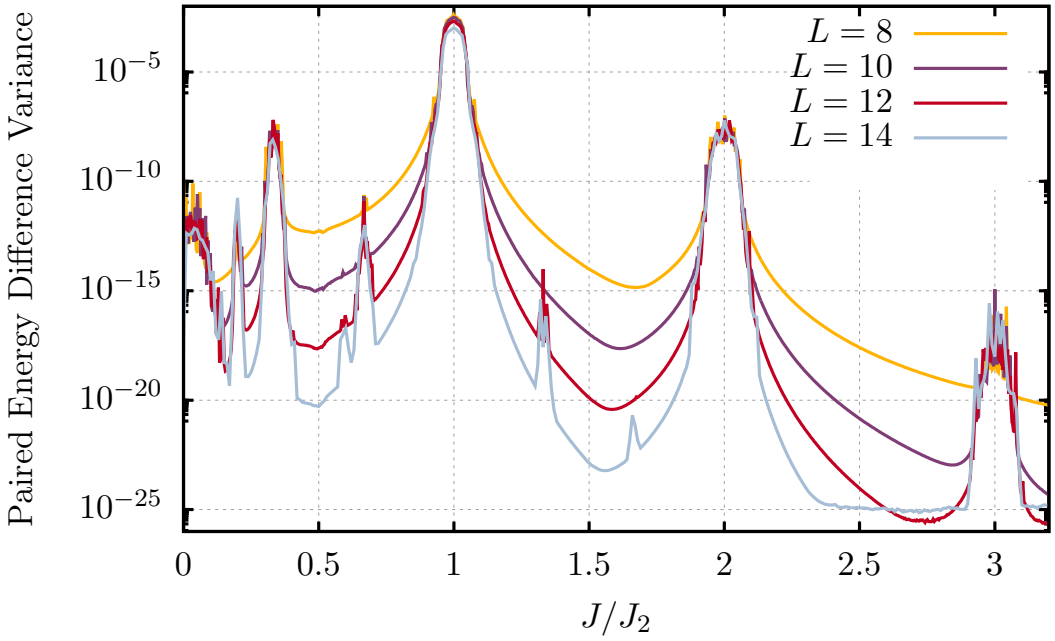

Figure 5.12: The PEDV (see text) calculated for $\Gamma = 0.05$ and $\Gamma = 0$ using exact diagonalisation, plotted against J/J_2 rather than J_2/J in figure 5.8. The width of the poles changes appropriately, and there are no resonances at $pJ = J_2$ for even p. The saturation of the PEDV for $L = 14$ at $J/J_2 > 2.5$ is not physical but rather due to limits in machine precision.

Figure 5.8 reveals the log scale is hiding a substantial (but not exponential) decrease in the peak of the pole with L. However, at larger system sizes, saturation of peak height does appear to occur. This implies that the decay time of the autocorrelation of the edge spin $A_\infty(t)$ will also saturate with L at and near the poles, rather than increasing exponentially (as it would if there were an exact strong zero mode), or decreasing (as it would if there were not even an almost strong zero mode).

The PEDVs here are calculated for small Γ and large J_2, which imply the existence of two very different scales. Widely separated scales can lead to spurious signs of localization in small-size numerics coming from 'minibands', gaps in the density of states, as detailed by Papic *et al.* [48]. Of course, given our relatively small system sizes, we also observe minibands in our numerics. However, there are two points which illustrate we are not merely observing a finite-size phenomenon. Firstly, the ADHH theroem relies on there being two different scales, J and Y, but given their existence, guarantees the long coherence time of the edge spin, *regardless* of the system size. In fact one the system size is much larger than the saturation point, the almost strong zero mode is unaffected

to further changes in system size. Whereas the gaps between minibands filling with states as the system size increased was fatal to Papic *et al.*'s localisation, it is immaterial to the ADHH theorem, which only requires that states with different eigenvalues of $\hat{N}$ are well-separated in energy compared to Y.

Alternatively, even from the system sizes shown and without appealing the ADHH theorem, we can see that the minibands are not responsible for the behaviour observed. The minibands are most prominent when J_2 is a rational (or even more so, an integer) multiple of J, as this reduces the number of minibands possible. On the other hand, the resonances depend strongly on *which* particular rational value. Furthermore, when we replace the Γ term by the Γ_2 term and repeat the calculation, as in figure 5.9 we find the poles change in position and relative magnitude exactly as predicted by the strong zero mode expansion. This behaviour is not explained by any miniband structure, which should not depend on which disordering term is used, but only the magnitude. Even for the rational values which the resonances do occur, they reduce the localisation, rather than increase it.

5.3 Eigenstate phase transitions and disorder

It is well known that at $J = \Gamma$ at $T = 0$ the transverse-field Ising model in one dimension undergoes a quantum phase transition from a long-range ordered ferromagnetic state (assuming $J > 0$) to a paramagnetic state [28]. This transition is marked by a change in properties of the *ground* state: for example, only on the ferromagnetic side of the transition is the $\mathbb{Z}_2$ symmetry spontaneously broken and the ground level twofold degenerate.

On the other hand, from our discussion above, we know that due to the exact strong zero mode that the entire spectrum of the transverse-field Ising model is twofold degenerate when $J < \Gamma$. Thus the phase transition is not just at zero temperature, but at *any* temperature. This is called an eigenstate phase transition [10]. At such transitions, not just the equilibrium properties but also the dynamic properties of the system change in a discontinuous manner. We have already discussed at great length, for example, how the autocorrelation time of the edge spin becomes infinite in the ordered phase, but is finite and small in the paramagnetic regime. Another example would be

McGinley *et al.*'s [27] slow logarithmic growth of the late-time entanglement entropy after a quench from an unentangled initial state in the ordered phase, which would be absent in the paramagnetic phase.

What happens if we turn on interactions, like Γ_2 and J_2? These are irrelevant from the point of view of renormalisation group so do not qualitatively change the ground-state phase transition. However, the exact strong zero mode becomes an almost strong zero mode. In the thermodynamic limit, which we need to consider to treat phase transitions, the pairing, and thus the degeneracy, vanishes. Nevertheless, the effect of adding a small Γ_2 term, for example, is qualitatively different to the transition at $J = \Gamma$. There is no jump in the autocorrelation time of edge spin – it smoothly decreases with Γ_2, remaining large, albeit not infinite. Similarly, although the degeneracy does indeed vanish, we have seen that some of the structure important to the dynamics of the system remains in the partner states which have quantifiably small energy difference from eigenstates in the opposite symmetry sector. Again, there is no such structure in the paramagnetic regime on the other side of the $J = \Gamma$ transverse-field Ising transition. Thus there are no sharp changes in the physical properties of the system, dynamic or equilibrium, as we go from exact to almost to no strong zero mode, in contrast to case where we skip the almost strong zero mode stage and transition directly from an exact strong zero mode to none.

The most famous example of an eigenstate phase transition is the many-body localisation transition [9]. This is the many-body counterpart to Anderson localisation, and occurs in disordered systems. The details are beyond our scope, but the important part for our purposes is that it is possible to show in transverse-field Ising with interactions that with sufficient disorder strength there is a eigenstate phase transition from a system which is thermal at long times, or more technically obeys the so-called 'eigenstate thermalisation hypothesis', to a system in a many-body localised spin-glass phase. In this phase each eigenstate is degenerate with a state in the opposite $\mathbb{Z}_2$ symmetry sector, and there are a macroscopic number of locally conserved quantities [10]. It is natural to assume that one of these is positioned at the edge of the system, and thus from both the pairing and the local conservation we recognise that the exact strong zero mode is restored by many-body localisation.

This leads to the following picture for transverse-field Ising. In the free fermion limit there is an exact strong zero mode in the appropriate parameter regime $\Gamma < J$, but as soon as we add interactions this becomes an almost strong zero mode, and the system thermalises at long times. The long-lived plateau due to the almost strong zero mode is an example of prethermalisation [8, 15]. For strong enough disorder, there is an eigenstate phase transition to an many-body localised spin glass phase and the exact strong zero mode is restored. Thus as we claimed in section 4.3, there is no translational symmetry requirement for the strong zero mode.

For transverse-field Ising without interactions the effect of disorder in either term of the Hamiltonian has a trivial effect on the strong zero mode. This is not surprising because the system remains free, as may be easily observed from a Jordan-Wigner transformation like (2.4), which regardless of disorder remains quadratic. In particular if we allow the constant couplings J and Γ to vary by site, J_i and Γ_i, then the exact strong zero mode becomes

$$\Psi = \mathcal{N}_{\text{Disorder}} \sum_{j=1}^{L} \left(\prod_{k=1}^{j} \frac{\Gamma_i}{J_i} \right) \sigma_j^z \prod_{k=1}^{j-1} \sigma_k^x$$
$$\mathcal{N}_{\text{Disorder}} = \left[1 + \sum_{j=1}^{L} \prod_{k=1}^{j} \left(\frac{\Gamma_i}{J_i} \right)^2 \right]^{-\frac{1}{2}} . \tag{5.5}$$

Of course we can no longer merely require $J > \Gamma$. For an exact strong zero mode to exist the normalisation $\mathcal{N}_{\text{Disorder}}$ must converge. Another necessary condition is that the error vanishes in the thermodynamic limit, which implies

$$\lim_{L\to\infty} \prod_{k=1}^{L} \frac{\Gamma_i}{J_i} \to 0 .$$

If we further require the physically reasonable condition that each J_i and Γ_i are finite and do not vanish, then it is seems likely that these conditions are also sufficient for the exact strong zero mode to exist.

How can disorder aid the strong zero mode? A simple example which illustrates this is in a system with resonances. Suppose, for example, we have $J = J_2$ in our transverse-field Ising model with interactions. This is a first-order resonance, so the edge spin has no enhancement of coherence time compared to the bulk. However, suppose we change the value of the first J_2 bond. Then the resonant process (3.19) cannot flip the

edge spin, and we are pushed away from the pole in the strong zero mode expansion at first order. There will still ultimately be a resonance, but it will be at higher order. This means that the edge spin will have enchancement of decay time versus a bulk spin. Thus disorder at the *edge* of the system can protect the edge zero mode. Of course, it could also introduce resonances, so for strong disorder these must be treated rigorously, as has already been done in the study of many-body localisation [49].

However, in a fully many-body localised system, the edge is no longer special, as the bulk is also localised. In a clean system, if we tried to calculate the explicit strong zero mode expansion starting from a bulk spin, we would fail at first order due to the 'first-order resonance' caused by moving a domain wall across the bulk spin for no cost in energy. If we break the translational symmetry, we disrupt this resonance in much the same way as adding disorder to the edge took us away from the $J = J_2$ resonance. Instead one could continue the 'strong zero mode' expansion starting at the bulk spin to higher orders, although there would be poles in the expansion at the values of the couplings which would restore translational symmetry. This explains why the edge spin is special for clean systems but not for disordered systems from the point of view of the strong zero mode expansion. If one did attempt to use the strong zero mode expansion to perturbatively construct the l-bits via successive local unitary transformations, one would presumably end up with an equivalent construction to that already detailed by Ros *et al.* [50].

Apart from transverse-field Ising, the other model with a proven exact strong zero mode is the XYZ model. It is not as trivial to add disorder to the XYZ model as to the transverse-field Ising model, however, because if we promote J_x, J_y, and J_z to be site-dependent then the system is no longer integrable, unlike Ising which remains free [51]. This means that an exact strong zero mode no longer exists, so that the coherence time is no longer infinite, at least for weak disorder.

One simple way of investigating this is to stagger the couplings. For example, we can take the XXZ model for $J_z > J_x = J_y$, which has an exact strong zero mode, and stagger the XX terms so that the value of the coupling is $J_x + \delta$ starting on even lattice sites and $J_x - \delta$ starting on odd sites. The decay times are shown in figure 5.13. Interestingly we see that for finite sizes non-vanishing δ can actually increase the decay time, although

it appears that the peak is trending closer to $\delta = 0$ as the system size increases. This behaviour is also predicted by the error in the strong zero mode expansion, which has a minimum for non-zero δ which also shifts towards $\delta = 0$ as the truncation order is increased. However, we know that in the thermodynamic limit the autocorrelation time is infinite for $\delta = 0$ and is presumably finite as soon as we turn on δ due to thermalisation. The interesting finite-size phenomenon wherein the decay time increases with δ for small δ could be interpreted physically as greater staggering more strongly inhibiting transport between the two ends of the chain.

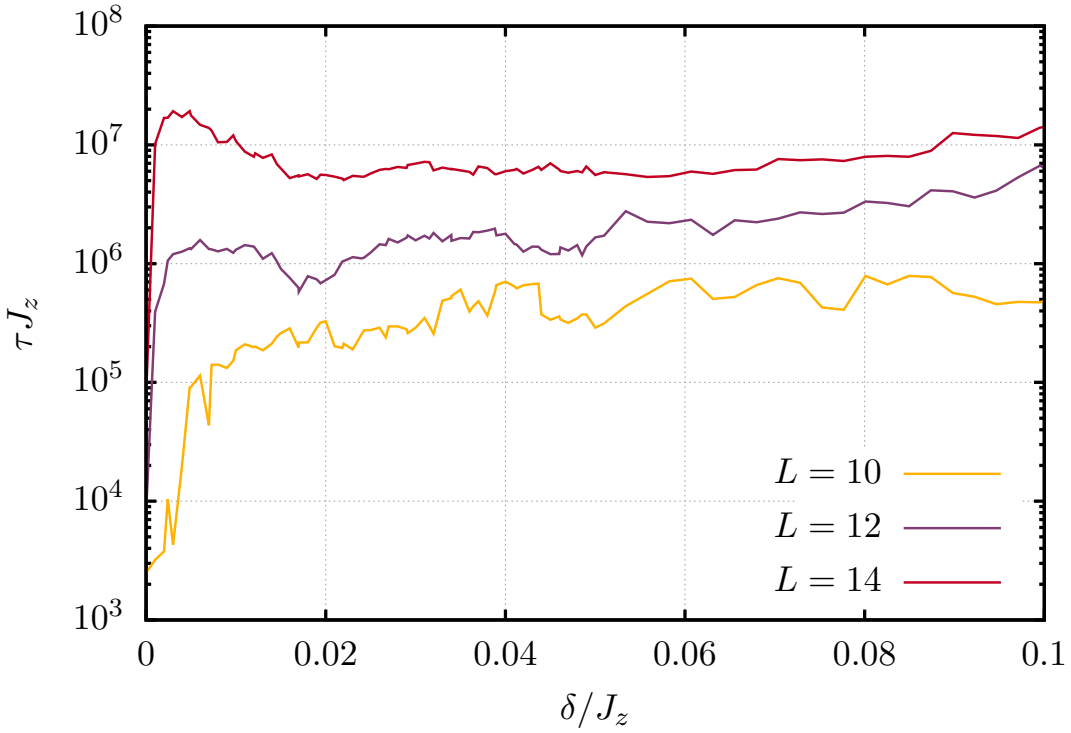

Figure 5.13: The decay time (on a logarithmic scale) of the edge spin at $T = \infty$ for $L = 10 - 14$ sites, as a function of the staggering δ in a staggered XXZ model with $J_x + \delta$ starting on even sites and $J_x - \delta$ starting on odd sites, and $J_x = J_y = 0.25J_z$. Th decay time has a peak at non-vanishing δ, although as the system size increases the position of the peak appears to be trending towards $\delta = 0$. Notice the increase in decay time visible for large δ is less surprising and occurs due to the proximity to the point $\delta = 0.25J_z$ at which the interactions starting at odd sites are cut off completely.

We could increase the period of the staggering to arrive systematically at a disordered XXZ model with no translational symmetry. In this case, because the disorder inherently breaks the integrability, we should expect the same story as for transverse-field Ising

with interactions to apply. Namely, for no disorder, there is an exact strong zero mode, with consequent pairing of the spectrum. For weak disorder, the exact strong zero mode becomes an almost strong zero mode, so the system ultimately thermalises and the pairing goes away. For strong enough disorder, an eigenstate phase transition restores the exact strong zero mode and the pairing between parity eigensectors. The many-body spectrum and phase diagram of the random-bond XXZ spin chain was studied in the context of many-body localisation by Vasseur *et al.* [52], who found a transition to a many-body localised spin-glass phase at strong disorder, suggesting that the exact strong zero mode is indeed restored.

6

Symmetry-protected topological order and qubits

6.1 Classical versus quantum coherence

We need to suppress dephasing in addition to depolarization of the edge spin in order to obtain a quantum coherent edge mode, a qubit; as we discussed in section 2.2 in the context of spins versus Majorana fermions. In particular, we require σ_1^x and σ_1^y to have long autocorrelation times in addtion to σ_1^z, which is not the case for the transverse-field Ising chain of equation (2.2).

This is manifest because the edge magnetisation in the Ising model discussed above is a classical phenomenon – though we have shown it has resistance to depolarisation, we should expect it to dephase quickly with merely local perturbations from the bulk. To rectify this, we construct a model in a SPT phase which has not just a solitary boundary mode but a pair of conjugate operators. This allows us to encode the qubit in non-local topological degrees of freedom, and use the enhanced edge coherence to protect it from both depolarisation and dephasing. Let us define the resulting edge operators as Σ^x, Σ^y and Σ^z. We show in figure 6.1 that the autocorrelation times for all of these operators is exponentially long, in contrast with Ising where only σ_1^z has a long autocorrelation time.

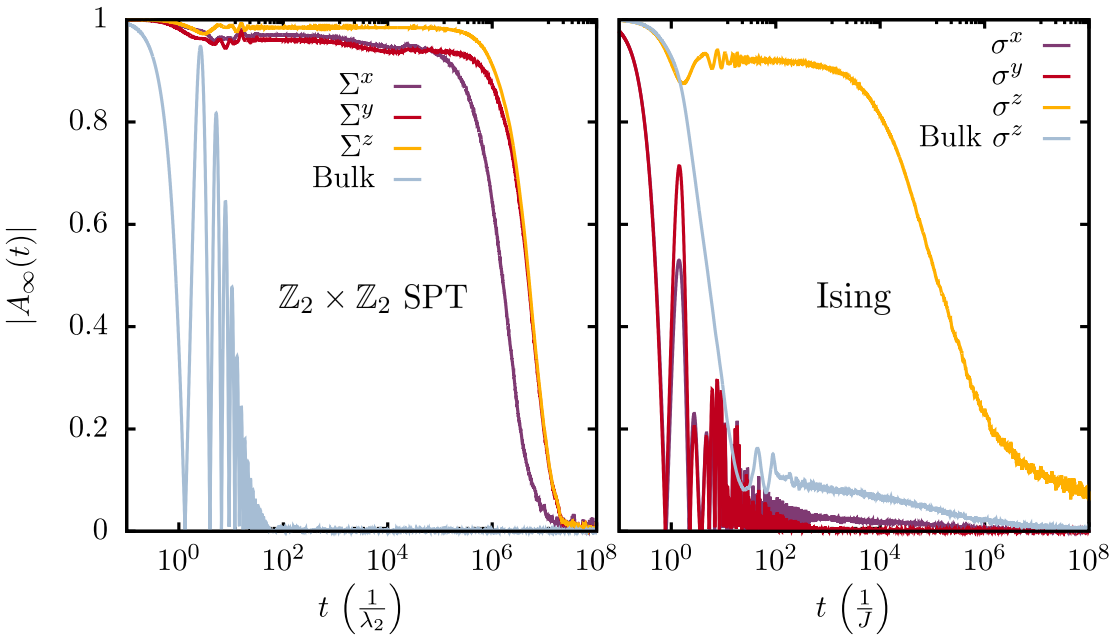

Figure 6.1: The auto-correlator of the edge spin operators at infinite temperature from exact diagonalisation for a ZXZ system of size 14 sites with $\Gamma = \Gamma_2 = 0.05$, $\lambda_2 = 1$, $\lambda_2 = 0.6$, compared with the same for transverse-field Ising with $J_2 = \Gamma = 0.25$.

6.2 The ZXZ Model and conjugate edge modes

In particular, we will consider the following Hamiltonian, on an open one-dimensional chain with $L = 2M$ sites

$$H_{\text{SPT}} = \lambda_1 \sum_{j=1}^{M-1} \sigma_{2j}^z \sigma_{2j+1}^x \sigma_{2j+2}^z + \lambda_2 \sum_{j=1}^{M-2} \sigma_{2j+1}^z \sigma_{2j+2}^x \sigma_{2j+3}^z + \Gamma \sum_{j=1}^{L} \sigma_j^x + \Gamma_2 \sum_{j=1}^{L-1} \sigma_j^x \sigma_{j+1}^x. \tag{6.1}$$

It may be shown that this Hamiltonian is related by a duality transformation to two coupled transverse-field Ising chains on the even and odd sites of the SPT system

$$H'_{\text{SPT}} = \lambda_1 \sum_{j=1}^{M-1} \sigma_{2j}^z \sigma_{2j+2}^z + \Gamma \sum_{j=1}^{L} \sigma_{2j}^x + \lambda_2 \sum_{j=1}^{M-2} \sigma_{2j+1}^z \sigma_{2j+3}^z + \Gamma \sum_{j=1}^{L-1} \sigma_{2j+1}^x + \Gamma_2 \sum_{i=1}^{L-1} \sigma_i^x \sigma_{i+1}^x. \tag{6.2}$$

See the Appendix for full details of this transformation, adapted from previous unpublished work by Laumann for inclusion in [21].

Importantly, note that if λ_1 and λ_2 are the dominant couplings, then the $\mathbb{Z}_2 \times \mathbb{Z}_2$ symmetry-protected Haldane phase transforms under duality to the global $\mathbb{Z}_2$ *symmetry-broken* phase of each Ising chain. As a direct consequence of the protection of the edge spins of these Ising chains, when we transform back under duality, the appropriate correlators of the edge spin of SPT will also be conserved, as given by

$$\begin{aligned} \Sigma^x &= \sigma_1^x \sigma_2^z \\ \Sigma^y &= \sigma_1^y \sigma_2^z \\ \Sigma^z &= \sigma_1^z. \end{aligned} \tag{6.3}$$

We have thus constructed a qubit which survives for exponentially long times, even at infinite temperature.

Unfortunately, as there are more types of bulk excitation in this Hamiltonian than just transverse-field Ising, we must be careful that they cannot dephase or depolarise the boundary qubit. Notice that if $\lambda_1 = \lambda_2$, then, after the duality transformation, the two coupled Ising chains will be symmetric. Let us denote the order parameters of the two chains Φ_1 and Φ_2 respectively. Now, as noted, this model has a $\mathbb{Z}_2 \times \mathbb{Z}_2$ symmetry, which protects the Haldane phase in the original SPT. One of these $\mathbb{Z}_2$ symmetries is Φ_1 to $-\Phi_1$, the other Φ_2 to $-\Phi_2$. However, if $\lambda_1 = \lambda_2$, then there is also an implicit Φ_1 to Φ_2 symmetry.

This symmetry *must* be broken in order for the edge spin to have a long coherence time. To show this, let us move a domain wall next to the edge spin of one of the Ising chains. Then using the Γ_2 term in the Hamiltonian, we may hop this domain wall in one step from one Ising chain to the other, in the process flipping both edge spins. But if $\lambda_1 = \lambda_2$, then there is *no* change in energy between having a domain wall on one chain as opposed to the other. Thus the protection of the edge spin fails at first order in perturbation theory, and it will not have a long coherence time. In fact this is just the first-order resonance already introduced for the equivalent coupled Ising chain model in section 4.3.

The dramatic increase in coherence time away from the symmetric point $\lambda_1 = \lambda_2$ is plotted using exact diagonalisation in Figure 6.2, for the two conjugate edge operators Σ^z, and the edge spin of the other Σ^x. The other salient feature of this figure is the dip in

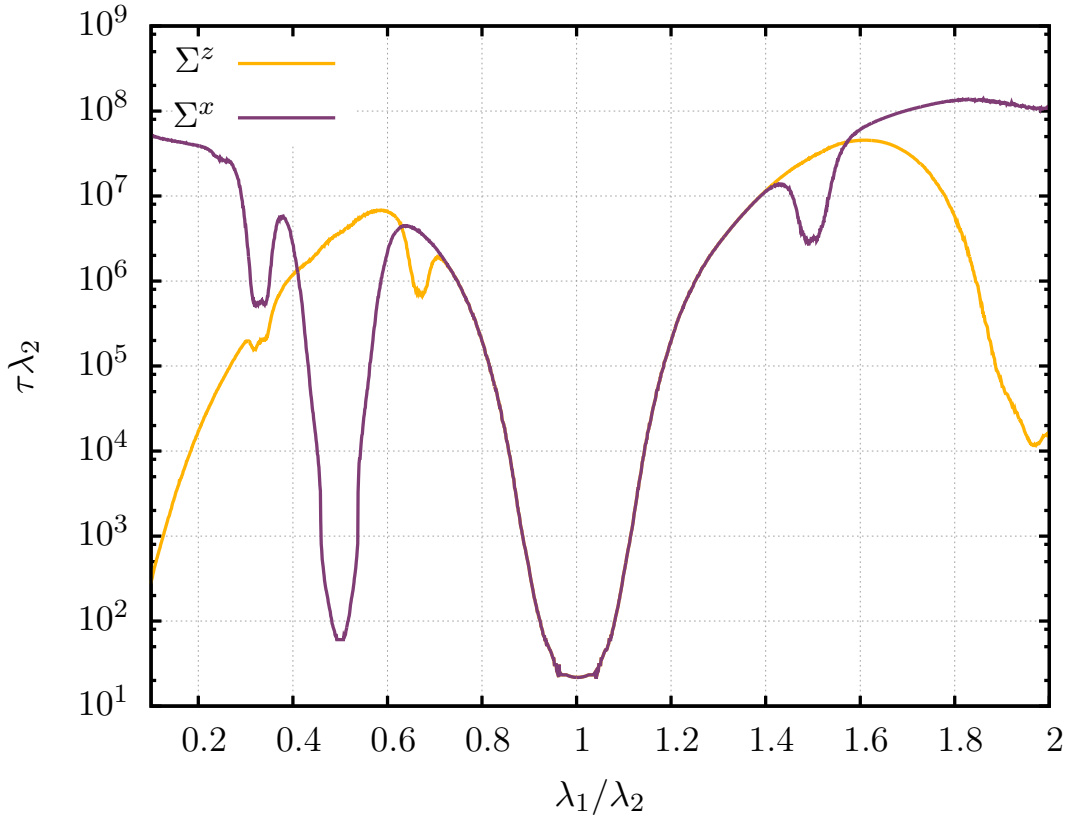

Figure 6.2: The mean lifetime τ of the autocorrelator of the conjugate edge operators Σ^z and Σ^x of the ZXZ model in equation (6.1), calculated using exact diagonalisation at infinite temperature, for a system 14 sites long with $\Gamma = \Gamma_2 = 0.05$.

the coherence time of Σ^x at $\lambda_1 = \lambda_2/2$. This occurs because, in the coupled-chain Ising picture, it is possible to hop a domain wall right on the edge of the second chain into the bulk of the first, creating *two* domain walls, a process which occurs for zero energy change at $\lambda_1 = \lambda_2/2$. This is a second-order resonance. However, if a domain wall is right on the edge of the first chain, its only option is to move to the end of second, so there is no corresponding dip in the coherence time of Σ^z.

For the ZXZ model, we can explicitly construct the two conjugate SZM with the computational method detailed above, starting from zeroth-order terms $\Psi_z^{(0)} = \Sigma^z$ and $\Psi_x^{(0)} = \Sigma^x$. We have explicitly constructed these up to 4th order. We stress that the existence of two such conjugate SZM is non-trivial and does not occur, for example, in

transverse-field Ising. For example, the explicit first-order terms are

$$\Psi_z^{(1)} = \frac{\Gamma}{\lambda_1}\sigma_1^x\sigma_2^x\sigma_3^z + \frac{\Gamma_2}{\lambda_1^2-\lambda_2^2}(\lambda_1\sigma_1^x\sigma_3^z + \lambda_2\sigma_1^y\sigma_2^y\sigma_3^x\sigma_4^z) \tag{6.4}$$

$$\begin{aligned}\Psi_x^{(1)} =& \frac{\Gamma}{\lambda_2}\sigma_1^x\sigma_2^x\sigma_3^x\sigma_4^z - \frac{\Gamma_2}{\lambda_1^2-\lambda_2^2}(\lambda_2\sigma_2^x\sigma_3^x\sigma_4^z + \lambda_1\sigma_1^z\sigma_2^z\sigma_3^z) \\ &+ \frac{\Gamma_2\lambda_1}{4\lambda_1^2-\lambda_2^2}\left(\sigma_1^y\sigma_2^z\sigma_3^y + (2\frac{\lambda_1}{\lambda_2} - \frac{\lambda_2}{\lambda_1})\sigma_1^x\sigma_2^x\sigma_4^z - \sigma_1^x\sigma_2^y\sigma_3^y\sigma_4^x\sigma_5^z - 2\frac{\lambda_1}{\lambda_2}\sigma_1^y\sigma_4^y\sigma_5^z\right)\end{aligned} \tag{6.5}$$

It is manifest from these expressions that at $|\lambda_1| = |\lambda_2|$ the perturbation theory breaks down even at first order, explaining the short coherence time at this point. Furthermore, one can read off the domain-wall emission processes which cause this breakdown from the Pauli matrices in the resonant terms. The resonance at $2|\lambda_1| = |\lambda_2|$ is also apparent in $\Psi_x^{(1)}$ but not in $\Psi_z^{(1)}$, as we would expect from the discussion above. At second order in the expansion, further poles at $|\lambda_1|/|\lambda_2| = 1/3, 2$ for Σ^z also appear, and at $1/3, 3/2$ for Σ^x, the effects of some of which are visible in Figure 6.2. The dip at $2/3$ is in fact due to a third order pole.

More generally, we can use the same sorts of argument as in section 3.3.2 to discern when each edge operator has a resonance. Suppose $\lambda_2/\lambda_1 = p/q$ for integers without common prime factors p and q – this ensures that the total $\hat{N}$ of the two chains has integer eigenvalues. Recall that there is a resonance if the change in energy of the unperturbed Hamiltonian due to flipping an edge spin can be matched by flipping bulk spins. For the ladder we have two edge spins, so we have the additional option of flipping the other edge spin to make the change in energy vanish. Following our previous notation, let us denote the change in energy due to flipping a spin at site j while the system is in configuration s as $2\lambda_1\Delta_j(s)/q$. Then $\Delta_1(s) = \pm q$ and $\Delta_2(s) = \pm p$, while flipping bulk spins results in a change equal to an arbitrary linear combination of $2p$ and $2q$, which has even parity. Thus if either p or q is even, the corresponding conjugate edge operator Σ^x or Σ^z will have a resonance. The other edge operator will not have a resonance at that point, because by construction if one of p or q is even the other must be odd. On the other hand, if both p and q are odd, their linear combination is even. This means that both edge operators suffer from a resonance at the same order when p and q are odd.

This unfortunately means there are no resonance-free values for both conjugate edge operators. Nevertheless, we can still choose values of λ_1 and λ_2 for which the resonances only occur at high orders in perturbation theory, which means we can still significantly enhance the coherence time, as can be seen from the numerics.

Just as with the single strong edge zero mode picture, the long coherence times of the conjugate edge operators Σ^α can be understood by their large overlap with their respective almost strong zero modes Ψ^α. The fact that the edge spin is not the almost strong zero mode itself explains the fast decay of $A^\alpha_\infty(t)$ in Figure 6.1 to a plateau $A^\alpha_\infty\big|_{\text{plateau}}$ less than one, on a timescale orders of magnitude less than its ultimate decay to zero. At infinite temperature, the plateau height can then be quantitatively predicted by

$$A^\alpha_\infty\big|_{\text{plateau}} = \frac{1}{2^L}\mathrm{Tr}(\Sigma^\alpha\Psi^\alpha)^2,$$

see the discussion in section 5.1. From our 4th order expressions, we find the plateau should be at $A^x_\infty\big|_{\text{plateau}} = 0.971$ and $A^z_\infty\big|_{\text{plateau}} = 0.985$, in good agreement with the values found from exact diagonalisation shown in Figure 6.1.

7 Experimental tests

7.1 Trapped ion chains

A possible experimental realization would be a trapped ion or neutral atom chain governed by a perturbed transverse-field Ising model [53, 54]. For example, in Ref. [55], the authors use chains of up to 22 $^{171}\mathrm{Yb}^{+}$ ions in linear radiofrequency (Paul) traps, encoding effective two-state systems in their $^{2}\mathrm{S}_{1/2}$ hyperfine ground states. Long-range spin-spin interactions are generated using laser-mediated spin-phonon interactions. In particular, using the beatnote between two overlapped laser beams to drive stimulated Raman transitions, they generate the effective Hamiltonian

$$\hat{H} = \sum_{i<j} J_{i,j}\sigma_i^z\sigma_j^z + B\sum_i \sigma_i^x \ , \tag{7.1}$$

where interaction is long-ranged and antiferromagnetic

$$J_{i,j} = \frac{J_I}{|i-j|^{\alpha}} \ . \tag{7.2}$$

with $J_I > 0$. For nearest-neighbor interactions in Ising, ferromagnet and antiferromagnet are unitarily equivalent. Here the distinction is important, because the ferromagnet has a phase with long-ranged order for $\alpha < 2$ and non-zero temperatures less than some critical temperature T_c,[56] while the antiferromagnet does not have such an ordered phase for $T > 0$, like the nearest-neighbor model [57]. Consequently, for initial states that are

near the *top* of the spectrum here, the end and bulk spin lifetimes will be infinite since these are low-energy state of the ferromagnetic Hamiltonian $-H$.

In the setup of Ref. [55], the experimentally realizable range of α is $0.5 < \alpha < 2$, while $J_I/2\pi \leq 1$kHz, achieved by changing the trap voltages and the detuning of the beatnote from resonance. The B term is generated by driving further resonant stimulated Raman transitions out of phase with the beatnote. It can range from negligible to a maximum of $B/2\pi = 10$kHz. So it should certainly be feasible to enter the regime $B \ll J_I$ in which the almost strong zero mode is significant.

The autocorrelators of individual spins $\langle \sigma_j^z(t)\sigma_j^z(0)\rangle$ may be measured up to times of order $100/J_I$. Thus, it should be possible to observe the protection of the edge spin through the survival of its autocorrelator, in contrast with the bulk spins, which would decay over experimentally accessible timescales. The one caveat is that, although the edge spin will be long-lived for any system temperature or any energy initial state, for very high-energy initial states near the top of the spectrum, or for negative temperatures, the protection comes from the long-ranged ferromagnetic order when $\alpha < 2$, rather than the almost strong zero mode. This case is easily distinguishable because the bulk spins will also be long-lived.

Simulations with ED at infinite temperature on similar system sizes confirm this picture, at least for $\alpha \gtrsim 1.25$, see Fig. 7.1. The main theoretical concern for the almost strong zero mode is the long-ranged nature of the interaction, because for the ADHH theorem to hold we require small J_0/J. In fact, as we discussed in section 4.4, the ADHH theorem has not yet been proven for power-law decay interactions. As long as $\alpha > 1$, however, the updated Lieb-Robinson bounds due to Else *et al.* [47] should apply. This cutoff agrees well with the value of α at which we start to see the strong edge zero mode fail in the numerics.

To gain some intuition, let us suppose $\hat{N}$ consists of just the nearest-neighbor interaction magnitude J_I. Then for $\alpha = 2$, the shortest-possible range in the experiments, the next-largest term is a quarter of the size, so we might be justified in putting it and longer-range terms in $\hat{Y}$. However, for smaller α we should include at least the next-nearest-neighbor term in $\hat{N}$ as well. We then have to deal with the possibilties

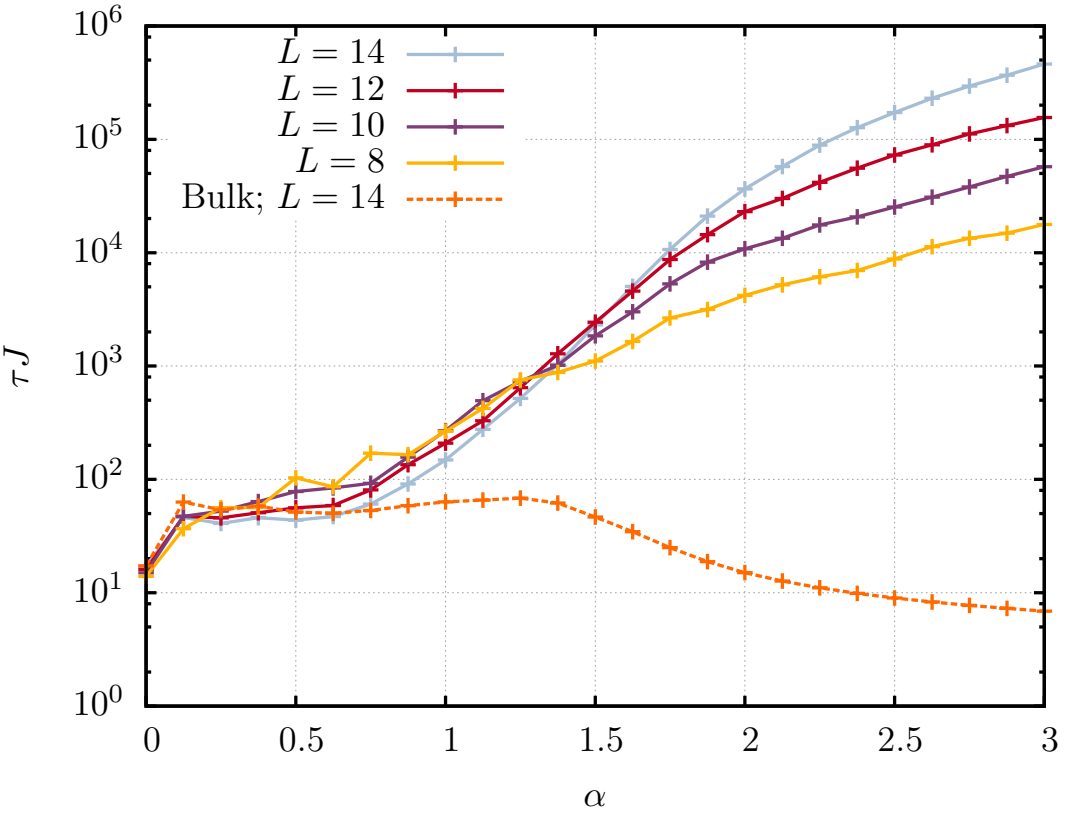

Figure 7.1: The decay time (on a logarithmic scale) of an MZM in the transverse-field Ising model with long-ranged interactions at $T = \infty$ for $L = 8 - 14$ sites and $h = 0.2$, as obtained by exact diagonalization. It is plotted as a function of α, the power of the decay of the long-ranged interaction. The lines are to guide the eye. The decay times for ferromagnetic and antiferromagnetic interactions are the same at $T = \infty$; it is only at lower temperatures where the effect of the long-ranged order for $\alpha < 2$ in the ferromagnetic case becomes important.

of resonances as dicussed above. Crucially, for there to be any chance for the ADHH theorem to hold, $\hat{N}$ must have integer eigenvalues, which is of course impossible to tune exactly experimentally for more than one coupling. However, for the system sizes $L \leq 22$ which are experimentally accessible, we do not expect this to be of practical issue in observing the protection of the edge spin in contrast to the bulk, and indeed the results from exact diagonalisation support this.

Of course, once $\alpha < 1$, the arguments above based on locality break down completely. The two ends of the chain come into contact, so that terms which flip the edge spin may be immediately added to $\hat{D}$, and the edge spin will no longer be protected. It is also worth noting that the smaller α, the less localised at the edge the zero mode is, and so the greater overlap it has with the bulk spins. This means that there may be some small

but observable part of the correlator of spins near the edge which survives to long times, albeit exponentially suppressed in magnitude compared to the edge, c.f. figure 4.10.

7.2 Other experimental realisations

For completeness' sake, we briefly describe two other experimental tests that have been proposed in the literature.

Given that it could be used to construct a qubit enjoying edge protection, it would be ideal if there were a possible experimental realisation for the ZXZ model of equation (6.2) in its SPT phase. There has been a proposal to construct such a model experimentally by exploiting the fact it appears as an effective time-independent Hamiltonian of a transverse-field Ising chain driven periodically at high driving frequencies [58], in the context of using many-body localisation to stabilise the edge modes. This driven Ising chain can in turn be simulated by a chain of Rydberg-dressed alkali-metal atoms in a 1D optical lattice. However, the stability of such effective time-independent Hamiltonians was in fact exactly what ADHH set out to prove with their theorem [17] – the time-independent result was in fact simply a corollary – and it is not yet clear how the two bounds interact. In addition, the first-order corrections to the effective Hamiltonian break the $\mathbb{Z}_2 \times \mathbb{Z}_2$ symmetry. More research is required to understand if such a setup could be used to probe the almsot strong zero mode.

In this thesis we have focussed on spin chains. Of course, as was detailed in section 2.2, these are equivalent by Jordan-Wigner transformation to fermionic systems. The long coherence time of the edge spin becomes the long coherence time of the unpaired Majorana fermions at the end of the chains [12]. It should be mentioned that Chetan Nayak has proposed in [20] a possible experimental test of the almost strong zero mode using quantum dot chains [59]. He finds a parameter regime in which the decay of the Majorana zero mode would naively be dominated by electron-electron interactions rather than electron-phonon interactions at finite temperature, and should therefore benefit greatly from the long edge coherence time due to the almost strong zero mode described in this thesis.

8
Conclusion

In summary, the main outcome of this thesis has been show to that coherence time of the edge spin in one-dimensional spin chains can be greatly enhanced compared to the bulk, even in interacting, non-integrable systems at infinite temperature, due to the presence of the almost strong zero mode. We have proved the existence of the almost strong zero mode given certain conditions on the Hamiltonian, which we will discuss further below, and placed a lower bound on its lifetime using the ADHH theorem. We explicitly constructed the almost strong zero mode up to 11^{th} order in perturbation theory with the aid of computer aided algebra. We have examined the parameter regime in which the almost strong zero mode exists, as well as the special 'resonant' couplings where it fails at lower order in perturbation theory than we would expect from the ADHH theorem. The current state of the art results for the existence of exact and almost strong zero modes is summarised in table 8.1. The physical consequences of both exact and almost strong edge zero modes were explored and contrasted – in particular the aforementioned long coherence time of the edge spin at infinite temperature. This is infinite for exact strong zero modes, but saturates in system size for almost strong zero modes at a finite time exponentially long in the small integrability breaking coupling. We explained how this saturation was related to the truncation of the strong zero mode expansion as an asymptotic series for almost strong zero modes, and how the expansion could be used calculate other observable quantities, such as the plateau height of the autocorrelator of the edge spin.

Systems	Strong Zero Mode	Status
Transverse-field Ising chain	Exact	Proven
XYZ spin chain	Exact	Proven
Integrable, without resonances	Exact	Conjecture
System with resonances	Almost/None if resonance is first order	Proven
Non-integrable	Almost	Proven
Long-ranged interactions	Almost, with modified ADHH theorem	Conjecture
ADHH not applicable	None	Conjecture

Table 8.1: A table detailing the proven or conjectured existence of the exact and almost strong zero modes in certain systems covered in this thesis. For all the entries except the last two we assume the ADHH theorem is applicable: that is, the system only has interactions with finite support and the unperturbed Hamiltonian has an integer spectrum.

We considered the effects of finite size, boundary conditions, and finite temperature on the almost strong zero mode in considerably more detail than in our paper [20], although we were limited in confirming definitive statements about intermediate temperatures – greater than the gap but not infinite – by the limited system size of our numerics. We showed numerically that the autocorrelation at late times for spins decayed exponentially the further removed they were from the edge, confirming the significance of the edge spin. We also demonstrated that adding further terms of the strong zero mode expansion increased the autocorrelator plateau height, but as expected did not increase the ultimate decay time.

We have also considered the effect of both exact and almost strong zero modes on the eigenstate spectrum. The degeneracy between eigenstates in even and odd sectors for the entire spectrum has of course been well-documented before [22], but we have shown how the long coherence time of the edge spin is related to this pairing. We also described how the normalisation of the edge spin can be used to calculate the mean of the matrix elements of the edge spin between paired eigenstates. For almost strong zero modes, we described how this mean pairing starts to go away at the same system sizes as the decay time of the autocorrelator saturates, but introduced another measure, the paired energy difference variance, to allow us to analyse the behaviour of the almost strong zero mode using the matrix elements of the edge spin in the eigenstate basis. We used the PEDV to study numerically the effects and positions of resonances in particular, in greater detail than would have been possible with the coherence time alone. We discussed

how the eigenstate phase transition when the system loses an exact strong zero mode becomes a smooth crossover once integrability was broken and the exact strong zero mode became an almost strong zero mode, and we described the effect of disorder on the strong zero mode and its relation to many-body localisation.

Turning to possible practical applications, we introduced the ZXZ model with a $\mathbb{Z}_2 \times \mathbb{Z}_2$ SPT phase and a unitary transform to a system of coupled transverse-field Ising chains in the their symmetry-broken phases. This system had a two conjugate edge modes which could be used to construct a qubit. Thus we promoted the classical edge coherence enhancement to a truly quantum phenomenon. We proposed an experimental test for the almost strong zero mode in trapped ion chains simulating a long-ranged transverse-field Ising model, feasible to implement with current technology. We also proposed a possibility for an experimental test for the almost strong zero mode in the ZXZ model using Rydberg-blockaded chains, although more research needs to be done to establish if signatures of almost strong zero mode would be observable.

We also started to consider which classes of systems can support strong zero modes. We argued that only integrable systems can support exacts strong zero modes – we will now discuss further lines of research into the possible deep connection between strong zero modes and integrability below. Because the Hamiltonian must have integer eigenvalues, we ruled out gapless systems. We also showed that too much symmetry can be fatal for the almost strong zero mode due to resonances, giving the chiral Potts model and coupled transverse-field Ising chains as examples. We argued that a small longitudinal magnetic field would not immediately destroy the almost strong zero mode, but more numerical research is needed to confirm this. In the final section of the thesis, we will discuss future avenues of research inspired by the work in this thesis, in large part looking to extend the types of systems in which we can prove exact or almost strong zero modes exist.

8.1 Further avenues of research

The first obvious generalisation is to consider systems in two dimensions or greater. We have already mentioned in the introduction that Else [20] considered almost strong edge zero modes in a toric code with open boundaries, while Vasiloiu [25] *et al.* studied

strong zero modes in a class of generalised Ising spin ladders with plaquette interactions. However, in both these cases the strong zero modes comprised the entire one-dimensional edge of a two-dimensional system. Thus they are still pseudo-one-dimensional, in the sense that the 'bulk' remains only one dimension larger than the 'edge'. One possible extension would therefore be to consider strong zero modes localised at the corners of system in two dimensions or higher. An inherent difficulty for finding such modes is avoiding resonances, which have the potential to proliferate exponentially as we increase the dimension, if we do not also incorporate disorder or ansiotropy, as we discussed for the transverse-field Ising ladder in section 4.3.

The original proof of the ADHH theorem [17] is applicable to higher dimensions – the difficulty for finding strong edge zero modes is in connecting tying the ADHH theorem to the conservation of an operator localised on the edge, rather than in applying the theorem itself. By contrast, the proof places strict bounds on the range of the terms in the operator $\hat{N}$, forcing them to be single site. This was relaxed to operators with finite support in Appendix A of reference [20]. Nevertheless, updating the theorem using the new Lieb-Robinson bounds for long-range interactions [46, 47] would provide a formal bound for the work in the thesis on almost strong zero modes and in particular the experimental test in trapped ion chains.

The original proof of the ADHH theorem also assumes that the Hamiltonian is Hermitian. Vasiloiu [26] *et al.* have studied the effects of adding dissipation to the strong zero modes in transverse-field Ising and the XYZ spin chain. These are systems with exact strong zero modes. They found that the coherence time remained long, although the oscillations in the transverse-field Ising model were replaced by a decay to zero, exactly as for the cases we have studied in this thesis when adding interactions rather than dissipation. They also showed that even and odd eigenspectrum of the Lindblad operator were paired by strong zero mode, which is itself promoted to a map acting on operators rather than vectors in the dissipative case. It would therefore be interesting to observe the effects of dissipation on a system supporting only an almost strong zero mode. Presumably as itself an integrability-breaking perturbation, the dissipation would act to reduce the saturated coherence time. The pairing in the Lindblad operator should

also ultimately disappear with system size, as we showed for Hermitian Hamiltonians. Generalising the ADHH theorem to non-Hermitian Hamiltonians would be one method to approach this problem formally.

On the subject of non-equilibrium physics, inspired by our papers [19, 20], Yates *et al.* [60] have found an almost strong edge zero mode in a periodically-driven, one-dimensional 'Floquet' system without disorder. They showed that the edge mode persisted for times much longer than the time taken for the bulk of the system to heat up to infinite temperature. Note that the ADHH theorem [17] was originally developed to show that clean, interacting Floquet systems are governed by an effective time-independent Hamiltonian up to times (quasi-)exponentially long in the driving frequency. This frequency is equivalent to the ratio J/J_0 for the time-independent version of the ADHH theorem which has been central to this thesis. Interestingly, Yates *et al.*'s work is carried out far from this high-frequency regime due to system size limitations. In order to provide a complete understanding of almost strong zero modes in Floquet systems and their relation to those in time-independent systems it would be extremely interesting to extend Yates *et al.*'s work into this high frequency regime.

We have discussed increasing the spatial dimension, but we can of course also increase the dimension of the Hilbert space on each lattice site. For the majority of this thesis we have considered spin-half chains. The sole exception to this has been the chiral Potts chain in section 4.3. Recall that this is equivalent to a one-dimensional chain of parafermions, in the same way as the transverse-field Ising model may be transformed into the Kitaev chain under a Jordan-Wigner transformation [22]. We discussed the resonance structure of the strong zero mode in chiral Potts chain in detail, and pointed out that in the parameter regime in which it is integrable, we might expect the strong zero mode to be exact. There is currently no proof of this, but the method which ultimately proved the existence of the exact strong zero mode in the XYZ chain, which we will discuss below, may well be a promising method for solving this problem also.

More generally, Munk *et al.* [61] considered extending the $\mathbb{Z}_2$ symmetry of the Ising model or $\mathbb{Z}_Q$ symmetry of the chiral Potts model to arbitrary discrete group G, which could be non-Abelian. They did this by defining a set of ladder models of gauge

fluxes that included the Ising and Potts as special cases. Under a generalised Jordan-Wigner transformation these models are equivalent to a one-dimensional chain of 'dyonic' operaors, which are defined by the group elements and irreducible representations of G, and are the extensions of Majorana fermions or parafermions. They prove that these systems have topological zero modes, but rule out exact strong zero modes in cases with non-Abelian G due to what we have described in this thesis as resonances. They argue that with a set of finely tuned spatially varying couplings the exact strong zero mode could be restored, which is equivalent to our argument in section 5.3 showing that the strong zero mode could be protected from a resonance at $J = J_2$ by adding in disorder starting from the edge. However, they do not consider the possibility of almost strong zero modes. Presumably the coherence of the edge dyonic operator remains long even at infinite temperature due to an almost strong zero mode. It would be illuminating to examine Munk *et al.*'s model using the apparatus developed in this thesis to see if this is indeed the case.

Throughout the thesis we have often remarked that the only known exact strong zero modes are in the free fermion Kitaev chain [12] and the XYZ chain [14]. From the point of view of the ADHH theorem the cutoff $n_* \to \infty$ and the emergent $U(1)$ symmetry, which we may associate with particle number conservation, becomes exact. It is natural to assume that $n_* \to \infty$ for all integrable systems, but there is currently no proof of this. If this is true, then in any integrable system in which one can show that the emergent $U(1)$ symmetry due to the ADHH theorem protects the edge spin, the resulting strong zero mode will be exact. One might also speculate whether there is some special non-integrable system, not many-body localised, which can support an exact strong zero mode. If such a system did exist it would have to evade the eigenstate thermalisation hypothesis by some other method. More plausibly, an intermediate edge zero mode might also exist between 'weak' and 'strong', which is exact in some subspace spanned by a special set of finite energy density eigenstates. Precedent has been set for stable long-lived dynamics in a special subset of eigenstates by recent research into 'quantum many-body scarring' [62].

Although in reference [14], Fendley provided an expression for the strong zero mode in the XYZ chain to all orders in perturbation theory and proved that the normalisation converged, technically he did not prove the existence of an exact strong edge zero mode.

This is because the condition which must be satisfied by an exact strong zero mode is that the error – that is, the commutator of the strong zero mode with the Hamiltonian – vanishes as we approach the thermodynamic limit. We have seen in this thesis that the almost strong zero mode can remain normalisable, but saturate in system size and be truncated anyway due to the divergence of the error. Fortunately, there is a proof that the strong zero mode in the XYZ chain is exact in unpublished work by Verstraete and Fendley [63]. They achieve this by rewriting Fendley's all orders perturbative expansion as a very simple translationally invariant matrix product operator.

A translationally invariant matrix product operator M [64] has the following form

$$M = \sum_{i_1 i_2 \ldots} \left\langle x \right| A^{i_1} A^{i_n} \ldots A^{i_L} \left| y \right\rangle O_{i_1} \otimes O_{i_2} \otimes \ldots O_{i_L} \ , \tag{8.1}$$

where the $\{O_{i_j}\}$ are a basis of operators on each lattice site – for example, $\{I, \sigma_j^x, \sigma_j^y, \sigma_j^z\}$ in the spin-half case. The A^{i_1} are a set of square matrices of dimension D, called the bond dimension, and $|x\rangle$ and $|y\rangle$ are vectors of the same dimension. It is described as 'translationally invariant' because each lattice site does not have a different set of matrices associated with it. Verstraete and Fendley [63] showed that the XYZ strong zero mode could be written as a matrix product operator with $D = 4$, which is an extreme simplification of the complicated sum of Pauli matrices previously required. Importantly, because of the translational invariance, an expression for the error can be found in terms of powers of a transfer matrix. It can be shown that all the eigenvalues of this transfer matrix are less than one, so that as the system size increases, the error necessarily vanishes.

A specific choice for $|x\rangle$ and $|y\rangle$ is required to obtain the strong zero mode. Fendley [65] has shown that using the same matrices A^{i_1} but changing these vectors yields a *set* of non-trivial conserved quantities which commute exactly with the Hamiltonian. This hints at a possible deep connection between the strong edge zero mode and integrability. Research is in progress, in part guided by the computer-aided algebra programs developed in this thesis, to find strong zero modes in other integrable systems, such as in spin-one systems, to test the generality of this connection.

One might also wonder whether the matrix product operator approach could be used fruitfully to describe almost strong zero modes. Unfortunately it appears that the bond

dimension D needed to describe an almost strong zero mode grows with system size, such that there is no simple translationally invariant formula as for the exact strong zero mode.

Appendices

A

Unitary transform of the ZXZ SPT chain

In this Appendix, we describe the duality transformation that takes the 1D Haldane-type $\mathbb{Z}_2 \times \mathbb{Z}_2$ SPT of equation (6.1) to the global symmetry breaking phase of two coupled Ising chains. This is adapted to fit our case from work by Chris Laumann [21]. This transformation generalizes the non-local unitary described by Kennedy and Tasaki [66], to reveal the hidden 'string' order of the AKLT model. We will derive it first for the ZXZ model of the $\mathbb{Z}_2 \times \mathbb{Z}_2$ SPT phase and then comment on how it generalizes to the full Hamiltonian. The ZXZ model of the $\mathbb{Z}_2 \times \mathbb{Z}_2$ SPT is given in the commuting limit by the Hamiltonian

$$H_{\text{ZXZ}} = \sum_{j=1}^{L-2} \sigma_j^z \sigma_{j+1}^x \sigma_{j+2}^z \,. \tag{A.1}$$

Pairs of spins that can be arranged into two-site unit cells on this open one dimensional chain, with $L = 2M$ spins in total. The model satisfies the two $\mathbb{Z}_2$ symmetries

$$G_e = \prod_{j=1}^{M} \sigma_{2j}^x \tag{A.2}$$

$$G_o = \prod_{j=1}^{M} \sigma_{2j+1}^x \,. \tag{A.3}$$

We see that in this version of the SPT, we may view the $\mathbb{Z}_2 \times \mathbb{Z}_2$ 'on- site' symmetry as being defined on the unit cells rather than the individual spins.

We now define the duality transformation U out of the following unitaries:

$$\begin{aligned} W &= \prod_{j\text{odd}} (-\sigma^x_{2j+1}) \\ V &= \prod_j (-\sigma^x_{2j} P_j + (1 - P_j)) \\ P_j &= \frac{1 - \prod_{i<j} \sigma^x_{2i+1}}{2} \\ U &= VW. \end{aligned}$$

All of these operators commute as they are formed only out of the X operators on various sites. It can be easily verified that U, V and W are unitary and Hermitian, which the P_j are projectors; that is $P_j = P_j^2 = P^\dagger$.

In order to determine the action of U on local operators, we need only determine its action on an operator basis for the chain. This is conveniently provided by the Pauli operators σ_i^x and σ_i^z on each site i, which are respectively symmetry even/odd under the relevant on-site symmetry

$$\begin{aligned} G_{e/o} \sigma^x_i G^\dagger_{e/o} &= \sigma^x_i \\ G_{e/o} \sigma^z_{2j} G^\dagger_{e/o} &= \pm \sigma^z_{2j} \\ G_{e/o} \sigma^z_{2j+1} G^\dagger_{e/o} &= \pm \sigma^z_{2j+1} \end{aligned}$$

Since U only involves σ^x terms, it is clear that σ^x_j commutes with U, and so that

$$\sigma^x_j i \xrightarrow{U} U^\dagger \sigma^x_i U = \sigma^x_i \tag{A.4}$$

For the even site σ^z operators:

$$\begin{aligned} \sigma^z_{2j} &\xrightarrow{U} U^\dagger \sigma^z_{2j} U \\ &= \left(\prod_{k<j} \sigma^x_{2k+1} \right) \sigma^z_{2j} \\ &= \mathcal{L}_j \sigma^z_{2j}, \end{aligned} \tag{A.5}$$

where we have defined the left-going string operator $\mathcal{L}_j$ which measures the odd-site Ising parity to the left of j.

Meanwhile for odd site operators we find similarly that

$$\begin{aligned}\sigma^z_{2j+1} &\xrightarrow{U} U^\dagger \sigma^z_{2j+1} U \\ &= (-1)^j \sigma^z_{2j} \left(\prod_{k>j} -\sigma^x_{2k} \right) \\ &= (-1)^{j+(M-j-1)} \sigma^z_{2j} \mathcal{R}_j, \end{aligned} \tag{A.6}$$

where $\mathcal{R}_j = \prod_{k>j} \sigma^x_{2k}$ is the right-going string measuring Ising parity.

From equations (A.4), (A.5) and (A.6), we can show that any locally supported operator which is even under both symmetries is mapped to a local operator under U. In particular, any strings generated by symmetry odd operators on different sites cancel. We also note that the duality squares to one, justifying the use of the term.

Now we have introduced the duality, we can examine its effect on the Hamiltonian in equation (6.1). Notice in particular that

$$\begin{gathered}\sigma^z_{2j}\sigma^x_{2j+1}\sigma^z_{2j+2} \overset{U}{\longleftrightarrow} \sigma^z_{2j}\sigma^z_{2j+2} \\ \sigma^z_{2j}\sigma^x_{2j+1}\sigma^z_{2j+2} \overset{U}{\longleftrightarrow} \sigma^z_{2j}\sigma^z_{2j+2} \\ \sigma^x_i \overset{U}{\longleftrightarrow} \sigma^x_i.\end{gathered}$$

Using these relations it is trivial to see that H_{SPT} and H'_{SPT} defined in the main text in equations (6.1) and (6.2) are indeed related by the duality transformation $H_{\text{SPT}} \overset{U}{\longleftrightarrow} H'_{\text{SPT}}$.

Furthermore, under the duality the SPT edge modes as defined in equation (6.3) become

$$\begin{aligned}\Sigma^x &= \sigma^x_1\sigma^z_2 \overset{U}{\longleftrightarrow} \sigma^x_1\sigma^z_2\mathcal{R}_1 = \sigma^z_2 G_e \\ \Sigma^y &= \sigma^y_1\sigma^z_2 \overset{U}{\longleftrightarrow} = i\sigma^z_0\sigma^z_1 G_e \\ \Sigma^z &= \sigma^z_1 \overset{U}{\longleftrightarrow} \sigma^z_1\end{aligned}$$

So, given that G_e is conserved, the autocorrelation times of the SPT edge modes directly follow from the lifetime of the edge magnetisation on each Ising chain.

References

[1] C. Nayak et al. “Non-Abelian anyons and topological quantum computation”. In: *Reviews of Modern Physics* 80 (July 2008), pp. 1083–1159. DOI: 10.1103/RevModPhys.80.1083. arXiv: 0707.1889 (cit. on p. 1).

[2] J. Alicea. “New directions in the pursuit of Majorana fermions in solid state systems”. In: *Reports on Progress in Physics* 75.7, 076501 (July 2012), p. 076501. DOI: 10.1088/0034-4885/75/7/076501. arXiv: 1202.1293 (cit. on p. 1).

[3] S. Das Sarma, M. Freedman, and C. Nayak. “Majorana Zero Modes and Topological Quantum Computation”. In: *NPJ Quantum Information* 1 (2015). DOI: doi:10.1038/npjqi.2015.1 (cit. on p. 1).

[4] Anindya Das et al. “Zero-bias peaks and splitting in an Al-InAs nanowire topological superconductor as a signature of Majorana fermions”. In: *Nat. Phys.* 8 (2012), pp. 887–895. DOI: 10.1038/nphys2479. arXiv: 1205.7073 (cit. on p. 1).

[5] J. M. Deutsch. “Quantum statistical mechanics in a closed system”. In: *Phys. Rev. A* 43.4 (Feb. 1991), pp. 2046–2049. DOI: 10.1103/PhysRevA.43.2046 (cit. on p. 2).

[6] Mark Srednicki. “Chaos and quantum thermalization”. In: *Phys. Rev. E* 50.2 (Aug. 1994), pp. 888–901. DOI: 10.1103/PhysRevE.50.888 (cit. on p. 2).

[7] Enej Ilievski et al. “Quasilocal charges in integrable lattice systems”. en. In: *J. Stat. Mech.* 2016.6 (June 2016), p. 064008. DOI: 10.1088/1742-5468/2016/06/064008 (cit. on pp. 2, 41).

[8] Bruno Bertini et al. “Prethermalization and Thermalization in Models with Weak Integrability Breaking”. In: *Phys. Rev. Lett.* 115.18 (Oct. 2015), p. 180601. DOI: 10.1103/PhysRevLett.115.180601 (cit. on pp. 2, 5, 83).

[9] Rahul Nandkishore and David A. Huse. “Many body localization and thermalization in quantum statistical mechanics”. In: *Annu. Rev. Condens. Matter Phys.* 6.1 (Mar. 2015), pp. 15–38. DOI: 10.1146/annurev-conmatphys-031214-014726. arXiv: 1404.0686 (cit. on pp. 2, 82).

[10] S. A. Parameswaran, Andrew C. Potter, and Romain Vasseur. “Eigenstate phase transitions and the emergence of universal dynamics in highly excited states”. In: *Annalen der Physik* 529.7 (2017), p. 1600302. DOI: 10.1002/andp.201600302. arXiv: 1610.03078 (cit. on pp. 2, 10, 81, 82).

[11] Marcos Rigol et al. “Relaxation in a Completely Integrable Many-Body Quantum System: An Ab Initio Study of the Dynamics of the Highly Excited States of 1D Lattice Hard-Core Bosons”. In: *Phys. Rev. Lett.* 98.5 (Feb. 2007), p. 050405. DOI: 10.1103/PhysRevLett.98.050405 (cit. on p. 2).

[12] A. Y. Kitaev. “Unpaired Majorana fermions in quantum wires”. In: *Physics Uspekhi* 44 (Oct. 2001), p. 131. DOI: 10.1070/1063-7869/44/10S/S29. arXiv: 0010440 (cit. on pp. 3, 10, 11, 41, 60, 65, 96, 102).

[13] J. Alicea and P. Fendley. "Topological phases with parafermions: theory and blueprints". In: *Annual Reviews of Condensed Matter Physics* 7 (2016), pp. 119–139. DOI: 10.1146/annurev-conmatphys-031115-011336. arXiv: 1504.02476 (cit. on pp. 4, 5, 10).

[14] P. Fendley. "Strong zero modes and eigenstate phase transitions in the XYZ/interacting Majorana chain". In: *J. Phys. A* 49, 30LT01 (July 2016), 30LT01. DOI: 10.1088/1751-8113/49/30/30LT01. arXiv: 1512.03441 (cit. on pp. 4, 5, 10, 11, 14, 41, 102).

[15] Michael Moeckel and Stefan Kehrein. "Interaction Quench in the Hubbard Model". In: *Phys. Rev. Lett.* 100 (17 2008), p. 175702. DOI: 10.1103/PhysRevLett.100.175702 (cit. on pp. 5, 83).

[16] F. H. L. Essler et al. "Quench dynamics in a model with tuneable integrability breaking". In: *Phys. Rev. B* 89 (16 2014), p. 165104. DOI: 10.1103/PhysRevB.89.165104. arXiv: 1311.4557 (cit. on p. 5).

[17] Dmitry Abanin et al. *A rigorous theory of many-body prethermalization for periodically driven and closed quantum systems*. 2015. arXiv: 1509.05386 (cit. on pp. 5, 15, 48, 96, 100, 101).

[18] G. Kells. "Many-body Majorana operators and the equivalence of parity sectors". In: *Phys. Rev. B* 92.8, 081401 (Aug. 2015), p. 081401. DOI: 10.1103/PhysRevB.92.081401. arXiv: 1409.6575 (cit. on p. 5).

[19] Jack Kemp et al. "Long coherence times for edge spins". en. In: *J. Stat. Mech.* 2017.6 (2017), p. 063105. DOI: 10.1088/1742-5468/aa73f0. arXiv: 1701.00797. (Visited on 07/26/2017) (cit. on pp. 5, 7, 101).

[20] Dominic V. Else et al. "Prethermal Strong Zero Modes and Topological Qubits". In: *Phys. Rev. X* 7.4 (Dec. 2017), p. 041062. DOI: 10.1103/PhysRevX.7.041062. arXiv: 1704.08703 (cit. on pp. 5–7, 15, 48, 62, 96, 98–101).

[21] J. Kemp, C. Laumann, and N. Yao. "Symmetry enhanced boundary qubits at infinite temperature". unpublished. 2019 (cit. on pp. 5, 19, 88, 106).

[22] P. Fendley. "Parafermionic edge zero modes in Z_n-invariant spin chains". In: *J. Stat. Mech.* 11 (Nov. 2012), p. 20. DOI: 10.1088/1742-5468/2012/11/P11020. arXiv: 1209.0472 (cit. on pp. 5, 10, 30, 41, 43, 44, 46, 98, 101).

[23] A.S. Jermyn et al. "Stability of zero modes in parafermion chains". In: *Phys. Rev. B* 90 (16 2014), p. 165106. DOI: 10.1103/PhysRevB.90.165106. arXiv: 1407.6376 (cit. on pp. 5, 10, 30, 44).

[24] Niall Moran et al. "Parafermionic clock models and quantum resonance". In: *Phys. Rev. B* 95.23 (June 2017). arXiv: 1701.05270, p. 235127. DOI: 10.1103/PhysRevB.95.235127. arXiv: 1701.05270. (Visited on 06/07/2019) (cit. on pp. 5, 45).

[25] Loredana M. Vasiloiu et al. "Strong zero modes in a class of generalised Ising spin ladders with plaquette interactions". In: arXiv preprint (Jan. 2019). arXiv: 1901.10211 (cit. on pp. 6, 99).

[26] Loredana M. Vasiloiu, Federico Carollo, and Juan P. Garrahan. "Enhancing correlation times for edge spins through dissipation". In: *Physical Review B* 98.9 (Sept. 2018). DOI: 10.1103/PhysRevB.98.094308. arXiv: 1805.10060. (Visited on 10/18/2018) (cit. on pp. 6, 100).

[27] Max McGinley, Andreas Nunnenkamp, and Johannes Knolle. "Slow growth of out-of-time-order correlators and entanglement in integrable disordered systems". In: *Phys. Rev. Lett.* 122.2 (Jan. 2019), p. 020603. DOI: 10.1103/PhysRevLett.122.020603 (cit. on pp. 6, 82).

[28] T. D. Schultz, D. C. Mattis, and E. H. Lieb. "Two-Dimensional Ising Model as a Soluble Problem of Many Fermions". In: *Rev. Mod. Phys.* 36 (3 1964), pp. 856–871. DOI: 10.1103/RevModPhys.36.856 (cit. on pp. 9, 81).

[29] M. B. Hastings. "An area law for one-dimensional quantum systems". In: *J. Stat. Mech.* 2007.08 (Aug. 2007), P08024–P08024. DOI: 10.1088/1742-5468/2007/08/P08024 (cit. on p. 10).

[30] Don N. Page. "Average entropy of a subsystem". In: *Phys. Rev. Lett.* 71.9 (Aug. 1993), pp. 1291–1294. DOI: 10.1103/PhysRevLett.71.1291 (cit. on p. 10).

[31] P. Pfeuty. "The One-Dimensional Ising Model with a Transverse Field". In: *Ann. Phys.* 57 (1970), p. 179 (cit. on p. 10).

[32] David Aasen et al. "Milestones Toward Majorana-Based Quantum Computing". In: *Phys. Rev. X* 6 (3 2016), p. 031016. DOI: 10.1103/PhysRevX.6.031016. arXiv: 1511.05153 (cit. on p. 13).

[33] Wolfram Research, Inc. *Some Notes on Internal Implementation*. 2019. URL: https://reference.wolfram.com/language/tutorial/SomeNotesOnInternalImplementation.html (visited on 04/22/2019) (cit. on p. 23).

[34] Daniel Richardson. "Some undecidable problems involving elementary functions of a real variable". In: *Journal of Symbolic Logic* 33.4 (1969), 514–520. DOI: 10.2307/2271358 (cit. on p. 23).

[35] Aaron Meurer et al. "SymPy: symbolic computing in Python". In: *PeerJ Computer Science* 3 (Jan. 2017), e103. DOI: 10.7717/peerj-cs.103. URL: https://doi.org/10.7717/peerj-cs.103 (cit. on p. 24).

[36] Wolfram Research, Inc. *Mathematica, Version 12.0*. Champaign, IL, 2019 (cit. on p. 24).

[37] *MATLAB (R2017b)*. The Mathworks, Inc. Natick, Massachusetts, 2017 (cit. on p. 24).

[38] Christian Bauer, Alexander Frink, and Richard Kreckel. "Introduction to the GiNaC Framework for Symbolic Computation within the C++ Programming Language". In: *Journal of Symbolic Computation* 33.1 (2002), pp. 1 –12. DOI: https://doi.org/10.1006/jsco.2001.0494. arXiv: cs/0004015 (cit. on p. 24).

[39] V. Ros, M. Müller, and A. Scardicchio. "Integrals of motion in the many-body localized phase". In: *Nucl. Phys.* B891 (2015). [Erratum: Nucl. Phys.B900,446(2015)], pp. 420–465. DOI: 10.1016/j.nuclphysb.2014.12.014,10.1016/j.nuclphysb.2015.09.017. arXiv: 1406.2175 (cit. on p. 30).

[40] Walter Selke. "The ANNNI model — Theoretical analysis and experimental application". In: *Physics Reports* 170.4 (Nov. 1988), pp. 213–264. DOI: 10.1016/0370-1573(88)90140-8 (cit. on pp. 36, 64).

[41] P. R. C. Guimarães et al. "Dynamics of the transverse Ising model with next-nearest-neighbor interactions". In: *Phys. Rev. E* 92.4 (Oct. 2015), p. 042115. DOI: 10.1103/PhysRevE.92.042115 (cit. on pp. 36, 64).

[42] Fabio Franchini. *An introduction to integrable techniques for one-dimensional quantum systems*. Vol. 940. Springer, 2017 (cit. on p. 41).

[43] Fabian H. L. Essler et al. *The One-Dimensional Hubbard Model*. Cambridge University Press, 2005. DOI: 10.1017/CBO9780511534843 (cit. on p. 42).

[44] G. von Gehlen and V. Rittenberg. "Operator content of the three-state Potts quantum chain". en. In: *J. Phys. A: Math. Gen.* 19.10 (July 1986), pp. L625–L629. DOI: 10.1088/0305-4470/19/10/013 (cit. on p. 46).

[45] Elliott H. Lieb and Derek W. Robinson. "The finite group velocity of quantum spin systems". en. In: *Commun.Math. Phys.* 28.3 (Sept. 1972), pp. 251–257. DOI: 10.1007/BF01645779 (cit. on p. 48).

[46] T. Matsuta, T. Koma, and S. Nakamura. "Improving the Lieb-Robinson bound for long-range interactions". In: *Ann. Henri Poincaré* 18.2 (Feb. 2017), pp. 519–528. DOI: 10.1007/s00023-016-0526-1. arXiv: 1604.05809 (cit. on pp. 48, 100).

[47] Dominic V. Else et al. "An improved Lieb-Robinson bound for many-body Hamiltonians with power-law interactions". In: arXiv preprint (Sept. 2018). arXiv: 1809.06369 (cit. on pp. 48, 94, 100).

[48] Z. Papic, E. M. Stoudenmire, and Dmitry A. Abanin. "Many-body localization in disorder-free systems: the importance of finite-size constraints". In: *Annals of Physics* 362 (Nov. 2015), pp. 714–725. DOI: 10.1016/j.aop.2015.08.024. arXiv: 1501.00477. (Visited on 06/23/2016) (cit. on p. 80).

[49] John Z. Imbrie. "On Many-Body Localization for Quantum Spin Chains". In: *J Stat Phys* 163.5 (June 2016), pp. 998–1048. DOI: 10.1007/s10955-016-1508-x. arXiv: 1403.7837 (cit. on p. 84).

[50] V. Ros, M. Mueller, and A. Scardicchio. "Integrals of motion in the Many-Body localized phase". In: *Nuclear Physics B* 891 (Feb. 2015), pp. 420–465. DOI: 10.1016/j.nuclphysb.2014.12.014. arXiv: 1406.2175 (cit. on p. 84).

[51] M. P. Grabowski and P. Mathieu. "Integrability test for spin chains". en. In: *J. Phys. A: Math. Gen.* 28.17 (Sept. 1995), pp. 4777–4798. DOI: 10.1088/0305-4470/28/17/013. (Visited on 06/14/2019) (cit. on p. 84).

[52] Romain Vasseur et al. "Particle-hole symmetry, many-body localization, and topological edge modes". In: *Phys. Rev. B* 93.13 (Apr. 2016), p. 134207. DOI: 10.1103/PhysRevB.93.134207 (cit. on p. 86).

[53] Brian Neyenhuis et al. "Observation of prethermalization in long-range interacting spin chains". In: *Science Advances* 3.8 (2017). DOI: 10.1126/sciadv.1700672. arXiv: 1608.00681 (cit. on p. 93).

[54] Sebastian Hild et al. "Far-from-equilibrium spin transport in Heisenberg quantum magnets". In: *Physical Review Letters* 113.14 (Oct. 2014). DOI: 10.1103/PhysRevLett.113.147205. arXiv: 1407.6934 (cit. on p. 93).

[55] P. W. Hess et al. “Non-thermalization in trapped atomic ion spin chains”. In: *Philosophical Transactions of the Royal Society A: Mathematical, Physical and Engineering Sciences* 375 (2108 2017). arXiv: 1704.02439 (cit. on pp. 93, 94).

[56] Amit Dutta and J. K. Bhattacharjee. “Phase transitions in the quantum Ising and rotor models with a long-range interaction”. In: *Phys. Rev. B* 64.18 (Oct. 2001), p. 184106. DOI: 10.1103/PhysRevB.64.184106 (cit. on p. 93).

[57] Azer Kerimov. “Uniqueness of Gibbs states in one-dimensional antiferromagnetic model with long-range interaction”. In: *Journal of Mathematical Physics* 40.10 (1999), pp. 4956–4974. DOI: 10.1063/1.533009 (cit. on p. 93).

[58] I.-D. Potirniche et al. “Floquet Symmetry-Protected Topological Phases in Cold-Atom Systems”. In: *Phys. Rev. Lett.* 119.12 (Sept. 2017), p. 123601. DOI: 10.1103/PhysRevLett.119.123601 (cit. on p. 96).

[59] I. C. Fulga et al. “Adaptive tuning of Majorana fermions in a quantum dot chain”. In: *New Journal of Physics* 15.4, 045020 (Apr. 2013), p. 045020. DOI: 10.1088/1367-2630/15/4/045020. arXiv: 1212.1355 [cond-mat.mes-hall] (cit. on p. 96).

[60] Daniel J. Yates, Fabian H. L. Essler, and Aditi Mitra. “Almost strong $0, \pi$ edge modes in clean, interacting 1D Floquet systems”. In: *Phys. Rev. B* 99.20 (May 2019), p. 205419. DOI: 10.1103/PhysRevB.99.205419. arXiv: 1902.09509. (Visited on 06/24/2019) (cit. on p. 101).

[61] Morten I. K. Munk, Asbjørn Rasmussen, and Michele Burrello. “Dyonic zero-energy modes”. In: *Phys. Rev. B* 98.24 (Dec. 2018), p. 245135. DOI: 10.1103/PhysRevB.98.245135 (cit. on p. 101).

[62] Christopher J. Turner et al. “Quantum many-body scars”. In: *Nature Physics* 14.7 (July 2018), pp. 745–749. DOI: 10.1038/s41567-018-0137-5. arXiv: 1711.03528 (cit. on p. 102).

[63] Frank Verstraete and Paul Fendley. Private communication. 2017 (cit. on p. 103).

[64] Jutho Haegeman and Frank Verstraete. “Diagonalizing Transfer Matrices and Matrix Product Operators: A Medley of Exact and Computational Methods”. In: *Annu. Rev. Condens. Matter Phys.* 8.1 (Mar. 2017), pp. 355–406. DOI: 10.1146/annurev-conmatphys-031016-025507 (cit. on p. 103).

[65] Paul Fendley. Private communication. 2018 (cit. on p. 103).

[66] Tom Kennedy and Hal Tasaki. “Hidden $Z_2 \times Z_2$ symmetry breaking in Haldane-gap antiferromagnets”. In: *Phys. Rev. B* 45 (1 1992), pp. 304–307. DOI: 10.1103/PhysRevB.45.304 (cit. on p. 106).